

A Volume-limited Sample of Ultracool Dwarfs. II. The Substellar Age and Mass Functions in the Solar Neighborhood

WILLIAM M. J. BEST,¹ ANIKET SANGHI,^{1,2} MICHAEL C. LIU,³ EUGENE A. MAGNIER,³ AND TRENT J. DUPUY⁴

¹*The University of Texas at Austin, Department of Astronomy, 2515 Speedway, C1400, Austin, TX 78712, USA*

²*Cahill Center for Astronomy and Astrophysics, California Institute of Technology, 1200 E. California Boulevard, MC 249-17, Pasadena, CA 91125, USA**

³*Institute for Astronomy, University of Hawaii, 2680 Woodlawn Drive, Honolulu, HI 96822*

⁴*Institute for Astronomy, University of Edinburgh, Royal Observatory, Blackford Hill, Edinburgh, EH9 3HJ, UK*

ABSTRACT

We present the most precise constraints to date for the mass and age distributions of single ultracool dwarfs in the solar neighborhood, based on an updated volume-limited sample of 504 L, T, and Y dwarfs within 25 pc. We develop a Monte Carlo approach using the $\langle V/V_{\max} \rangle$ statistic to correct for incompleteness and obtain a space density of $(1.83^{+0.16}_{-0.15}) \times 10^{-2} \text{ pc}^{-3}$ for spectral types L0–Y2. We calculate bolometric luminosities for our sample, using an updated “super-magnitude” method for the faintest objects. We use our resulting luminosity function and a likelihood-based population synthesis approach to simultaneously constrain the mass and age distributions. We employ the fraction of young L0–L7 dwarfs as a novel input for this analysis that is crucial for constraining the age distribution. For a power-law mass function $\frac{dN}{dM} \propto M^{-\alpha}$ we find $\alpha = 0.58^{+0.16}_{-0.20}$, indicating an increase in numbers toward lower masses, consistent with measurements in nearby star-forming regions. For an exponential age distribution $b(t) \propto e^{-\beta t}$ we find $\beta = -0.44 \pm 0.14$, i.e., a population with fewer old objects than often assumed, which may reflect dynamical heating of the Galactic plane as much as the historical brown dwarf birthrate. We compare our analysis to Kirkpatrick et al. (2021), who used a similar volume-limited sample. Although our mass function measurements are numerically consistent, their assumption of a flat age distribution is disfavored by our analysis, and we identify several important methodological differences between our two studies. Our calculation of the age distribution of solar neighborhood brown dwarfs is the first based on a volume-limited sample.

Keywords: Brown dwarfs (185), Infrared photometry (792), Initial mass function (796), L dwarfs (894), Late-type dwarf stars (906), Luminosity function (942), Stellar mass functions (1612), T dwarfs (1679), Trigonometric parallax (1713), Y dwarfs (1827), Stellar evolutionary models (2046)

1. INTRODUCTION

Brown dwarfs are substellar objects more massive than planets but less massive than stars ($\approx 13\text{--}70 M_{\text{Jup}}$; Dupuy & Liu 2017). Given this intermediate station, studies of brown dwarf formation have sought to determine whether the objects are extreme low-mass outcomes of standard star formation processes or high-mass products of planet formation (i.e., in disks around

stars), or have some other origin. Observations of nearby ($\approx 100\text{--}500$ pc) star-forming regions indicate that brown dwarfs form like stars, via turbulent fragmentation and core collapse in molecular clouds (Luhman 2012), but it is unclear whether other mechanisms such as massive disk instability (Boss 1997) or ejection from young multiple systems (Reipurth & Clarke 2001) may contribute significantly to the field population (Chabrier et al. 2014).

Closer to the Sun (i.e., within a few tens of parsecs), the lack of large and complete samples has hampered our understanding of the history of brown dwarf formation. Most brown dwarfs have been discovered by way

Corresponding author: William M. J. Best
wbest@utexas.edu

* NSF Graduate Research Fellow.

of searches in wide-field sky surveys such as the Sloan Digital Sky Survey (SDSS; York et al. 2000) and the Two Micron All Sky Survey (2MASS; Skrutskie et al. 2006) that are severely magnitude-limited for the fainter brown dwarf spectral types. Selection of brown dwarfs from wide-field surveys has become efficient only with multi-wavelength data (e.g. Mace et al. 2013a; Best et al. 2015), in particular including the red-optical bands from the Panoramic Survey Telescope And Rapid Response System (Pan-STARRS1) 3π Survey (PS1; Chambers et al. 2020) and the mid-infrared bands from the Wide-Field Infrared Survey Explorer (*WISE*; Wright et al. 2010). In addition, the parallaxes needed to confirm membership in volume-limited samples are expensive to obtain since most brown dwarfs are too faint to be observed by *Gaia*, and have only recently become available in sufficient numbers to build large, complete samples (e.g. Dupuy & Liu 2012; Faherty et al. 2012; Dahn et al. 2017; Smart et al. 2018; Best et al. 2020; Kirkpatrick et al. 2021).

Precise values for the local brown dwarf mass and age distributions would help to discern the dominant formation mechanism(s), but these quantities have been difficult to ascertain (e.g., Marocco et al. 2015). Brown dwarfs cool throughout their lifetimes, with more massive brown dwarfs beginning as late-M dwarfs and progressing through L, T and Y spectral types over billions of years, while less massive objects reach the cooler spectral types more quickly (e.g., Burrows et al. 1997; Kirkpatrick 2005). This continuous cooling means that a younger, less massive brown dwarf can have the same directly-observable properties (e.g., T_{eff} and luminosity) as an older, more massive brown dwarf. Further, there is no evolutionary phase analogous to the stellar main sequence where T_{eff} can serve as a proxy for mass over any given age range. The masses and ages of field brown dwarfs are therefore not usually measurable from observations; exceptions include dynamical masses from orbital monitoring of binaries and spectroscopic features of unusually old and young brown dwarfs. Kinematic distributions have provided statistical measures of age (Wielen 1977; Faherty et al. 2009), but have not proven capable of distinguishing between a constant, evolving, or largely stochastic birth history (e.g., Burgasser 2004; Day-Jones et al. 2013; Kirkpatrick et al. 2021).

A statistical approach that can overcome the mass-age degeneracy is to synthesize model populations of brown dwarfs characterized by an initial mass function (IMF) and age distribution, evolve the populations to present-day luminosity and T_{eff} using an evolutionary model, and compare the synthetic populations to observations of a well-characterized sample of brown dwarfs. If the

IMF has not changed over time, and no external influences have altered the mass distribution of nearby ultracool dwarfs, then the present-day mass function will be the same as the IMF. Previous efforts in this vein established the first estimates of the local low-mass IMF and formation history (e.g., Burgasser 2004; Allen et al. 2005; Deacon & Hambly 2006; Metchev et al. 2008; Pinfeld et al. 2008; Burningham et al. 2010a; Reyl e et al. 2010; Kirkpatrick et al. 2012; Burningham et al. 2013; Day-Jones et al. 2013; Marocco et al. 2015). These studies used the best space density, luminosity function, binary fraction, and evolutionary models available at the time, but were unable to place significant constraints on either the mass or age distribution for ultracool dwarfs (spectral types M6 and later). Collectively, they only constrained the substellar mass function slope to $-1 \lesssim \alpha \lesssim 1$ (for space density as a function of object mass given by $\Psi(M) \propto M^{-\alpha}$) and could only infer broad agreement with a constant formation rate over the history of the Galaxy. However, new well-characterized volume-limited samples of brown dwarfs in the solar neighborhood — those of Best et al. (2021, hereinafter Paper I) and Kirkpatrick et al. (2021, hereinafter K21) — have breathed new life into the population synthesis approach, enabling precise measurements of observable distributions such as bolometric luminosity (L_{bol}) or T_{eff} needed to constrain the underlying mass and age functions. K21 presented a full-sky 20 pc volume-limited sample from which they derive a mass function estimate of $\alpha = 0.6 \pm 0.1$, assuming a uniform age distribution. In this paper, we present new simultaneous constraints on both the mass and age distributions of very low-mass stars and brown dwarfs in the solar neighborhood using bolometric luminosities from a 25-pc volume-limited sample of L, T, and Y dwarfs.

2. VOLUME-LIMITED SAMPLE

2.1. Sample Definition

In Paper I, we presented a volume-limited sample of 369 L0–T8 dwarfs out to 25 pc defined entirely by parallaxes. Our sample was the first to comprehensively map the L/T transition (spectral types \approx L8–T4), and its 22 young ($\lesssim 200$ Myr) members suggested a young-leaning age distribution. We have now updated our volume-limited sample to include recent nearby brown dwarf discoveries and parallax measurements from the literature (e.g., K21, Zhang et al. 2021; Gaia Collaboration et al. 2023). The boundaries of the sample remain the same — declination $-30^\circ \leq \delta \leq 60^\circ$ (covering 68% of the sky) out to 25 pc from the Sun — but we have extended the coolest spectral type from T8

to Y2, i.e., to include the coldest known types¹. We now also require parallax uncertainties to be less than 1/7 of the parallaxes, rather than 1/5 as in Paper I. This excised only one object from the Paper I sample: SDSS J152103.24+013142.7 (spectral type T3, parallax 43.3 ± 6.2 mas).

We present our updated volume-limited sample in Table 1. The sample now contains 504 objects, increasing from 369 in Paper I primarily due to the inclusion of 86 objects with spectral types T8.5 and cooler. Nearly all of these were discovered or discussed by K21. While

we previously required parallaxes and spectroscopic confirmation for inclusion in our sample, we have allowed 73 objects (15% of our new sample) lacking one or both of these measurements that K21 concluded were bona fide brown dwarfs², so that our volume-limited sample will more completely represent the coldest members of the solar neighborhood. All members of our updated volume-limited sample and associated photometry are tabulated in the UltracoolSheet³ (which also identifies the Paper I volume-limited sample).

¹ WISE J085510.83–071442.5, the coldest brown dwarf identified to date (Luhman 2014a), does not yet have a spectroscopically confirmed spectral type. We adopt the photometric type of $\geq Y2$ (Leggett et al. 2015) for convenience, but note the Y4 photometric estimate of Kirkpatrick et al. (2019).

² 16 have no parallax measurement; 16 have no spectroscopic confirmation; 41 have neither.

³ <http://bit.ly/UltracoolSheet>

Table 1. Our volume-limited 25 pc sample of L0–Y2 dwarfs

Object	Parallax a (mas)	Spectral Type a, b (Optical/NIR)	Flag C	Y_{MKO} (mag)	J_{MKO} (mag)	H_{MKO} (mag)	K_{MKO} (mag)	M_{bol} (mag)	Source d	References (Disc; ϖ ; SpT; Flag; Phot)
SDSS J000013.54+255418.6	70.8 ± 1.9	T5/T4.5	...	15.80 ± 0.06	14.73 ± 0.03	14.74 ± 0.03	14.82 ± 0.03	16.75 ± 0.18	D	123; 73; 0,32; −; 73,123
WISE J000517.48+373720.5	126.9 ± 2.1	.../T9	...	18.48 ± 0.02	17.59 ± 0.02	17.98 ± 0.02	17.99 ± 0.02	20.02 ± 0.05	S	159; 122; 159; −; 134
2MASS J00132229−1143006	40.3 ± 3.1	.../T3pec	16.05 ± 0.02	15.74 ± 0.22	15.76 ± 0.22	16.58 ± 0.24	D	110; 14; 110; −; 14,15
2MASSW J0015447+351603	58.8 ± 0.3	L2/L1.0	...	14.95 ± 0.05	13.74 ± 0.02	12.96 ± 0.02	12.25 ± 0.02	14.40 ± 0.10	D	114; 89; 0,6; −; 15,14
PSO J004.6359+56.8370	46.5 ± 3.9	.../T4.5	16.22 ± 0.02	17.03 ± 0.23	J	14; 14; 14; −; 14
2MASS J00282091+2249050	42.9 ± 1.6	.../L7:	...	16.82 ± 0.05	15.49 ± 0.02	14.55 ± 0.06	13.77 ± 0.06	15.25 ± 0.14	D	39; 89; 39; −; 15,14
WISE J003110.04+574936.3	71.0 ± 3.2	.../L9	BY	15.92 ± 0.05	14.770 ± 0.010	13.862 ± 0.014	13.21 ± 0.03	15.71 ± 0.13	D	218; 122; 12; 16,146; 15,78,12
PSO J007.9194+33.5961	45.4 ± 3.8	.../L9	...	17.48 ± 0.06	16.38 ± 0.02	15.46 ± 0.05	14.67 ± 0.05	16.06 ± 0.16	D	13; 14; 13; −; 15,14
2MASS J00320509+0219017	41.3 ± 0.3	L1.5/M9	...	15.443 ± 0.004	14.220 ± 0.002	13.446 ± 0.002	12.797 ± 0.002	14.15 ± 0.10	D	194; 89; 0,228; −; 126
2MASS J00332386−1521309	43.5 ± 0.8	L4 β /L1; FLD-G	Y	16.38 ± 0.08	15.22 ± 0.06	14.26 ± 0.04	13.39 ± 0.04	14.92 ± 0.12	D	96; 89; 0,3; 54,3; 15
ULAS J003402.77−005206.7	68.7 ± 1.4	.../T9	...	18.90 ± 0.10	18.15 ± 0.03	18.49 ± 0.04	18.48 ± 0.05	19.18 ± 0.18	D	226; 73; 42; −; 226
2MASS J00345157+0523050	118.8 ± 2.7	.../T6.5	...	16.213 ± 0.007	15.140 ± 0.004	15.576 ± 0.010	16.07 ± 0.03	18.45 ± 0.18	D	29; 122; 32; −; 126
2MASSW J0036159+182110	114.47 ± 0.14	L3.5/L4:	B	13.58 ± 0.06	12.30 ± 0.03	11.64 ± 0.03	11.04 ± 0.03	14.66 ± 0.11	D	190; 89; 0,123; 11,186; 73,123
WISE J003829.05+275852.1	88.2 ± 2.0	.../T9	18.61 ± 0.02	18.92 ± 0.04	...	20.35 ± 0.09	S	159; 122; 159; −; 159
HD 3651B	90.02 ± 0.05	.../T7.5	C	17.12 ± 0.06	16.16 ± 0.03	16.68 ± 0.04	16.87 ± 0.05	18.60 ± 0.18	D	174; 89; 154; −; 15,154
WISE J004024.88+090054.8	69.8 ± 1.5	.../T7	...	17.15 ± 0.02	16.131 ± 0.011	16.56 ± 0.02	16.55 ± 0.05	17.91 ± 0.18	D	159; 121; 159; −; 126
2MASSW J0045214+163445	65.4 ± 0.2	L2 β /L2; VI-G	BY	14.22 ± 0.05	12.930 ± 0.010	12.12 ± 0.02	11.33 ± 0.02	13.59 ± 0.10	D	228; 89; 0,3; 186,54,3; 15,78
WISE J004542.56+361139.1	57.0 ± 3.7	.../T5	...	16.81 ± 0.05	15.91 ± 0.02	16.13 ± 0.05	16.07 ± 0.05	17.24 ± 0.20	D	159; 122; 159; −; 15,14
WISE J004851.21+250814.9	74.0 ± 10.4	.../T8.5	19.51 ± 0.16	20.45 ± 0.40	S	171; 122; 171; −; 78
WISEPC J004928.48+044100.1	62.6 ± 2.9	.../L9	...	16.903 ± 0.012	15.767 ± 0.008	14.802 ± 0.006	14.131 ± 0.006	16.16 ± 0.12	D	117; 14; 117; −; 126
WISE J004945.61+215120.0	140.4 ± 2.1	.../T8.5	...	17.29 ± 0.17	16.36 ± 0.02	16.72 ± 0.02	16.80 ± 0.17	19.13 ± 0.19	D	159; 122; 159; −; 15,122,121
SIP5 J0050−1538	40.4 ± 0.2	L1/L0.5	...	14.68 ± 0.05	13.69 ± 0.02	13.15 ± 0.03	12.62 ± 0.03	13.89 ± 0.11	D	62; 89; 0,6; −; 15,14
CFBDS J005910.90−011401.3	103.2 ± 2.1	.../T8.5	...	18.82 ± 0.02	18.06 ± 0.03	18.27 ± 0.05	18.71 ± 0.05	19.92 ± 0.06	S	71; 73; 55; −; 71,131
WISEA J010202.11+035541.4	40.2 ± 2.8	.../L9	...	17.82 ± 0.03	16.67 ± 0.02	15.753 ± 0.012	15.066 ± 0.012	16.14 ± 0.20	D	203; 14; 203; −; 126
SDSSp J010752.33+004156.1	64.1 ± 4.5	L8/L7pec	...	16.91 ± 0.03	15.75 ± 0.03	14.56 ± 0.03	13.58 ± 0.03	15.82 ± 0.15	D	91; 225; 0,85; −; 128
2MASS J01311838+3801554	40.9 ± 0.5	L4/L1.5	...	15.91 ± 0.05	14.63 ± 0.02	13.77 ± 0.03	13.03 ± 0.03	14.39 ± 0.11	D	53; 89; 0,39; −; 15,14
CFBDS J013302.27+023128.4	53.1 ± 2.6	.../T8.5	...	19.36 ± 0.11	18.34 ± 0.08	18.51 ± 0.15	...	19.50 ± 0.14	S	2; 122; 2; −; 126
WISE J013525.64+171503.4	46.7 ± 3.5	.../T6	...	18.03 ± 0.06	17.07 ± 0.02	17.52 ± 0.03	17.74 ± 0.07	18.16 ± 0.23	D	159; 14; 159; −; 15,14,122
2MASSW J0135358+120522	40.1 ± 0.4	L1.5/L0.6	...	15.558 ± 0.005	14.343 ± 0.003	13.558 ± 0.002	12.862 ± 0.002	14.15 ± 0.10	D	114; 89; 0,6; −; 125,126
SIMP J013656.5+093347.3	163.4 ± 0.5	T2/T2.5	Y	14.392 ± 0.003	13.252 ± 0.002	12.809 ± 0.002	12.585 ± 0.002	16.50 ± 0.18	D	4; 89; 0,4; 87; 125,126
WISEPC J013836.59−032221.2	43.9 ± 2.9	.../T3	...	17.290 ± 0.014	16.144 ± 0.007	15.656 ± 0.008	15.27 ± 0.05	16.39 ± 0.20	D	117; 14; 117; −; 170,15
2MASSW J0141032+180450	42.3 ± 0.2	L1/L4.5	...	15.01 ± 0.06	13.83 ± 0.03	13.10 ± 0.03	12.48 ± 0.03	13.83 ± 0.11	D	228; 89; 0,228; −; 15
2MASS J01443536−0716142	78.5 ± 0.5	L5/L5	...	15.52 ± 0.05	14.15 ± 0.02	13.09 ± 0.02	12.26 ± 0.02	15.07 ± 0.10	D	138; 89; 0,164; −; 15,14
WISE J014656.66+423410.0	51.7 ± 2.0	.../T9.5	B	21.60 ± 0.15	20.69 ± 0.07	21.30 ± 0.12	22.40 ± 0.40	20.04 ± 0.12	S	118; 122; 136; 75; 75
CWISE J014837.51−104805.6	66.8 ± 9.3	.../T8.5	18.14 ± 0.03	[[17.94 ± 0.21]]	[[17.96 ± 0.30]]	18.87 ± 0.31	D	122; 122; 122; −; 1,122
WISEPA J015010.86+382724.3	44.6 ± 3.2	.../T0	B	17.05 ± 0.05	15.93 ± 0.02	15.11 ± 0.05	14.54 ± 0.05	15.94 ± 0.15	D	117; 122; 117; 16; 15,14
SDSS J015141.69+124429.6	46.7 ± 3.4	.../T1	...	17.40 ± 0.02	16.388 ± 0.012	15.597 ± 0.012	15.288 ± 0.013	16.49 ± 0.20	D	91; 225; 32; −; 126
2MASS J01550354+0950003	45.0 ± 0.6	L5/L3.2 INT-G	Y	16.109 ± 0.007	14.731 ± 0.004	13.884 ± 0.003	13.11 ± 0.04	14.71 ± 0.11	D	194; 89; 0,85; 85; 126,15

Table 1 continued

Table 1 (continued)

Object	Parallax ^a (mas)	Spectral Type ^{a,b} (Optical/NIR)	Flag ^c	γ_{MKO} (mag)	δ_{MKO} (mag)	H_{MKO} (mag)	K_{MKO} (mag)	M_{bol} (mag)	Source ^d	References (Disc; π ; SpT; Flag; Phot)
HIP 9269B	40.44 ± 0.03	.../L6	C	17.30 ± 0.05	16.13 ± 0.02	15.082 ± 0.014	14.30 ± 0.02	15.60 ± 0.10	D	66; 89; 66; -, 15,66
2MASS J0205034+125142	42.5 ± 3.0	L5/L5.5	...	17.018 ± 0.013	15.561 ± 0.006	14.513 ± 0.004	13.637 ± 0.004	15.11 ± 0.18	D	114; 14; 0,39; -, 126
DENIS J020529.0-115925	49.3 ± 1.6	L7/L5.5::	B	15.55 ± 0.03	16.43 ± 0.05	13.61 ± 0.05	12.99 ± 0.05	14.79 ± 0.14	D	69; 89; 0,123; 124,19; 128
WISEPA J020625.26+264023.6	52.1 ± 1.4	.../L8 (red)	...	17.60 ± 0.12	14.42 ± 0.11	15.16 ± 0.08	14.50 ± 0.08	16.14 ± 0.12	D	117; 145; 145; -, 15
2MASS J0208183+254253	43.1 ± 0.3	L1/L1.5	...	15.06 ± 0.05	13.91 ± 0.02	13.18 ± 0.03	12.57 ± 0.03	13.99 ± 0.11	D	114; 89; 0,201; -, 15,14
2MASS J02132062+3648506C	70.0 ± 0.2	.../T3	C	16.28 ± 0.02	15.158 ± 0.013	14.89 ± 0.02	14.93 ± 0.02	16.80 ± 0.18	D	68; 89; 68; -, 68
2MASS J0213288+444445	51.7 ± 0.2	L1.5/...	13.41 ± 0.02	12.81 ± 0.02	12.19 ± 0.02	14.01 ± 0.10	D	51; 89; 51; -, 14,15
CWISE J021705.51+075849.9	49.1 ± 6.9	.../T6.5	...	18.43 ± 0.04	17.23 ± 0.02	17.75 ± 0.07	17.90 ± 0.13	18.37 ± 0.31	D	122; 122; 122; -, 126
WISEPC J022322.39-293258.1	80.7 ± 2.6	.../T7.5	...	18.08 ± 0.07	17.10 ± 0.05	17.30 ± 0.11	17.59 ± 0.08	18.94 ± 0.19	D	117; 121; 117; -, 15,117
WISEPA J022623.98-021142.8	51.1 ± 2.3	.../T7	B	...	18.41 ± 0.02	18.88 ± 0.10	...	19.56 ± 0.17	J	117; 14; 117; 121; 14,121
2MASS J02271036-1624479	49.9 ± 0.2	L1/L0.5:	...	14.66 ± 0.05	13.53 ± 0.02	12.70 ± 0.03	12.13 ± 0.03	13.84 ± 0.11	D	194; 89; 0,164; -, 15,14
2MASS J02284243+1639329	46.1 ± 0.2	L0;/M8.7	...	14.05 ± 0.05	13.09 ± 0.02	12.38 ± 0.02	11.80 ± 0.02	13.25 ± 0.10	D	194; 89; 0,6; -, 15,14
GJ 1048B	46.4 ± 0.2	L1/L1	C	13.82 ± 0.50	12.66 ± 0.50	12.80 ± 0.08	12.17 ± 0.08	13.71 ± 0.14	D	94; 89; 0,94; -, 15,79
CWISEP J023842.60-133210.7	55.6 ± 7.8	.../Y1 (or later)	Y	21.65 ± 0.35	S	172; 122; 172; 172; 0
2MASS J0243137-245329	93.6 ± 3.6	T5.5/T6	...	16.13 ± 0.06	15.13 ± 0.03	15.39 ± 0.03	15.34 ± 0.03	17.48 ± 0.19	D	24; 225; 0,32; -, 73,123
WISE J024714.52+372523.5	64.8 ± 2.0	.../T8	18.02 ± 0.02	19.88 ± 0.11	S	159; 14; 159; -, 14
2MASS J0251148-035245	86.3 ± 0.2	L3/L1	12.94 ± 0.02	12.30 ± 0.02	11.64 ± 0.02	14.65 ± 0.10	D	51; 89; 0,228; -, 14,15
PSO J043.5395+02.3995	146.1 ± 1.5	.../T8	...	17.000 ± 0.014	15.916 ± 0.009	16.29 ± 0.02	16.73 ± 0.05	19.15 ± 0.18	D	142,207; 121; 142; -, 126
WISEA J025756.40-265528.8	47.2 ± 6.6	.../T9.5	20.99 ± 0.07	20.80 ± 0.38	S	122; 122; 171; -, 122
WISE J025934.00-034645.7	43.9 ± 6.1	.../T5	18.78 ± 0.49	S	159; 122; 159; -, 0
CFBDS J030135.11-161418.0	49.1 ± 3.8	.../T7	...	19.38 ± 0.05	18.34 ± 0.07	18.99 ± 0.10	18.07 ± 0.06	18.51 ± 0.22	D	2; 1; 2; -, 2
WISE J030449.03-270508.3	73.1 ± 2.6	.../X0pec	20.79 ± 0.09	21.02 ± 0.16	...	21.22 ± 0.14	S	185; 122; 185; -, 185
2MASS J03140344+1603056	72.6 ± 0.2	L0/L0; FLD-g	...	[13.47 ± 0.05]	12.410 ± 0.010	11.87 ± 0.02	11.21 ± 0.02	13.72 ± 0.10	D	194; 89; 0,3; -, 1,78,15
WISE J031614.68+382008.0	44.2 ± 3.1	.../T3	15.90 ± 0.02	[[15.56 ± 0.08]]	[[15.38 ± 0.10]]	16.47 ± 0.21	D	159; 122; 159; -, 1,14,122
WISE J031624.35+430709.1	74.7 ± 2.1	.../T8	19.47 ± 0.04	19.70 ± 0.09	...	20.24 ± 0.10	S	159; 122; 159; -, 159
WISEA J032301.86+562558.0	51.9 ± 3.0	.../L7	...	17.06 ± 0.05	15.78 ± 0.02	14.70 ± 0.05	13.75 ± 0.05	15.59 ± 0.15	D	157; 122; 157; -, 15,14
WISE J032547.72+083118.2	76.3 ± 2.8	.../T7	...	[16.96 ± 0.05]	16.090 ± 0.010	[16.41 ± 0.05]	[16.28 ± 0.05]	17.85 ± 0.19	D	159; 122; 159; -, 1,78
SDSS J032553.17+042540.1	44.0 ± 3.2	.../T5.5	...	17.168 ± 0.014	15.996 ± 0.009	16.26 ± 0.02	16.52 ± 0.04	17.17 ± 0.21	D	50; 14; 50; -, 126
PSO J052.2746+13.3754	44.3 ± 3.0	.../T3.5	...	17.34 ± 0.05	16.23 ± 0.02	15.93 ± 0.05	15.73 ± 0.05	16.69 ± 0.20	D	14; 14; 14; -, 15,14
PSO J052.7214-03.8409	59.2 ± 3.3	.../L9;	...	17.36 ± 0.05	16.26 ± 0.02	15.24 ± 0.02	14.58 ± 0.05	16.37 ± 0.19	D	13; 122; 13; -, 15,13
WISE J033515.01+431045.1	84.8 ± 1.7	.../T9	...	19.95 ± 0.03	19.32 ± 0.02	19.87 ± 0.04	20.86 ± 0.11	20.37 ± 0.08	S	159; 122; 159; -, 134
WISE J033605.05-014350.4	99.8 ± 2.1	.../Y0;	19.44 ± 0.14	21.21 ± 0.07	S	159; 122; 168; -, 169
CWISE J034146.12+471530.5	46.7 ± 6.5	.../T1.5	...	17.38 ± 0.02	16.269 ± 0.011	15.729 ± 0.013	15.53 ± 0.02	16.63 ± 0.25	D	122; 122; 122; -, 126
2MASS J03552337+1133437	109.1 ± 0.5	L5 γ /L3; VL-g	BY	15.46 ± 0.06	13.940 ± 0.010	12.60 ± 0.02	11.502 ± 0.001	15.03 ± 0.10	D	193; 89; 0,3; 11,54,3; 15,78,125
UGPS J03553200+4743588	66.4 ± 3.2	.../T6;	16.20 ± 0.02	16.58 ± 0.02	16.50 ± 0.04	17.79 ± 0.20	D	214; 122; 214; -, 214
WISE J040137.21+284951.7	80.4 ± 0.2	L3/L2.5	...	14.61 ± 0.05	13.34 ± 0.02	12.50 ± 0.02	11.80 ± 0.02	14.65 ± 0.10	D	49; 89; 0,49; -, 15,14
CWISEP J040235.55-265145.4	82.5 ± 11.6	.../Y1 (or later)	20.12 ± 0.16	21.62 ± 0.33	S	172; 122; 172; -, 170
WISE J040418.01+412735.6	61.7 ± 0.3	L2/L2pec	...	15.37 ± 0.05	14.08 ± 0.02	13.17 ± 0.02	12.343 ± 0.002	14.62 ± 0.10	D	49; 89; 0,49; -, 15,14,153
2MASS J04070885+1514565	56.7 ± 2.1	.../T5	Y	16.88 ± 0.05	15.67 ± 0.02	15.84 ± 0.05	15.88 ± 0.03	17.10 ± 0.18	D	29; 122; 32; 122; 15,14,126
2MASS J0408290-145033	45.6 ± 0.3	L2/L4.5	...	15.33 ± 0.05	14.15 ± 0.02	13.41 ± 0.02	12.80 ± 0.02	14.39 ± 0.10	D	228; 89; 0,228; -, 15,14

Table 1 continued

Table 1 (continued)

Object	Parallax ^a (mas)	Spectral Type ^{a, b} , (Optical/NIR)	Flag ^c	γ_{MKO} (mag)	δ_{MKO} (mag)	H_{MKO} (mag)	K_{MKO} (mag)	M_{bol} (mag)	Source ^d	References (Disc; ϖ ; SpT; Flag; Phot)
PSO J062.3459+11.1794	45.7 ± 2.7	.../T3.5	16.17 ± 0.02	15.73 ± 0.15	15.88 ± 0.02	16.81 ± 0.19	D	14; 14; 14; -; 14,15,126
WISEPA J041022.71+150248.5	151.3 ± 2.0	.../Y0	...	19.61 ± 0.04	19.44 ± 0.03	20.02 ± 0.05	19.91 ± 0.07	21.50 ± 0.04	S	55; 122; 117; -; 133
CWISE J041102.41+471422.6	61.0 ± 8.5	.../T7	17.67 ± 0.02	18.11 ± 0.07	...	19.20 ± 0.34	J	122; 122; 122; -; 126
Gaia J041246.85-073416.8	60.0 ± 0.2	.../L2pec	13.480 ± 0.010	12.82 ± 0.03	[[12.25 ± 0.03]]	14.45 ± 0.11	D	122; 89; 122; -; 1,169,59
2MASS J04134574+3709087	51.9 ± 0.2	L1/...	[[13.73 ± 0.04]]	13.04 ± 0.04	[[12.47 ± 0.02]]	14.35 ± 0.10	D	116,195; 89; 195; -; 1,59
2MASS J0415195-093506	175.2 ± 1.7	T8/T8	...	16.39 ± 0.06	15.32 ± 0.03	15.70 ± 0.03	15.83 ± 0.03	18.89 ± 0.18	D	24; 73; 0,32; -; 15,123
WISEA J041743.13+241506.3	84.0 ± 11.8	.../T6	15.520 ± 0.010	[[15.71 ± 0.14]]	15.77 ± 0.02	17.62 ± 0.29	D	104; 122; 104; -; 1,78,59,126
SDSSP J042348.57-041403.5	70.2 ± 0.9	L7.5/T0	B	15.41 ± 0.03	14.30 ± 0.03	13.51 ± 0.03	12.96 ± 0.03	15.48 ± 0.11	D	91; 89; 0,32; 30; 128
WISE J042417.94+072744.1	43.7 ± 1.5	.../T7.5	18.32 ± 0.02	19.13 ± 0.16	J	159; 14; 159; -; 14
CWISEP J042455.68+000221.4	53.2 ± 7.5	.../T9;	19.67 ± 0.07	20.45 ± 0.41	S	122; 122; 122; -; 122
WISE J043052.92+463331.6	96.1 ± 2.9	.../T8	19.06 ± 0.02	19.25 ± 0.13	...	20.40 ± 0.08	S	159; 122; 159; -; 14,159
CWISE J043309.36+100902.3	46.3 ± 6.5	.../T8	17.94 ± 0.04	18.89 ± 0.34	J	122; 122; 122; -; 78
2MASS J0439010-235308	80.7 ± 0.4	L6.5/L6	...	15.51 ± 0.06	14.31 ± 0.03	13.44 ± 0.03	12.77 ± 0.02	15.58 ± 0.10	D	51; 89; 0,39; -; 15,79
WISEPA J044853.29-193548.5	57.6 ± 3.0	.../T5pec	...	17.51 ± 0.06	16.63 ± 0.02	16.94 ± 0.06	17.30 ± 0.08	18.17 ± 0.21	D	117; 122; 117; -; 15,14
WISE J045746.08-020719.2	82.0 ± 2.9	.../T2	14.64 ± 0.02	14.187 ± 0.004	13.986 ± 0.004	16.44 ± 0.18	D	17; 14; 17; -; 14,126
WISEPA J050003.05-122343.2	84.6 ± 2.2	.../T8	...	18.69 ± 0.06	17.88 ± 0.02	18.13 ± 0.12	18.06 ± 0.08	19.19 ± 0.18	D	117; 14; 117; -; 15,14,117
2MASS J05002100+0330501	75.6 ± 0.3	L4/L4.2 FLD-G	...	14.93 ± 0.05	13.60 ± 0.02	12.76 ± 0.02	12.04 ± 0.02	14.77 ± 0.10	D	194; 89; 0,85; -; 15
WISEA J050048.17+044214.2	43.9 ± 0.3	.../L0.5pec	[[13.75 ± 0.03]]	13.11 ± 0.03	[[12.49 ± 0.03]]	13.94 ± 0.11	D	120; 89; 120; -; 1,59
2MASS J05012406-0010452	47.8 ± 0.8	L4 γ /L3; VL-G	Y	16.26 ± 0.06	14.89 ± 0.04	13.78 ± 0.04	12.92 ± 0.04	14.64 ± 0.11	D	194; 89; 0,3; 54,3; 15
WISEA J050238.28+100750.0	42.7 ± 4.6	.../T7.5	18.90 ± 0.11	19.73 ± 0.36	S	122; 122; 122; -; 78
PSO J076.7092+52.6087	61.3 ± 3.1	.../T4.5	...	16.61 ± 0.05	15.44 ± 0.02	15.47 ± 0.02	15.60 ± 0.03	17.03 ± 0.19	D	13; 122; 13; -; 15,13
WISE J050854.88+331920.8	53.0 ± 0.5	L2/...	[[14.15 ± 0.04]]	13.29 ± 0.04	[[12.60 ± 0.03]]	14.54 ± 0.11	D	156; 89; 120; -; 1,59
2MASS J0512063-294954	49.6 ± 2.8	L5 γ /L3.8 INT-G	Y	16.86 ± 0.08	15.300 ± 0.010	14.26 ± 0.04	13.25 ± 0.04	15.06 ± 0.16	D	51; 1; 0,85; 81,85; 15,169
WISEPA J051317.28+060814.7	70.8 ± 1.5	.../T6.5	15.97 ± 0.06	16.19 ± 0.08	16.17 ± 0.11	17.64 ± 0.20	D	117; 121; 117; -; 15
CWISE J051427.35+200447.7	54.1 ± 7.6	.../T0.5	...	17.09 ± 0.02	15.885 ± 0.010	[[15.08 ± 0.08]]	14.537 ± 0.005	16.22 ± 0.26	D	122; 122; 122; -; 1,126,59
2MASS J05160945-0445499	47.8 ± 2.8	.../T5.5	...	16.813 ± 0.013	15.545 ± 0.008	15.773 ± 0.011	15.79 ± 0.02	16.82 ± 0.19	D	28; 122; 32; -; 125,126
2MASS J05185995-2828372	43.7 ± 0.8	L7/T1pec	B	17.12 ± 0.11	15.87 ± 0.10	14.86 ± 0.07	14.11 ± 0.07	15.58 ± 0.12	D	52; 73; 0,32; 33; 15,79
WISE J052126.29+102528.4	150.2 ± 3.0	.../T7.5	...	15.71 ± 0.05	14.87 ± 0.02	15.27 ± 0.05	15.00 ± 0.05	18.00 ± 0.18	D	17; 122; 17; -; 15,14
UGPS J052127.27+364048.6	122.2 ± 1.6	.../T8.5	...	[[18.08 ± 0.05]]	16.93 ± 0.02	17.28 ± 0.04	17.32 ± 0.09	19.20 ± 0.18	D	46; 121; 46; -; 1,153
2MASS J0523382-140302	78.5 ± 0.2	L2.5/L5	13.02 ± 0.03	12.27 ± 0.03	11.62 ± 0.03	14.40 ± 0.11	D	51; 89; 0,228; -; 15
SDSSP J053951.99-005902.0	78.9 ± 0.4	L5/L5	...	15.02 ± 0.03	13.85 ± 0.03	13.04 ± 0.03	12.40 ± 0.03	15.21 ± 0.10	D	83; 89; 0,123; -; 127
PSO J085.1080-18.0445	59.2 ± 4.0	.../T5	15.99 ± 0.02	...	[[16.13 ± 0.04]]	17.34 ± 0.20	D	14; 14; 122; -; 1,14,169
WISE J054047.00+483232.4	69.4 ± 2.1	.../T8.5	18.49 ± 0.02	18.62 ± 0.05	...	20.07 ± 0.10	S	159; 122; 159; -; 159
WISEPA J054231.26-162829.1	61.3 ± 2.6	.../T6.5	16.28 ± 0.02	16.63 ± 0.10	16.76 ± 0.14	17.85 ± 0.22	D	117; 14; 117; -; 14,15
WISE J054601.19-095947.5	50.4 ± 3.6	.../T5	...	17.04 ± 0.05	15.98 ± 0.02	16.24 ± 0.05	16.43 ± 0.06	17.30 ± 0.21	D	159; 14; 159; -; 15,14
WISEA J055007.94+161051.9	49.2 ± 0.5	.../L2	...	15.64 ± 0.05	14.36 ± 0.02	13.56 ± 0.03	12.81 ± 0.03	14.59 ± 0.11	D	119; 89; 119; -; 15,14
PSO J089.1751-09.4513	44.3 ± 2.5	.../T5.5	...	17.66 ± 0.06	16.46 ± 0.02	16.58 ± 0.06	16.66 ± 0.07	17.27 ± 0.20	D	14; 14; 14; -; 15,14
2MASS J05591914-1404488	95.3 ± 0.7	T5/T4.5	...	14.69 ± 0.02	13.57 ± 0.03	13.64 ± 0.03	13.73 ± 0.03	16.48 ± 0.18	D	23; 89; 0,32; -; 128
CWISE J060149.45+141955.2	54.3 ± 7.6	.../T2.5	15.784 ± 0.005	15.321 ± 0.006	14.816 ± 0.009	16.40 ± 0.26	D	122; 122; 122; -; 126
2MASS J06020638+4043588	76.4 ± 3.1	.../T4.5	...	16.38 ± 0.05	15.28 ± 0.02	15.39 ± 0.05	15.41 ± 0.05	17.22 ± 0.19	D	150; 122; 150; -; 15,14

Table 1 continued

Table 1 (continued)

Object	Parallax a (mas)	Spectral Type a, b (Optical/NIR)	Flag c	γ_{MKO} (mag)	δ_{MKO} (mag)	H_{MKO} (mag)	K_{MKO} (mag)	M_{bol} (mag)	Source d	References (Disc; ϖ ; SpT; Flag; Phot)
LSR J0602+3910	85.76 ± 0.13	L1/L2: INT-G	Y	[13.29 ± 0.05]	12.160 ± 0.010	11.51 ± 0.02	10.83 ± 0.02	13.70 ± 0.10	D	197; 89; 0.3; 3; 1,78,15
WISEP J060738.65+242953.4	138.1 ± 0.5	L8/L9	...	15.35 ± 0.06	14.12 ± 0.03	13.12 ± 0.03	12.46 ± 0.02	16.19 ± 0.18	D	48; 89; 0.49; -; 15
Gl 229B	173.57 ± 0.02	.../T7pec	C	15.17 ± 0.10	14.01 ± 0.05	14.36 ± 0.05	14.36 ± 0.05	17.74 ± 0.18	D	177; 89; 32; -; 129
WISEPA J061135.13-041024.0	47.2 ± 3.2	.../T0	B	16.614 ± 0.010	15.398 ± 0.006	14.743 ± 0.005	14.292 ± 0.005	15.85 ± 0.15	D	117; 92; 117; 92; 125,92,126
WISEP J061348.70+480820.5	49.7 ± 4.9	.../T5	15.940 ± 0.010	[16.03 ± 0.05]	[16.06 ± 0.07]	17.04 ± 0.23	D	122; 122; 122; -; 1,78,212
WISEPA J061407.49+391236.4	53.7 ± 1.7	.../T6	B	...	16.340 ± 0.010	16.42 ± 0.25	...	17.58 ± 0.16	J	117; 121; 117; 121; 78,15
WISE J061437.73+095135.0	64.9 ± 2.0	.../T7	...	17.54 ± 0.05	16.44 ± 0.02	16.66 ± 0.05	16.51 ± 0.05	17.76 ± 0.19	D	159; 122; 159; -; 15,14
2MASS J061438.18+3950357	44.0 ± 2.6	.../L9;	...	17.63 ± 0.05	16.54 ± 0.02	15.67 ± 0.05	15.04 ± 0.05	16.26 ± 0.20	D	176; 14; 176; -; 15,14
DENIS-P J0615493-010041	45.0 ± 0.2	L2;L1.0	...	14.75 ± 0.06	13.70 ± 0.03	13.05 ± 0.03	12.52 ± 0.03	14.04 ± 0.11	D	180; 89; 0.6; -; 15
WISEA J061557.21+152626.1	52.8 ± 3.1	.../T8.5	18.94 ± 0.05	20.11 ± 0.20	S	168; 122; 168; -; 168
CWISE J061741.79+194512.8	133.0 ± 18.6	.../L6.5	B	...	13.930 ± 0.010	13.180 ± 0.010	12.490 ± 0.010	16.15 ± 0.22	D	122; 122; 122; 122; 126
WISEPA J062309.94-045624.6	86.5 ± 1.7	.../T8	...	18.04 ± 0.06	17.10 ± 0.02	17.34 ± 0.07	17.26 ± 0.09	18.83 ± 0.19	D	117; 14; 117; -; 15,14
Gaia J062317.14+263131.8	48.6 ± 0.5	.../L3pec	14.560 ± 0.010	13.59 ± 0.03	[12.85 ± 0.03]	14.60 ± 0.11	D	122; 89; 122; -; 1,78,59
WISEPA J062542.21+1564625.5	49.5 ± 2.0	.../T6	16.73 ± 0.02	16.96 ± 0.10	16.96 ± 0.15	17.65 ± 0.22	D	117; 121; 117; -; 14,15
WISEPA J062720.07-111428.8	74.8 ± 3.6	.../T6	...	[16.38 ± 0.05]	15.240 ± 0.010	15.50 ± 0.18	15.51 ± 0.18	17.26 ± 0.22	D	117; 121; 117; -; 1,169,15
CWISEP J063428.10+504925.9	62.0 ± 4.2	.../Y0	21.49 ± 0.19	S	172; 122; 122; -; 0
Gaia J064025.19-235219.4	49.8 ± 0.6	.../L5	[14.99 ± 0.05]	14.14 ± 0.05	[13.42 ± 0.05]	15.23 ± 0.11	D	122; 89; 122; -; 1,59
WISE J064205.58+410155.5	64.1 ± 1.1	.../L9 (red)	Y	17.30 ± 0.05	16.15 ± 0.02	15.113 ± 0.014	14.306 ± 0.012	16.31 ± 0.18	D	159; 1; 13; 13,122; 15,13
WISEA J064223.48+042343.1	41.1 ± 5.8	.../T8	17.65 ± 0.02	18.07 ± 0.07	...	18.34 ± 0.34	J	168; 122; 168; -; 153
WISE J064336.71-022315.4	71.3 ± 1.2	.../L8	15.35 ± 0.05	14.44 ± 0.05	13.60 ± 0.06	16.00 ± 0.11	D	161; 89; 161; -; 15
WISEA J064503.72+524054.1	53.5 ± 4.2	.../T8.5	18.93 ± 0.09	20.07 ± 0.24	S	122; 122; 122; -; 78
WISE J064528.38-030248.2	54.1 ± 3.0	.../T6	16.934 ± 0.011	17.33 ± 0.03	17.34 ± 0.09	18.10 ± 0.21	D	222; 122; 222; -; 125
CWISE J064749.87-160022.7	49.0 ± 6.9	.../T6	16.90 ± 0.02	...	[17.47 ± 0.12]	18.03 ± 0.31	D	122; 122; 122; -; 1,170
WISEA J064750.85-154616.4	62.7 ± 3.3	.../L9.5	B	...	15.15 ± 0.02	14.35 ± 0.06	13.72 ± 0.06	15.88 ± 0.14	D	209; 122; 209; 16; 14,15
DENIS-P J0652197-253450	62.26 ± 0.09	L0/L2 β	Y	13.67 ± 0.05	12.72 ± 0.02	12.09 ± 0.02	11.49 ± 0.02	13.66 ± 0.10	D	180; 89; 0.7; 7; 15
PSO J103.0927+41.4601	57.6 ± 3.3	.../T0	B	16.47 ± 0.05	15.361 ± 0.014	14.51 ± 0.03	13.95 ± 0.03	15.92 ± 0.20	D	12; 122; 12; 16; 15,12
2MASS J0652307+471034	109.8 ± 0.3	L4.5/L6.5	...	14.74 ± 0.05	13.38 ± 0.02	12.47 ± 0.02	11.67 ± 0.02	15.20 ± 0.10	D	51; 89; 0.39; -; 15,14
WISEPA J065609.60+420531.0	63.0 ± 4.1	T2/T3	...	16.19 ± 0.05	15.27 ± 0.02	14.98 ± 0.05	14.99 ± 0.05	16.70 ± 0.20	D	117; 14; 0,117; -; 15,14
2MASS J07003664+3157266	89.0 ± 0.4	L3.5/...	B	...	12.82 ± 0.02	11.98 ± 0.02	11.27 ± 0.02	14.31 ± 0.10	D	219; 89; 219; 193,76; 79
WISE J071322.55-291751.9	109.3 ± 2.1	.../Y0	...	20.34 ± 0.08	19.98 ± 0.05	20.19 ± 0.08	21.30 ± 0.31	20.88 ± 0.08	S	118; 122; 118; -; 134
WISEA J071552.38-114532.9	55.5 ± 0.3	.../L4pec	...	15.41 ± 0.05	14.18 ± 0.02	13.58 ± 0.05	12.78 ± 0.04	14.84 ± 0.11	D	119; 89; 119; -; 15,14
DENIS-P J0716478-063037	40.8 ± 0.2	L1;L1.1	...	14.85 ± 0.05	13.799 ± 0.002	13.131 ± 0.001	12.556 ± 0.002	13.84 ± 0.10	D	180; 89; 0.6; -; 15,153
UGPS J072227.51-054031.2	242.8 ± 2.4	T9/T9	...	17.37 ± 0.02	16.518 ± 0.010	16.90 ± 0.02	17.07 ± 0.08	20.39 ± 0.04	S	152; 132; 0.55; -; 152
WISE J072312.44+340313.5	60.8 ± 2.1	.../T9;	18.19 ± 0.02	18.63 ± 0.06	...	19.59 ± 0.11	S	159; 122; 159; -; 122,121
2MASS J0727182+171001	112.5 ± 0.9	T8/T7	...	16.16 ± 0.06	15.19 ± 0.03	15.67 ± 0.03	15.69 ± 0.03	18.05 ± 0.18	D	24; 73; 0.32; -; 73,123
2MASS J07414279-0506464	43.3 ± 1.5	.../L5;	14.100 ± 0.010	13.19 ± 0.05	[12.36 ± 0.03]	13.76 ± 0.14	D	210,58; 89; 58; -; 1,169,59
SDSS J074149.15+235127.5	73.2 ± 3.4	.../T5	...	17.129 ± 0.013	15.886 ± 0.005	16.10 ± 0.02	16.28 ± 0.04	17.78 ± 0.19	D	123; 122; 32; -; 126
GDSS J074201.41+205520.5	63.5 ± 3.1	.../T5	...	16.98 ± 0.06	15.60 ± 0.03	15.95 ± 0.03	16.06 ± 0.03	17.39 ± 0.19	D	123; 122; 32; -; 15,123
WISEPA J074457.15+562821.8	65.3 ± 2.0	.../T8	17.27 ± 0.02	17.65 ± 0.12	17.70 ± 0.20	18.70 ± 0.23	D	117; 122; 117; -; 14,15
ULAS J074502.79+233240.3	51.5 ± 7.2	.../T8.5	...	20.00 ± 0.15	18.88 ± 0.07	47; 122; 47; -; 126

Table 1 continued

Table 1 (continued)

Object	Parallax a (mas)	Spectral Type a, b (Optical/NIR)	Flag c	Y_{MKO} (mag)	J_{MKO} (mag)	H_{MKO} (mag)	K_{MKO} (mag)	M_{bol} (mag)	Source d	References (Disc; τ ; SpT; Flag; Phot)
2MASS J09054654+5623117	41.3 ± 1.1	L5/L6	...	16.67 ± 0.06	15.33 ± 0.02	14.37 ± 0.04	13.71 ± 0.04	15.12 ± 0.12	D	194; 89; 0.39; -, 15,14
WISEPA J090649.36+473538.6	47.0 ± 2.9	.../T8	B	...	17.85 ± 0.04	17.87 ± 0.16	18.67 ± 0.34	18.85 ± 0.29	D	117; 122; 117; 77; 78,15
2MASS J0908380+503208	95.9 ± 0.6	L5/L9;	...	15.52 ± 0.05	14.43 ± 0.02	13.56 ± 0.03	12.93 ± 0.03	15.98 ± 0.10	D	51; 89; 0.123; -, 15,14
DENIS-P J090957.1-065806	40.6 ± 0.2	L0/L0;	...	14.90 ± 0.05	13.81 ± 0.02	13.12 ± 0.02	12.50 ± 0.03	13.75 ± 0.11	D	70; 89; 0.164; -, 15,79
CWISE J091105.02+214645.1	72.8 ± 10.2	.../T9	17.480 ± 0.010	17.88 ± 0.05	...	19.55 ± 0.37	S	122; 122; 122; -, 122
Gl 337CD	49.2 ± 0.3	L8/T0	BC	16.68 ± 0.05	15.53 ± 0.02	14.65 ± 0.08	14.00 ± 0.06	15.70 ± 0.11	D	227; 89; 0.32; 31; 15,14,79
2MASS J09153413+0422045	56.7 ± 0.9	L6/L6	B	15.770 ± 0.005	14.518 ± 0.003	13.632 ± 0.003	12.887 ± 0.002	14.99 ± 0.11	D	194; 89; 0.201; 193; 126
WISE J092055.40+453856.3	81.3 ± 1.5	.../L9.5	...	16.14 ± 0.05	15.04 ± 0.01	14.19 ± 0.02	13.766 ± 0.011	16.29 ± 0.18	D	159; 89; 12; -, 15,12
2MASS J09211410-2104446	79.6 ± 0.2	L1.5/L4: (blue)	...	13.77 ± 0.05	12.71 ± 0.02	12.23 ± 0.02	11.66 ± 0.02	14.48 ± 0.10	D	194; 89; 0.36; -, 15,14
SDSS J092308.70+234013.7	40.6 ± 0.3	L1/L2.3	...	14.82 ± 0.05	13.79 ± 0.02	13.23 ± 0.02	12.78 ± 0.02	14.09 ± 0.11	D	200; 89; 0.6; -, 15,14
SDSSp J092615.38+584720.9	43.4 ± 1.0	T5/T4.5	B	16.90 ± 0.08	15.71 ± 0.06	15.38 ± 0.19	15.53 ± 0.19	16.54 ± 0.21	D	91; 76; 0.32; 33; 15
WISEPC J092906.77+040957.9	41.0 ± 2.2	.../T6.5	...	17.890 ± 0.010	16.870 ± 0.010	17.240 ± 0.010	17.61 ± 0.02	17.83 ± 0.20	D	117; 121; 117; -, 47
2MASS J0937347+293142	163.4 ± 1.8	T7/T6pec	...	15.18 ± 0.06	14.29 ± 0.03	14.67 ± 0.03	15.39 ± 0.06	18.46 ± 0.18	D	24; 198; 0.32; -, 73,123
CWISEP J093852.89+063440.6	53.2 ± 7.5	.../Y0	21.03 ± 0.12	21.12 ± 0.37	S	172; 122; 172; -, 172
2MASS J09393548-2448279	187.3 ± 4.6	T8/T8	...	16.47 ± 0.09	15.61 ± 0.09	15.96 ± 0.09	16.83 ± 0.09	19.00 ± 0.07	S	221; 37; 0.32; -, 130
CWISEP J094005.50+523359.2	75.0 ± 10.5	.../Y1 (or later)	21.72 ± 0.33	S	172; 122; 172; -, 0
WISE J094305.98+360723.5	97.1 ± 2.9	.../T9.5	19.74 ± 0.05	20.32 ± 0.04	...	20.67 ± 0.10	S	56; 122; 56; -, 56,202
2MASS J09490860-1545485	42.2 ± 2.7	.../T8	...	17.09 ± 0.05	15.82 ± 0.02	[15.22 ± 0.05]	[15.22 ± 0.05]	16.31 ± 0.20	D	221; 122; 32; -, 15,14,1
ULAS J095047.28+011734.3	51.00 ± 0.03	.../T8	C	18.90 ± 0.03	18.02 ± 0.03	18.40 ± 0.03	18.85 ± 0.07	19.08 ± 0.18	D	47; 89; 159; -, 47
WISEPC J095259.29+195507.3	40.0 ± 3.0	.../T6	B	17.88 ± 0.08	16.91 ± 0.02	17.28 ± 0.10	17.51 ± 0.08	17.72 ± 0.22	D	117; 122; 117; 77; 15,78
ULAS J095429.90+062309.6	40.9 ± 3.2	.../T5	...	17.730 ± 0.010	16.600 ± 0.010	16.870 ± 0.010	17.050 ± 0.010	17.42 ± 0.21	D	208,47; 14; 47; -, 47
PSO J149.0341-14.7857	65.4 ± 3.4	.../L9	...	17.18 ± 0.05	15.99 ± 0.02	15.073 ± 0.013	14.46 ± 0.02	16.43 ± 0.19	D	13; 14; 13; -, 15,13
G 196-3B	46.2 ± 0.6	L3 β /L3; VL-G	CY	16.23 ± 0.07	14.73 ± 0.05	13.72 ± 0.03	12.73 ± 0.03	14.35 ± 0.11	D	189; 89; 0.3; 54,3; 15
DENIS J1004403-131818	40.4 ± 0.5	L0/L1:	14.62 ± 0.04	13.93 ± 0.04	13.34 ± 0.04	14.70 ± 0.11	D	167; 89; 0.164; -, 15
SDSS J100711.74+193056.2	45.6 ± 2.0	.../L8;	...	17.78 ± 0.06	16.70 ± 0.02	15.88 ± 0.05	15.24 ± 0.05	16.42 ± 0.19	D	50; 14; 50; -, 15,14
CWISEP J100854.84+203136.6	53.8 ± 7.5	.../T9.5	20.73 ± 0.39	20.80 ± 0.39	S	122; 122; 122; -, 122
2MASS J1010148-040649	57.7 ± 3.6	L6/L6	...	16.67 ± 0.05	15.40 ± 0.02	14.43 ± 0.04	13.57 ± 0.05	15.63 ± 0.15	D	51; 122; 0.116; -, 15,14,79
ULAS J101243.54+102101.7	59.7 ± 1.8	.../T5.5	...	18.02 ± 0.03	16.880 ± 0.014	17.25 ± 0.05	17.45 ± 0.08	18.36 ± 0.19	D	205; 14; 44; -, 126
WISEPC J101808.05-244557.7	83.0 ± 2.8	.../T8	17.40 ± 0.03	19.61 ± 0.16	J	117; 122; 117; -, 169
DENIS J1019245-270717	43.1 ± 0.2	L0.5/M9.5	...	14.42 ± 0.05	13.50 ± 0.02	12.97 ± 0.02	12.45 ± 0.02	13.85 ± 0.10	D	167; 89; 0.112; -, 15,14
2MASS J10224821+5825453	54.0 ± 0.2	L1 β /L1; FLD-G	Y	14.55 ± 0.06	13.400 ± 0.010	12.69 ± 0.03	12.13 ± 0.03	14.05 ± 0.10	D	194; 89; 0.3; 54,3; 15,78
WISE J102557.72+030755.7	83.6 ± 2.3	.../T8.5	...	18.92 ± 0.05	17.84 ± 0.03	18.36 ± 0.05	...	19.88 ± 0.08	S	159; 122; 159; -, 126,159
CFBDS J02841.01+565401.9	46.6 ± 2.6	.../T8	...	18.85 ± 0.02	17.98 ± 0.04	18.38 ± 0.08	18.85 ± 0.09	18.97 ± 0.20	D	2; 122; 2; -, 2
2MASS J1029216+162652	53.3 ± 0.4	L2.5/L2.8	...	15.52 ± 0.05	14.23 ± 0.02	13.41 ± 0.02	12.60 ± 0.02	14.55 ± 0.10	D	114; 89; 0.6; -, 15,14
ULAS J102940.52+093514.6	68.6 ± 1.7	.../T8	...	18.24 ± 0.02	17.280 ± 0.010	17.630 ± 0.010	17.64 ± 0.02	18.74 ± 0.18	D	47; 14; 47; -, 47
CWISEP J103453.14+161228.0	52.1 ± 7.3	.../T7.5	17.68 ± 0.03	18.88 ± 0.34	J	172; 122; 172; -, 172
WISE J103907.73-160002.9	45.3 ± 2.0	.../T7.5	...	18.19 ± 0.03	16.89 ± 0.02	17.19 ± 0.04	17.09 ± 0.07	17.60 ± 0.20	D	159; 14; 159; -, 169,15
2MASS J10430758+2225236	52.4 ± 2.9	L8/L9;	...	17.03 ± 0.06	15.85 ± 0.02	14.82 ± 0.04	13.98 ± 0.04	15.79 ± 0.14	D	53; 14; 0.39; -, 15,14
SDSS J104335.08+121314.1	59.9 ± 3.1	.../L9	...	17.049 ± 0.012	15.865 ± 0.007	14.910 ± 0.005	14.212 ± 0.005	16.15 ± 0.19	D	50; 14; 116; -, 126
2MASS J1045240-014957	58.8 ± 0.2	L1/L1; FLD-G	...	14.231 ± 0.002	13.084 ± 0.001	12.402 ± 0.001	11.780 ± 0.001	13.85 ± 0.10	D	95; 89; 0.3; -, 126

Table 1 continued

Table 1 (continued)

Object	Parallax a (mas)	Spectral Type a, b (Optical/NIR)	Flag c	Y_{MKO} (mag)	J_{MKO} (mag)	H_{MKO} (mag)	K_{MKO} (mag)	M_{bol} (mag)	Source d	References (Disc; π ; SpT; Flag; Phot)
2MASS J1047538+212423	94.7 \pm 3.8	T7/T6.5	...	16.44 \pm 0.03	15.46 \pm 0.03	15.83 \pm 0.03	16.20 \pm 0.03	18.16 \pm 0.19	D	21; 225; 0,32; -; 128
CWISEP J104756.81+545741.6	46.3 \pm 6.5	.../Y0	21.11 \pm 0.39	S	172; 122; 172; -; 0
SDSS J104842.84+011158.5	66.6 \pm 0.2	L1/L4	...	13.945 \pm 0.002	12.797 \pm 0.001	12.157 \pm 0.001	11.579 \pm 0.001	13.94 \pm 0.10	D	107; 89; 0,111; -; 126
WISE J105047.90+505606.2	45.3 \pm 2.2	.../T8	17.94 \pm 0.02	18.31 \pm 0.03	...	18.84 \pm 0.18	J	159; 14; 159; -; 159
2MASS J10511900+5613086	63.92 \pm 0.13	L2/L0.8	...	14.31 \pm 0.05	13.18 \pm 0.02	12.49 \pm 0.02	11.88 \pm 0.02	14.19 \pm 0.10	D	194; 89; 0,6; -; 15,14
WISE J105130.01-213859.7	64.0 \pm 2.3	.../T8.5	...	19.53 \pm 0.09	18.61 \pm 0.08	19.19 \pm 0.39	...	19.71 \pm 0.12	S	159; 122; 168; -; 169,159
WISE J105257.95-194250.2	67.8 \pm 2.2	.../T7.5	...	17.72 \pm 0.05	16.83 \pm 0.02	17.08 \pm 0.05	17.00 \pm 0.05	18.22 \pm 0.19	D	218; 14; 218; -; 15,14
CWISE J105512.11+544328.3	145.0 \pm 14.7	.../T8	21.64 \pm 0.23	S	122; 122; 122; -; 0
WISE J105553.59-165216.3	71.7 \pm 2.3	.../T9.5	20.79 \pm 0.02	20.82 \pm 0.10	S	222,168; 122; 168; -; 222
DENIS-P J1058.7-1548	55.1 \pm 0.3	L3/L2.2 FLD-G	...	15.31 \pm 0.04	14.12 \pm 0.05	13.29 \pm 0.05	12.55 \pm 0.05	14.58 \pm 0.11	D	69; 89; 0,85; -; 128
CWISE J110201.76+350334.7	59.3 \pm 8.3	.../T9	19.12 \pm 0.13	20.36 \pm 0.41	S	122; 122; 171; -; 78
2MASS J1104012+195921	55.7 \pm 0.4	L4/L5.5	...	15.64 \pm 0.05	14.34 \pm 0.02	13.56 \pm 0.03	12.93 \pm 0.03	15.00 \pm 0.11	D	51; 89; 0,39; -; 15,14
2MASS J11061197+2754225	49.3 \pm 1.2	.../T2.5	...	16.10 \pm 0.06	14.96 \pm 0.04	14.20 \pm 0.05	13.84 \pm 0.05	15.58 \pm 0.12	D	150; 89; 150; -; 15,162
SDSSp J111010.01+011613.1	52.1 \pm 1.2	.../T5.5	Y	17.338 \pm 0.012	16.161 \pm 0.008	16.20 \pm 0.02	16.05 \pm 0.03	17.10 \pm 0.18	D	91; 73; 32; 123,86; 126
GH 417BC	42.2 \pm 1.1	L4.5/L5: FLD-G	BC	15.83 \pm 0.05	14.47 \pm 0.02	13.55 \pm 0.03	12.67 \pm 0.03	14.06 \pm 0.12	D	114; 89; 0,3; 18; 15,14,79
2MASS J11145133-2618235	179.2 \pm 1.4	T8/T7.5	...	16.36 \pm 0.05	15.650 \pm 0.010	16.04 \pm 0.02	16.54 \pm 0.05	19.91 \pm 0.10	K	221; 73; 0,32; -; 131,169
2MASS J11181292-0856106	43.7 \pm 2.0	L6/L6pec	...	16.85 \pm 0.10	15.65 \pm 0.09	14.85 \pm 0.08	14.16 \pm 0.08	15.62 \pm 0.14	D	116; 89; 0,116; -; 15
WISE J111838.70+312537.9	114.5 \pm 0.4	.../T8.5	C	19.18 \pm 0.12	17.79 \pm 0.05	18.15 \pm 0.06	...	19.90 \pm 0.03	S	229; 89; 229; -; 229
WISEPC J112254.73+255021.5	66.3 \pm 2.3	.../T6	C	17.29 \pm 0.06	16.29 \pm 0.02	16.67 \pm 0.06	16.67 \pm 0.06	17.92 \pm 0.19	D	117; 121; 117; -; 15,14
WISE J112438.12-042149.7	59.4 \pm 2.9	.../T7	...	17.35 \pm 0.05	16.37 \pm 0.02	16.77 \pm 0.05	16.64 \pm 0.06	17.71 \pm 0.20	D	159; 122; 159; -; 15,14
CWISE J113019.19-115811.3	41.2 \pm 5.8	.../sdT5?	S	18.25 \pm 0.05	17.21 \pm 0.02	17.51 \pm 0.11	...	17.87 \pm 0.37	S	122; 122; 122; 122; 170,122
CWISE J114120.42-211024.5	57.9 \pm 8.1	.../T9;	19.71 \pm 0.19	20.51 \pm 0.41	S	122; 122; 122; -; 170
ULAS J115239.94+113407.6	56.7 \pm 2.7	.../T8.5	...	19.30 \pm 0.06	18.26 \pm 0.04	18.66 \pm 0.10	18.32 \pm 0.17	18.91 \pm 0.21	D	47; 122; 47; -; 126
ULAS J115508.39+044502.3	49.1 \pm 2.3	.../T7	...	19.35 \pm 0.07	18.31 \pm 0.02	19.37 \pm 0.17	J	47; 14; 47; -; 126,14
SDSS J115553.86+055957.5	46.5 \pm 3.9	.../L6.8 FLD-G	...	16.928 \pm 0.011	15.720 \pm 0.006	14.749 \pm 0.006	14.109 \pm 0.006	15.69 \pm 0.17	D	123; 14; 85; -; 126
PSO J180.1475-28.6160	40.7 \pm 5.4	.../T0	...	17.06 \pm 0.05	15.96 \pm 0.02	15.15 \pm 0.01	14.75 \pm 0.05	15.94 \pm 0.27	D	13; 14; 13; -; 15,13
SDSSp J120358.19+001550.3	66.3 \pm 0.5	L3/L5.0	...	15.257 \pm 0.005	13.931 \pm 0.002	13.114 \pm 0.002	12.440 \pm 0.002	14.88 \pm 0.10	D	83; 89; 0,6; -; 126
2MASS J1204303+321259	41.2 \pm 0.2	L0/M9	...	14.84 \pm 0.05	13.80 \pm 0.02	13.16 \pm 0.03	12.49 \pm 0.03	13.78 \pm 0.11	D	51; 89; 0,228; -; 15,14
CWISE J120502.74-180215.5	52.3 \pm 7.3	.../T8	...	18.91 \pm 0.04	17.92 \pm 0.03	19.13 \pm 0.34	J	122; 122; 122; -; 170
SDSS J120747.17+024424.8	44.8 \pm 3.6	L8/T0	...	16.616 \pm 0.009	15.455 \pm 0.006	14.710 \pm 0.005	14.187 \pm 0.007	15.68 \pm 0.17	D	107; 14; 0,32; -; 126
2MASS J12095613-1004008	45.8 \pm 1.0	T3.5/T3	B	16.56 \pm 0.03	15.55 \pm 0.03	15.24 \pm 0.03	15.17 \pm 0.03	16.39 \pm 0.18	D	29; 73; 0,32; 141; 50
2MASS J1213033-043243	59.1 \pm 0.6	L5/L4.2	Y	[15.82 \pm 0.05]	14.540 \pm 0.010	13.660 \pm 0.010	13.00 \pm 0.03	15.18 \pm 0.11	D	51; 89; 0,6; 88; 1,169,15
CWISE J121557.87+270154.2	45.0 \pm 6.3	.../T7	...	18.71 \pm 0.05	17.63 \pm 0.03	18.05 \pm 0.07	...	18.51 \pm 0.34	J	122; 122; 122; -; 126
2MASS J1217110-031113	91.7 \pm 2.2	T7/T7.5	...	16.58 \pm 0.03	15.56 \pm 0.03	15.98 \pm 0.03	15.92 \pm 0.03	17.88 \pm 0.18	D	21; 220,121; 0,32; -; 128
WISEPC J121756.91+162640.2	107.4 \pm 3.5	.../T9	B	18.38 \pm 0.04	17.800 \pm 0.010	18.18 \pm 0.05	18.80 \pm 0.04	19.49 \pm 0.09	S	117; 122; 117; 143; 143,122,117
SDSS J121951.45+312849.4	52.0 \pm 3.8	.../L8	...	17.146 \pm 0.014	15.951 \pm 0.009	15.025 \pm 0.007	14.348 \pm 0.006	16.04 \pm 0.15	D	50; 14; 50; -; 125,126
WISEA J122036.38+540717.3	47.6 \pm 5.1	.../T9.5	20.45 \pm 0.10	20.54 \pm 0.32	S	168; 122; 168; -; 168
2MASS J12212770+0257198	53.8 \pm 0.2	L0/M9.7 FLD-G	...	14.121 \pm 0.002	13.072 \pm 0.001	12.438 \pm 0.001	11.912 \pm 0.001	13.78 \pm 0.10	D	194; 89; 0,85; -; 126
2MASS J12255432-2739466	76.0 \pm 2.5	T6/T6	B	15.84 \pm 0.03	14.88 \pm 0.03	15.17 \pm 0.03	15.28 \pm 0.03	17.13 \pm 0.18	D	21; 220,121; 0,32; 26; 128
DENIS-P J122813.8-154711	48.1 \pm 1.7	L5/L6::	B	15.53 \pm 0.03	14.28 \pm 0.05	13.40 \pm 0.05	12.71 \pm 0.05	14.43 \pm 0.14	D	69; 76; 0,123; 166; 128

Table 1 continued

Table 1 (continued)

Object	Parallax ^a (mas)	Spectral Type ^{a, b} (Optical/NIR)	Flag ^c	Y_{MKO} (mag)	J_{MKO} (mag)	H_{MKO} (mag)	K_{MKO} (mag)	M_{bol} (mag)	Source ^d	References (Disc; π ; SpT; Flag; Phot)
2MASS J12314753+0847331	70.2 ± 3.6	T6/T5.5	...	16.340 ± 0.008	15.153 ± 0.004	15.456 ± 0.008	15.55 ± 0.02	17.19 ± 0.19	D	29; 14; 0,32; -, 126
ULAS J123828.51+095351.3	44.1 ± 6.1	.../T8.5	...	19.61 ± 0.08	18.95 ± 0.02	19.20 ± 0.02	...	19.49 ± 0.36	S	42; 121; 42; -, 126,42
2MASSW J1239272+551537	42.4 ± 2.1	L5/L4.5	B	15.94 ± 0.03	14.62 ± 0.03	13.63 ± 0.03	12.76 ± 0.03	14.17 ± 0.16	D	114; 73; 0,201; 96; 73
2MASSW J1246467+402715	44.7 ± 0.6	L4/L4.0	...	16.29 ± 0.05	14.90 ± 0.02	14.04 ± 0.04	13.25 ± 0.04	14.84 ± 0.11	D	114; 89; 0,6; -, 15,14
SDSS J125011.65+392553.9	42.8 ± 3.2	.../T4	16.14 ± 0.02	16.24 ± 0.25	16.18 ± 0.25	16.91 ± 0.25	D	50; 14; 50; -, 14,15
WISE J125015.56+262846.9	57.5 ± 3.7	.../T6	...	17.75 ± 0.02	16.404 ± 0.012	16.74 ± 0.02	16.79 ± 0.05	17.77 ± 0.21	D	159; 14; 13; -, 126
WISE J125448.52-072828.4	41.1 ± 2.7	.../T7	...	18.41 ± 0.05	17.300 ± 0.010	17.63 ± 0.03	17.40 ± 0.07	17.68 ± 0.21	D	218; 14; 218; -, 15,218
SDSSp J125453.90-012247.4	74.2 ± 2.3	T2/T2	...	15.858 ± 0.006	14.667 ± 0.003	14.136 ± 0.003	13.886 ± 0.005	16.24 ± 0.18	D	127; 89; 0,32; -, 126
VHS J125601.92-125729.9 b	47.3 ± 0.5	L8; /L7; VL-G	CY	18.56 ± 0.05	17.14 ± 0.02	15.78 ± 0.02	14.55 ± 0.12	16.03 ± 0.13	D	90; 89; 0,90; 90,90; 169,15
WISE J125715.90+400854.2	57.0 ± 1.8	.../T7	...	18.14 ± 0.06	16.89 ± 0.02	17.14 ± 0.06	17.18 ± 0.06	18.06 ± 0.19	D	159; 14; 159; -, 15,14
Ross 458C	86.90 ± 0.12	.../T8	C	17.72 ± 0.03	16.69 ± 0.01	17.01 ± 0.04	16.90 ± 0.06	18.57 ± 0.18	D	101; 89; 55; -, 126
2MASSW J1300425+191235	72.1 ± 0.2	L1/L3 (blue)	...	13.65 ± 0.05	12.63 ± 0.02	12.16 ± 0.02	11.60 ± 0.02	14.16 ± 0.10	D	93; 89; 0,36; -, 15,14
WISE J130141.62-030212.9	54.5 ± 4.5	.../T8.5	18.00 ± 0.02	18.39 ± 0.06	...	19.34 ± 0.22	S	159; 122; 159; -, 159
ULAS J130217.21+130851.2	65.0 ± 5.0	.../T8.5	...	19.12 ± 0.03	18.11 ± 0.04	18.60 ± 0.06	18.28 ± 0.03	19.05 ± 0.19	D	44; 162; 44; -, 44
Kelnu-1	49.0 ± 0.7	L2/L2	B	14.52 ± 0.03	13.23 ± 0.05	12.45 ± 0.05	11.78 ± 0.05	13.38 ± 0.12	D	196; 89; 0,116; 140; 131
2MASSI J1305410+204639	50.2 ± 0.7	L5/L6.5	C	[16.25 ± 0.05]	14.910 ± 0.010	14.13 ± 0.04	13.35 ± 0.04	15.18 ± 0.11	D	51; 89; 0,6; -, 1,78,15
CWISE J130841.31-032157.7	47.8 ± 6.7	.../T9	...	18.89 ± 0.05	18.03 ± 0.04	18.36 ± 0.10	...	19.02 ± 0.34	J	122; 122; 122; -, 126
WISEPC J131106.24+012252.4	68.8 ± 2.7	.../T6	...	19.90 ± 0.10	18.97 ± 0.08	19.09 ± 0.07	...	20.06 ± 0.12	S	117; 121; 117; -, 126,10
ULAS J131508.42+082627.4	50.5 ± 5.7	.../T7.5	...	20.00 ± 0.08	18.86 ± 0.04	19.50 ± 0.10	19.60 ± 0.12	20.16 ± 0.30	S	182; 121; 182; -, 182
2MASSI J1315309-264951	54.6 ± 0.8	L5.5/L6.7	B	[16.16 ± 0.05]	14.970 ± 0.010	14.14 ± 0.04	13.45 ± 0.04	15.43 ± 0.11	D	105; 89; 0,6; 40; 1,169,15
WISE J131833.98-175826.5	63.5 ± 2.2	.../T8	...	19.38 ± 0.06	18.27 ± 0.04	17.76 ± 0.23	...	19.59 ± 0.13	S	159; 122; 168; -, 169,15
WISEPA J132233.66-234017.1	77.5 ± 4.2	.../T8	...	17.98 ± 0.02	16.84 ± 0.02	[17.20 ± 0.06]	[17.39 ± 0.07]	18.74 ± 0.20	D	117; 121; 117; -, 169,1
2MASSW J1326201-272937	54.7 ± 5.9	L5/L6.6;	B	17.02 ± 0.05	15.74 ± 0.02	14.83 ± 0.05	13.83 ± 0.05	15.74 ± 0.21	D	95; 14; 0,6; 16; 15,14
SDSSp J132629.82-003831.5	47.9 ± 2.9	L8/L7	...	17.59 ± 0.02	16.221 ± 0.011	15.111 ± 0.007	14.171 ± 0.006	15.79 ± 0.14	D	83; 14; 0,165; -, 126
SDSS J133148.92-0111651.4	47.1 ± 1.4	L6/L6;	...	16.498 ± 0.009	15.330 ± 0.006	14.671 ± 0.004	14.051 ± 0.005	15.67 ± 0.11	D	107; 89; 0,165; -, 126
WISEA J133300.03-160754.4	52.8 ± 3.5	.../T9	...	19.78 ± 0.09	18.73 ± 0.07	18.37 ± 0.13	...	19.50 ± 0.18	S	121; 122; 122; -, 169,121
ULAS J133553.45+113005.2	99.9 ± 1.6	.../T9	...	18.81 ± 0.04	17.900 ± 0.010	18.250 ± 0.010	18.28 ± 0.03	20.08 ± 0.05	S	42; 73; 42; -, 42
WISE J133750.46+263648.6	40.4 ± 2.1	.../T5	...	17.72 ± 0.02	16.56 ± 0.01	16.81 ± 0.03	17.02 ± 0.06	17.38 ± 0.20	D	159; 14; 159; -, 126
2MASSW J1338261+414034	47.6 ± 0.2	L2.5/L2.4	...	15.33 ± 0.05	14.13 ± 0.02	13.38 ± 0.02	12.75 ± 0.02	14.45 ± 0.10	D	114; 89; 0,6; -, 15,14
SDSSp J134646.45-003150.4	69.2 ± 2.3	T7/T6.5	...	16.795 ± 0.010	15.641 ± 0.006	15.973 ± 0.011	15.96 ± 0.02	17.45 ± 0.18	D	224; 220,121; 0,32; -, 126
LHS 2803B	55.03 ± 0.02	.../T5.5	C	17.49 ± 0.05	16.39 ± 0.02	16.57 ± 0.04	16.90 ± 0.08	17.78 ± 0.19	D	65; 89; 65; -, 65
SDSS J135852.68+374711.9	49.6 ± 3.1	.../T4.5;	...	17.32 ± 0.05	16.24 ± 0.02	16.50 ± 0.05	16.70 ± 0.06	17.46 ± 0.20	D	50; 14; 50; -, 15,14
SDSS J140023.12+433822.3	40.8 ± 3.2	.../L7;	...	17.33 ± 0.05	16.20 ± 0.02	15.21 ± 0.05	14.45 ± 0.05	15.73 ± 0.17	D	50; 14; 50; -, 15,14
WISEPC J140518.40+553421.4	158.2 ± 2.6	.../Y0.5 pec	...	21.24 ± 0.10	21.06 ± 0.06	21.41 ± 0.08	21.61 ± 0.12	21.59 ± 0.05	S	55; 122; 0; -, 133,134
ULAS J141623.94+134836.3	107.7 ± 0.2	.../(sd)/T7.5	CS	18.16 ± 0.03	17.26 ± 0.02	17.58 ± 0.03	18.42 ± 0.09	19.02 ± 0.03	S	206,45; 89; 38; 206,45,38; 126,15
SDSS J141624.08+134826.7	107.7 ± 0.2	sdL7/sdL7	CS	14.352 ± 0.003	13.066 ± 0.001	12.503 ± 0.001	12.107 ± 0.002	15.55 ± 0.10	D	20,199,45; 89; 0,230; 206,45,116,230; 126
2MASSW J1421314+182740	52.9 ± 0.2	L0/M8.9	...	14.16 ± 0.05	13.14 ± 0.02	12.49 ± 0.02	11.92 ± 0.02	13.75 ± 0.10	D	93; 89; 0,6; -, 15,14
BD +01 2920B	57.27 ± 0.04	.../T8	C	19.51 ± 0.14	18.55 ± 0.03	18.96 ± 0.07	19.89 ± 0.33	19.54 ± 0.07	S	183; 89; 159; -, 126,159,183
2MASS J14283132+5923354	45.6 ± 0.4	L4/L4.4	...	16.03 ± 0.05	14.73 ± 0.02	13.95 ± 0.03	13.25 ± 0.03	14.88 ± 0.11	D	194; 89; 0,6; -, 15,14
VHS J143311.46-083736.3	56.5 ± 2.8	.../T8	...	20.14 ± 0.25	19.01 ± 0.02	19.22 ± 0.14	...	19.92 ± 0.14	S	149; 122; 149; -, 149,14

Table 1 continued

Table 1 (continued)

Object	Parallax ^a (mas)	Spectral Type ^{a, b} , (Optical/NIR)	Flag ^c	γ_{MKO} (mag)	δ_{MKO} (mag)	H_{MKO} (mag)	K_{MKO} (mag)	M_{bol} (mag)	Source ^d	(Disc; ϖ ; SpT; Flag; Phot)	References
WISEPA J143602.19-181421.8	50.9 ± 2.0	.../T8pec	...	17.40 ± 0.02	[[17.58 ± 0.10]]	18.18 ± 0.20	D		117; 122; 117; -, 1, 14, 169
2MASSW J1439284+192915	70.6 ± 0.2	L1/L1	...	13.67 ± 0.02	12.66 ± 0.03	12.05 ± 0.03	11.47 ± 0.03	13.96 ± 0.11	D		113; 89; 0, 201; -, 128
SDSSP J144600.60+0024520	45.5 ± 3.2	L6/L5	...	16.895 ± 0.014	15.584 ± 0.007	14.657 ± 0.005	13.921 ± 0.005	15.49 ± 0.16	D		91; 225; 0, 123; -, 126
CWISEP J144606.62-231717.8	86.4 ± 12.1	.../Y1 (or later)	22.19 ± 0.31	S		172; 122; 172; -, 0
WISE J144806.48-253420.3	54.8 ± 2.1	.../T8	...	18.90 ± 0.02	18.91 ± 0.12	18.91 ± 0.12	...	19.84 ± 0.12	S		218; 122; 218; -, 14, 121
2MASSW J1448256+103159	69.6 ± 0.5	L4;/L4.7; FLD-G	...	15.804 ± 0.006	14.420 ± 0.002	13.510 ± 0.003	12.674 ± 0.002	15.22 ± 0.11	D		228; 89; 0, 81; -, 126
HD 130948BC	54.95 ± 0.03	.../L4;	BC	13.20 ± 0.08	12.42 ± 0.15	12.42 ± 0.15	11.69 ± 0.04	13.57 ± 0.11	D		187; 89; 103; 187; 72
Gliese 570D	169.88 ± 0.07	T7/T7.5	C	15.78 ± 0.10	14.82 ± 0.05	15.28 ± 0.05	15.52 ± 0.05	18.62 ± 0.18	D		22; 89; 0, 32; -, 131
WISEPC J145715.03+581510.2	55.0 ± 2.3	T8/T7	...	17.81 ± 0.05	16.79 ± 0.02	17.14 ± 0.06	17.21 ± 0.06	18.02 ± 0.20	D		117; 121; 0, 117; -, 15, 14
PSO J224.3820+47.4057	49.5 ± 2.9	.../T7	...	18.01 ± 0.05	17.11 ± 0.02	17.36 ± 0.02	17.08 ± 0.06	17.74 ± 0.21	D		13; 14; 13; -, 15, 14, 122
CWISEP J145837.91+173450.1	46.3 ± 6.5	.../T8	...	18.39 ± 0.07	19.34 ± 0.34	J		172; 122; 172; -, 172
2MASS J15031961+2525196	155.8 ± 0.8	T6/T5	...	14.76 ± 0.06	13.55 ± 0.03	13.90 ± 0.03	13.99 ± 0.03	17.31 ± 0.18	D		27; 89; 0, 32; -, 123
SDSS J150411.63+102718.4	46.1 ± 1.5	.../T7	...	17.63 ± 0.02	16.506 ± 0.011	16.99 ± 0.05	17.12 ± 0.08	17.65 ± 0.19	D		50; 73; 50; -, 126
HIP 73786B	52.50 ± 0.02	.../sdT5.5	CS	17.65 ± 0.02	16.59 ± 0.02	17.05 ± 0.04	17.41 ± 0.09	18.10 ± 0.19	D		205, 175; 89; 231; 231; 126
PSO J226.2599-28.8959	42.5 ± 3.5	.../T1.5	B	16.84 ± 0.05	15.75 ± 0.02	15.24 ± 0.08	14.73 ± 0.05	16.00 ± 0.16	D		63; 122; 63; 16; 15, 14, 126
2MASSW J1506544+132106	85.4 ± 0.2	L3/L4	...	14.52 ± 0.05	13.23 ± 0.02	12.46 ± 0.02	11.72 ± 0.02	14.71 ± 0.10	D		93; 89; 0, 39; -, 15, 14
2MASSW J1507476-162738	134.9 ± 0.3	L5/L5.5	...	13.91 ± 0.03	12.70 ± 0.03	11.90 ± 0.02	11.29 ± 0.03	15.26 ± 0.10	D		190; 89; 0, 123; -, 128
2MASSW J1515008+484742	102.0 ± 0.3	L6/L6	...	15.14 ± 0.05	13.97 ± 0.02	13.18 ± 0.02	12.48 ± 0.02	15.75 ± 0.10	D		228; 89; 0, 228; -, 15, 14
SDSS J151643.01+305344.4	48.2 ± 2.7	.../T0.5;	...	17.96 ± 0.03	16.77 ± 0.01	16.00 ± 0.02	15.160 ± 0.013	16.45 ± 0.19	D		50; 14; 50; -, 126
WISE J151721.13+052929.3	46.1 ± 2.1	.../T8	...	19.57 ± 0.07	18.52 ± 0.02	18.85 ± 0.04	...	19.46 ± 0.17	J		159; 14; 159; -, 126, 14, 121
SDSS J152039.82+354619.8	57.4 ± 4.8	.../T0;	...	16.61 ± 0.05	15.49 ± 0.02	14.58 ± 0.05	14.01 ± 0.05	15.95 ± 0.17	D		50; 14; 50; -, 15, 14, 179
WISE J152305.10+312537.6	65.0 ± 3.5	.../T6.5pec	18.24 ± 0.07	18.69 ± 0.18	...	19.32 ± 0.14	S		159; 122; 159; -, 78, 159
GI 584C	56.0 ± 0.8	L8/L8	C	17.27 ± 0.01	16.052 ± 0.007	15.084 ± 0.006	14.376 ± 0.007	16.16 ± 0.18	D		114; 233; 0, 91; -, 126
2MASSI J1526140+204341	48.3 ± 0.8	L7/L5.5	...	16.57 ± 0.05	15.41 ± 0.02	14.52 ± 0.04	13.88 ± 0.05	15.57 ± 0.11	D		114; 89; 0, 39; -, 15, 14, 79
CWISE J153347.50+175306.7	51.3 ± 7.0	.../T8	18.21 ± 0.03	18.59 ± 0.05	...	19.38 ± 0.33	J		122; 122; 122; -, 122
WISEA J153429.75-104303.3	50.0 ± 7.0	.../T5	20.23 ± 0.42	S		172; 122; 172; -, 0
2MASSI J1534498-295227	63.0 ± 1.1	T6/T5.5	B	15.68 ± 0.06	14.60 ± 0.03	14.74 ± 0.03	14.91 ± 0.03	16.65 ± 0.18	D		24; 76; 0, 32; 26; 15, 123
SDSS J153453.33+121949.2	50.1 ± 1.5	.../L4;	...	16.56 ± 0.06	15.30 ± 0.02	14.38 ± 0.04	13.80 ± 0.04	15.57 ± 0.12	D		50; 89; 50; -, 15, 14
CWISEP J153859.39+482659.1	48.3 ± 6.0	.../T9	20.26 ± 0.10	20.68 ± 0.36	S		172; 122; 122; -, 172
DENIS-P J153941.96-052042.4	59.3 ± 0.3	L4;/L2	...	15.101 ± 0.005	13.777 ± 0.002	13.120 ± 0.010	12.54 ± 0.03	14.74 ± 0.11	D		111; 89; 0, 111; -, 169, 79
SDSS J154009.36+374230.3	40.8 ± 4.7	.../L9;	...	17.44 ± 0.06	16.35 ± 0.02	15.40 ± 0.05	14.63 ± 0.05	15.86 ± 0.21	D		50; 14; 50; -, 15, 14
WISEPA J154151.66-225025.2	169.9 ± 2.0	.../Y1	...	21.46 ± 0.13	21.12 ± 0.06	21.07 ± 0.07	21.70 ± 0.20	21.76 ± 0.07	S		55; 122; 202; -, 134, 133
WISE J154214.00+223005.2	84.3 ± 3.0	.../T9.5	...	20.46 ± 0.03	19.94 ± 0.03	20.52 ± 0.05	...	21.06 ± 0.10	S		159; 122; 159; -, 202
WISE J154459.27+584204.5	49.1 ± 1.9	.../T7.5	18.09 ± 0.02	18.39 ± 0.29	...	19.16 ± 0.16	J		159; 14; 159; -, 14, 15
2MASS J15461461+4932114	53.0 ± 4.4	.../T2.5;	...	16.78 ± 0.05	15.64 ± 0.02	15.35 ± 0.12	15.08 ± 0.05	16.53 ± 0.21	D		173; 122; 173; -, 15, 14, 179
2MASSW J1552591+294849	48.9 ± 0.2	L0 β /L0; INT-G	Y	14.55 ± 0.06	13.41 ± 0.03	12.66 ± 0.03	11.98 ± 0.03	13.62 ± 0.11	D		228; 89; 0, 3; 54, 3; 15
2MASSI J1553022+153236	75.1 ± 0.9	.../T7	B	16.37 ± 0.06	15.34 ± 0.03	15.76 ± 0.03	15.94 ± 0.03	17.56 ± 0.18	D		24; 73; 32; 33; 123
2MASSW J1555157-095605	73.98 ± 0.14	L1/L1.6	...	13.55 ± 0.05	12.470 ± 0.010	12.010 ± 0.010	11.42 ± 0.02	14.02 ± 0.10	D		95; 89; 0, 6; -, 15, 169
WISEPA J161441.45+173936.7	98.2 ± 2.7	.../T9	19.08 ± 0.06	19.31 ± 0.04	...	20.52 ± 0.07	S		117; 122; 117; -, 117, 134
2MASS J16150413+1340079	55.4 ± 2.1	.../T6	...	[17.18 ± 0.05]	16.130 ± 0.010	[16.57 ± 0.05]	[16.61 ± 0.05]	17.58 ± 0.19	D		150; 122; 150; -, 1, 78

Table 1 continued

Table 1 (continued)

Object	Parallax a (mas)	Spectral Type a, b (Optical/NIR)	Flag c	γ_{MKO} (mag)	δ_{MKO} (mag)	H_{MKO} (mag)	K_{MKO} (mag)	M_{bol} (mag)	Source d	References (Disc; ϖ ; SpT; Flag; Phot)
2MASSW J1615441+355900	50.2 ± 0.3	L3/L3.6	...	15.73 ± 0.05	14.43 ± 0.02	13.60 ± 0.03	12.91 ± 0.03	14.75 ± 0.11	D	114; 89; 0.6; -, 15, 14
WISEPA J161705.75+180714.3	78.0 ± 3.1	T8/T8	17.57 ± 0.02	18.23 ± 0.08	...	19.51 ± 0.11	S	117; 14; 0, 117; -, 14, 117
SIMP J1619275+031350	44.9 ± 3.3	.../T2.5	B	...	15.330 ± 0.010	15.08 ± 0.12	[15.04 ± 0.13]	16.28 ± 0.22	D	5; 122; 5; 5; 1, 78, 59
SDSSP J162414.37+002915.6	91.8 ± 1.2	T6/T6	...	16.28 ± 0.05	15.190 ± 0.010	15.48 ± 0.05	15.61 ± 0.05	17.64 ± 0.18	D	216; 220, 121; 0.32; -, 216, 78
PSO J246.1033-19.6194	43.6 ± 3.0	.../T2	16.35 ± 0.02	15.87 ± 0.02	15.82 ± 0.02	16.72 ± 0.20	D	14; 14; 14; -, 14, 126
WISEPA J162725.64+325525.5	54.4 ± 1.9	.../T6	...	17.33 ± 0.05	16.23 ± 0.02	16.56 ± 0.05	16.87 ± 0.05	17.74 ± 0.19	D	117; 121; 117; -, 15, 14
SDSS J162838.77+230821.1	75.1 ± 0.9	.../T7	...	17.27 ± 0.03	16.25 ± 0.03	16.63 ± 0.03	16.72 ± 0.03	18.17 ± 0.18	D	50; 73; 50; -, 50
PSO J247.3273+03.5932	81.2 ± 3.0	T3/T2	...	16.19 ± 0.02	15.100 ± 0.010	14.530 ± 0.010	14.28 ± 0.02	16.60 ± 0.18	D	63; 122; 0.63; -, 63
SDSS J163022.92+081822.0	55.8 ± 3.4	.../T5.5	16.18 ± 0.03	16.35 ± 0.03	16.41 ± 0.03	17.44 ± 0.20	D	50; 122; 50; -, 50
SDSS J163030.53+434404.0	44.7 ± 2.6	.../L7	...	17.66 ± 0.05	16.53 ± 0.02	15.56 ± 0.05	14.77 ± 0.05	16.10 ± 0.20	D	123; 14; 123; -, 15, 14
CWISE J163041.79-064338.3	55.3 ± 7.7	.../T5	16.280 ± 0.014	...	[16.73 ± 0.06]	17.67 ± 0.29	D	122; 122; 122; -, 1, 170
2MASSW J1632291+190441	66.3 ± 1.6	L8/L8	...	16.86 ± 0.05	15.77 ± 0.05	14.68 ± 0.05	13.97 ± 0.05	16.14 ± 0.11	D	113; 61; 0.32; -, 128
WISEA J163932.75+184049.4	61.9 ± 4.7	.../T9.5	20.82 ± 0.22	S	171; 122; 122; -, 0
2MASSW J1645221-131951	88.70 ± 0.12	L1.5/L1	...	13.47 ± 0.06	12.37 ± 0.03	11.71 ± 0.03	11.11 ± 0.03	14.12 ± 0.11	D	95; 89; 0.201; -, 15, 79
WISEPA J164715.59+563208.2	42.7 ± 2.1	L7/L9pec	...	17.71 ± 0.05	16.49 ± 0.02	15.41 ± 0.05	14.48 ± 0.05	15.83 ± 0.13	D	117; 14; 0, 117; -, 15, 14
Gaia J164824.31-291310.0	49.9 ± 0.6	.../L5pec	14.650 ± 0.010	13.84 ± 0.03	[13.11 ± 0.03]	14.94 ± 0.11	D	122; 89; 122; -, 1, 169, 59
CWISE J165013.37+565257.0	68.1 ± 9.5	.../T8	[15.44 ± 0.07]	[14.73 ± 0.06]	[14.24 ± 0.08]	16.34 ± 0.26	D	122; 122; 122; -, 1, 59
WISEPA J165311.05+444423.9	75.7 ± 1.9	T8/T8	...	18.11 ± 0.06	17.08 ± 0.02	17.59 ± 0.05	17.07 ± 0.06	18.46 ± 0.19	D	117; 14; 0, 117; -, 15, 14
2MASS J16573454+1054233	41.6 ± 0.3	L2/L1.4	B	15.23 ± 0.05	14.09 ± 0.02	13.40 ± 0.03	12.78 ± 0.03	14.15 ± 0.11	D	194; 89; 0.6; 16; 15, 14
DENIS-P J170548.38-051645.7	53.1 ± 0.2	L0.5/L1: FLD-G	...	14.32 ± 0.06	13.260 ± 0.010	12.60 ± 0.02	12.00 ± 0.02	13.86 ± 0.10	D	111; 89; 0.3; -, 15, 169
2MASS J17065487-1314396	50.8 ± 0.5	.../L5.0 FLD-G	14.370 ± 0.010	13.68 ± 0.03	13.08 ± 0.03	14.95 ± 0.11	D	85; 89; 85; -, 169, 15
WISE J170745.85-174452.5	86.0 ± 2.8	.../T5	16.35 ± 0.02	16.58 ± 0.03	[16.51 ± 0.05]	18.24 ± 0.19	D	159; 122; 159; -, 1, 159, 169
WISEPA J171104.60+350036.8	43.3 ± 1.9	.../T8	B	18.51 ± 0.03	17.59 ± 0.03	18.05 ± 0.03	18.24 ± 0.03	18.43 ± 0.19	D	117; 122; 117; 143; 143
2MASS J17114559+4028578	47.4 ± 0.5	.../L5.0	C	16.17 ± 0.05	14.96 ± 0.02	14.38 ± 0.05	13.78 ± 0.05	15.46 ± 0.11	D	188; 89; 6; -, 15, 14
2MASS J1721039+334415	61.8 ± 0.2	L3/L5	...	14.63 ± 0.05	13.500 ± 0.010	13.03 ± 0.03	12.46 ± 0.02	14.74 ± 0.10	D	51; 89; 0.36; -, 15, 78
WISE J172134.46+111739.4	50.4 ± 2.9	.../T6	...	17.45 ± 0.06	16.42 ± 0.02	16.69 ± 0.06	16.50 ± 0.06	17.35 ± 0.20	D	159; 122; 159; -, 15, 14
VVV BD001	54.5 ± 0.3	.../L5: blue	...	14.290 ± 0.012	13.200 ± 0.010	12.670 ± 0.010	12.21 ± 0.03	14.16 ± 0.11	D	9; 89; 9; -, 215, 15
2MASS J17312974+2721233	83.65 ± 0.09	L0/L0: FLD-G	...	13.06 ± 0.06	12.060 ± 0.010	11.45 ± 0.02	10.89 ± 0.02	13.71 ± 0.10	D	194; 89; 0.3; -, 15, 78
DENIS-P J1733423-165449	54.9 ± 0.2	L0.5/L0.9	...	14.59 ± 0.07	13.48 ± 0.05	12.87 ± 0.03	12.33 ± 0.03	14.32 ± 0.11	D	180; 89; 0.6; -, 15
WISEPA J173835.53+273258.9	130.9 ± 2.1	.../Y0	...	19.79 ± 0.07	19.63 ± 0.05	20.24 ± 0.08	20.58 ± 0.10	21.49 ± 0.08	S	55; 122; 117; -, 135, 133
2MASS J17392515+2454421	41.9 ± 0.7	.../L4	...	16.92 ± 0.09	15.73 ± 0.07	14.73 ± 0.05	13.93 ± 0.05	15.35 ± 0.12	D	116; 89; 116; -, 15
WISEPA J174124.26+255319.5	214.3 ± 2.8	T9/T9	...	17.09 ± 0.05	16.18 ± 0.02	16.31 ± 0.04	17.02 ± 0.20	20.13 ± 0.05	S	117, 207; 121; 0, 117; -, 15, 74
WISE J174303.71+421150.0	59.2 ± 3.3	.../T4.5	...	16.82 ± 0.05	15.62 ± 0.02	15.64 ± 0.05	15.66 ± 0.06	17.03 ± 0.19	D	159; 122; 159; -, 15, 14
DENIS-P J1745346-164053	50.9 ± 0.2	L1.5/L1.3	...	[14.58 ± 0.05]	13.540 ± 0.010	12.95 ± 0.02	[12.45 ± 0.05]	14.28 ± 0.12	D	180; 89; 0.6; -, 1, 169, 15
2MASS J17461199+5034036	48.3 ± 0.4	L5/L5.7	...	16.23 ± 0.05	14.95 ± 0.02	14.12 ± 0.04	13.51 ± 0.04	15.26 ± 0.11	D	194; 89; 0.6; -, 15, 14
2MASS J17502484-0016151	108.6 ± 0.2	L5/L5.5	...	14.40 ± 0.05	13.21 ± 0.02	12.44 ± 0.02	11.81 ± 0.02	15.31 ± 0.10	D	112; 89; 0, 112; -, 15, 79
SDSSP J175032.96+175903.9	44.5 ± 3.0	T4/T3.5	...	17.19 ± 0.05	16.16 ± 0.02	15.94 ± 0.05	16.02 ± 0.05	16.86 ± 0.20	D	91; 14; 0.32; -, 128, 14
2MASS J17545447+1649196	74.0 ± 3.1	T5/T5.5	...	16.53 ± 0.05	15.49 ± 0.02	15.64 ± 0.13	15.61 ± 0.05	17.31 ± 0.19	D	79, 35; 122; 0.79; -, 15, 14, 79
WISE J175510.28+180320.2	53.6 ± 3.1	.../T2.5	...	16.87 ± 0.05	15.82 ± 0.02	15.32 ± 0.02	15.24 ± 0.02	16.63 ± 0.19	D	159; 122; 122; -, 15, 13
CWISE J175517.35+250147.3	45.9 ± 6.4	.../T7	17.66 ± 0.04	18.58 ± 0.34	J	122; 122; 122; -, 78

Table 1 continued

Table 1 (continued)

Object	Parallax a (mas)	Spectral Type a, b (Optical/NIR)	Flag c	Y_{MKO} (mag)	J_{MKO} (mag)	H_{MKO} (mag)	K_{MKO} (mag)	M_{bol} (mag)	Source d	References (Disc; ϖ ; SpT; Flag; Phot)
SDSS J175805.46+463311.9	71.50 ± 0.02	.../T6.5	C	16.91 ± 0.06	15.86 ± 0.03	16.20 ± 0.03	16.12 ± 0.03	17.62 ± 0.18	D	123; 89; 32; −; 73,123
2MASS J18000116−1559235	81.2 ± 0.2	L4.5/L4.3	...	14.67 ± 0.05	13.34 ± 0.02	12.60 ± 0.03	11.96 ± 0.03	14.85 ± 0.10	D	6; 89; 0.6; −; 15,14
WISEP J180026.60+013453.1	128.1 ± 0.5	L7.5/L7.5	...	15.30 ± 0.05	14.17 ± 0.02	13.20 ± 0.03	12.41 ± 0.03	16.05 ± 0.10	D	98; 89; 0.98; −; 15,14
WISEPA J180435.40+311706.1	62.2 ± 2.7	.../T9.5	18.70 ± 0.05	19.21 ± 0.11	...	19.70 ± 0.13	S	117; 122; 117; −; 117
2MASS J18071509+501531	68.47 ± 0.10	L1.5/L1	...	14.02 ± 0.06	12.88 ± 0.02	12.20 ± 0.03	11.58 ± 0.03	14.01 ± 0.10	D	51; 89; 0.228; −; 15
PSO J272.0887−04.9943	42.8 ± 2.0	.../T1.5pec	...	17.99 ± 0.05	16.98 ± 0.02	16.27 ± 0.04	15.82 ± 0.05	16.69 ± 0.19	D	13; 14; 13; −; 15,14,13
WISE J180901.07+383805.4	52.4 ± 2.3	.../T7.5	...	18.23 ± 0.06	17.39 ± 0.02	17.66 ± 0.02	17.32 ± 0.06	18.03 ± 0.20	D	155; 14; 159; −; 15,14,122
WISE J180952.53−044812.5	49.2 ± 2.9	.../T1	B	16.21 ± 0.05	15.147 ± 0.007	14.44 ± 0.05	13.977 ± 0.006	15.68 ± 0.14	D	159; 122; 12; 67; 15,12
WISEPA J181210.85+272144.3	98.5 ± 4.4	.../T8.5	18.19 ± 0.06	18.83 ± 0.16	...	20.36 ± 0.11	S	117; 121; 117; −; 117
WISE J181243.14+200746.4	48.2 ± 2.8	.../T9	18.54 ± 0.02	18.95 ± 0.06	...	19.37 ± 0.17	S	159; 122; 159; −; 159
WISE J181329.40+283533.3	73.6 ± 2.0	.../T8	...	17.86 ± 0.05	16.91 ± 0.02	17.11 ± 0.05	16.93 ± 0.06	18.30 ± 0.19	D	159; 14; 159; −; 15,14
2MASS J18212815+1414010	107.0 ± 0.2	L4.5pec/L5; FLD-G	...	14.63 ± 0.06	13.300 ± 0.010	12.46 ± 0.02	11.62 ± 0.02	15.10 ± 0.10	D	151; 89; 0.145; −; 15,78
LSR J1826+3014	90.09 ± 0.08	sdL0/d/sdM8.5	S	...	11.52 ± 0.08	11.28 ± 0.08	10.82 ± 0.11	13.82 ± 0.17	D	137; 89; 0.6; 230.6; 15
CWISE J182755.05+564507.8	48.7 ± 6.8	.../T9.5	20.65 ± 0.40	S	122; 122; 122; −; 0
WISEPA J182831.08+265037.8	100.3 ± 2.0	.../Y2 (or later)	...	23.03 ± 0.17	23.48 ± 0.23	22.73 ± 0.13	23.48 ± 0.36	20.87 ± 0.08	S	55; 122; 118; −; 134,133
Gaia J183610.72+031524.6	54.9 ± 0.6	.../L6 v. red	[[14.71 ± 0.05]]	13.93 ± 0.04	13.208 ± 0.003	15.23 ± 0.10	D	223,122; 89; 122; −; 1,59,153
WISE J185101.83+593508.6	49.2 ± 0.6	.../L9	...	16.04 ± 0.05	14.846 ± 0.013	14.03 ± 0.02	13.45 ± 0.05	15.23 ± 0.11	D	218; 89; 13; −; 15,12
CWISE J185104.34−245232.1	47.6 ± 6.7	.../T4	16.331 ± 0.012	...	[[16.57 ± 0.06]]	17.31 ± 0.27	D	122; 122; 122; −; 1,169
WISEPA J185215.78+353716.3	72.0 ± 1.9	.../T7	...	17.41 ± 0.05	16.32 ± 0.02	16.73 ± 0.05	16.51 ± 0.05	17.93 ± 0.19	D	117; 121; 117; −; 15,14
2MASS J19010601+4718136	67.3 ± 3.4	.../T5	...	16.58 ± 0.05	15.53 ± 0.02	15.66 ± 0.05	15.72 ± 0.05	17.25 ± 0.19	D	29; 122; 32; −; 15,14
WISEPA J190624.75+450808.2	64.1 ± 1.6	.../T6	...	17.03 ± 0.05	15.98 ± 0.02	16.37 ± 0.08	16.40 ± 0.05	17.65 ± 0.18	D	117; 121; 117; −; 15,14
WISEP J190648.47+401106.8	59.67 ± 0.10	L1/L1	...	[[14.05 ± 0.05]]	12.950 ± 0.010	12.33 ± 0.02	11.75 ± 0.02	13.86 ± 0.10	D	97; 89; 0.97; −; 1,78,15
DENIS-P J1909081−193748	45.8 ± 0.4	L1/...	14.46 ± 0.02	13.59 ± 0.03	12.90 ± 0.03	14.52 ± 0.11	D	180; 89; 180; −; 14,15
WISE J191915.54+304558.4	62.5 ± 3.3	.../L9	...	16.68 ± 0.05	15.52 ± 0.02	14.557 ± 0.014	13.96 ± 0.05	16.05 ± 0.13	D	218; 122; 13; −; 15,13
GJ 758B	64.07 ± 0.02	.../T7;	C	...	18.57 ± 0.20	19.15 ± 0.20	217; 89; 178; −; 108
2MASS J19251275+0700362	89.0 ± 0.6	.../L7	[[14.65 ± 0.05]]	[[13.75 ± 0.03]]	[[12.92 ± 0.04]]	15.85 ± 0.10	D	210,82; 89; 82; −; 1,59
CWISE J192537.88+290159.0	76.2 ± 10.7	.../T8.5	18.01 ± 0.06	20.21 ± 0.41	S	122; 122; 122; −; 78
WISE J192841.35+235604.9	146.4 ± 1.2	.../T6	...	15.09 ± 0.05	13.98 ± 0.02	14.24 ± 0.05	14.18 ± 0.05	17.35 ± 0.18	D	159; 89; 159; −; 15,14
WISEA J193054.55−205949.4	106.3 ± 4.9	.../Y1 (or later)	22.03 ± 0.14	S	171; 122; 122; −; 0
CWISEP J193518.59−154620.3	69.3 ± 3.8	.../Y1 (or later)	21.37 ± 0.17	S	172; 122; 122; −; 0
WISENF J193656.08+040801.2	113.9 ± 3.8	.../Y0	21.55 ± 0.09	S	172; 122; 172; −; 0
CWISE J193824.10+350025.0	50.7 ± 7.1	.../T8	18.69 ± 0.11	19.90 ± 0.44	S	122; 122; 122; −; 78
Gaia J195557.27+321518.2	55.1 ± 1.0	L6.3:/...	15.130 ± 0.010	14.39 ± 0.04	[[13.72 ± 0.04]]	15.67 ± 0.11	D	211; 89; 211; −; 1,125,59
WISE J200050.19+362950.1	133.4 ± 2.2	.../T8	...	16.31 ± 0.05	15.440 ± 0.010	15.850 ± 0.010	16.13 ± 0.04	18.68 ± 0.18	D	56; 122; 56; −; 15,56,153
2MASS J20025073−0521524	56.7 ± 1.4	L5 β /L7	Y	16.52 ± 0.05	15.22 ± 0.02	14.38 ± 0.04	13.39 ± 0.04	15.45 ± 0.11	D	53; 89; 0.164; 81,85; 15,14
HR 7672B	56.27 ± 0.04	.../L4.5	C	14.10 ± 0.14	13.02 ± 0.10	15.10 ± 0.14	D	139; 89; 139; −; 15
WISE J200520.38+542433.9	60.30 ± 0.03	.../sdT8	CS	...	19.64 ± 0.09	19.57 ± 0.08	...	19.54 ± 0.07	S	160; 89; 160; 160; 160
WISE J200804.71−083428.5	57.8 ± 3.3	.../T5.5	...	17.16 ± 0.05	16.03 ± 0.02	16.31 ± 0.05	16.36 ± 0.05	17.46 ± 0.20	D	159; 122; 159; −; 15,14
CWISE J201342.27−032643.7	41.9 ± 5.9	.../T7	18.24 ± 0.12	18.96 ± 0.36	J	122; 122; 122; −; 169
WISE J201404.13+042408.5	45.5 ± 2.4	.../T6.5pec	18.01 ± 0.02	18.71 ± 0.30	17.97 ± 0.29	18.30 ± 0.30	D	159; 14; 159; −; 14,15

Table 1 continued

Table 1 (continued)

Object	Parallax a (mas)	Spectral Type a , (Optical/NIR)	Flag c	Y_{MKO} (mag)	J_{MKO} (mag)	H_{MKO} (mag)	K_{MKO} (mag)	M_{bol} (mag)	Source d	References (Disc; ϖ ; SpT; Flag; Phot)
WISEA J201833.67-141720.3	64.9 ± 9.1	.../T9	19.13 ± 0.11	20.44 ± 0.40	S	171; 122; 171; -, 170
WISE J201920.76-114807.5	79.9 ± 2.7	.../T8;	18.09 ± 0.06	18.23 ± 0.07	...	19.78 ± 0.09	S	159; 122; 159; -, 159
WISE J203042.79+074934.7	102.8 ± 0.8	.../T1.5	...	15.220 ± 0.012	14.046 ± 0.011	13.51 ± 0.04	13.36 ± 0.04	16.36 ± 0.18	D	159; 89; 159; -, 15,12
2MASS J20360316+1051295	41.0 ± 0.4	L3/L3.5	B	15.12 ± 0.06	13.89 ± 0.03	13.09 ± 0.03	12.42 ± 0.03	13.69 ± 0.11	D	194; 89; 0.39; 89,77; 15
CWISEP J203821.53-064930.9	43.7 ± 6.1	.../T9.5	19.35 ± 0.14	20.15 ± 0.43	S	172; 122; 172; -, 170
WISEPC J205628.90+145953.3	140.8 ± 2.0	.../Y0	...	19.77 ± 0.05	19.43 ± 0.04	19.96 ± 0.04	20.01 ± 0.06	21.07 ± 0.04	S	55; 122; 117; -, 134,133
CWISE J205701.64-170407.3	51.0 ± 7.1	.../T8.5	...	19.62 ± 0.08	18.58 ± 0.02	19.94 ± 0.43	S	122; 122; 122; -, 170,122
2MASS J2057540-025230	64.7 ± 0.2	L1.5/L2; FLD-G	...	14.19 ± 0.05	13.020 ± 0.010	12.32 ± 0.03	11.69 ± 0.03	14.00 ± 0.10	D	51; 89; 0.3; -, 15,169
CWISEP J210007.87-293139.8	52.7 ± 7.4	.../T9.5	21.31 ± 0.12	21.08 ± 0.38	S	172; 122; 172; -, 122
2MASS J2104149-103736	58.0 ± 0.3	L2.5/L2	...	15.030 ± 0.003	13.773 ± 0.002	13.05 ± 0.02	12.35 ± 0.02	14.48 ± 0.10	D	51; 89; 0.39; -, 169,15
PSO J318.5338-22.8603	45.1 ± 1.7	.../L7; VL-G	Y	18.81 ± 0.10	17.15 ± 0.04	15.68 ± 0.02	14.41 ± 0.02	15.87 ± 0.12	D	144; 145; 144; 144; 144
WISEA J211456.86-180519.0	55.0 ± 7.7	.../T8	...	19.46 ± 0.08	18.34 ± 0.06	19.80 ± 0.44	S	171; 122; 171; -, 170
PSO J319.3102-29.6682	76.1 ± 3.5	.../T0;	...	16.59 ± 0.02	15.45 ± 0.02	14.655 ± 0.012	14.17 ± 0.05	16.45 ± 0.19	D	13; 122; 13; -, 15,13
WISE J212321.92-261405.1	40.5 ± 3.3	.../T5.5	...	18.07 ± 0.06	17.03 ± 0.02	17.52 ± 0.06	17.69 ± 0.07	17.88 ± 0.23	D	159; 122; 159; -, 15,14
SDSS J212413.89+010000.3	57.0 ± 3.2	.../T5	...	17.21 ± 0.02	15.829 ± 0.008	16.05 ± 0.02	16.09 ± 0.03	17.25 ± 0.19	D	123; 14; 32; -, 126
2MASS J21371044+1450475	42.4 ± 0.2	L2/L0.8	...	15.21 ± 0.05	14.07 ± 0.02	13.37 ± 0.02	12.80 ± 0.03	14.21 ± 0.11	D	194; 89; 0.6; -, 15,14
2MASS J21373742+0808463	66.4 ± 0.7	L5/L5	14.64 ± 0.02	13.67 ± 0.03	13.00 ± 0.03	15.41 ± 0.10	D	194; 89; 0.39; -, 14,15
2MASS J21392676+0220226	96.5 ± 1.1	T2/T1.5	Y	[15.85 ± 0.05]	14.701 ± 0.005	[14.05 ± 0.05]	[13.57 ± 0.05]	16.40 ± 0.18	D	194,34; 232; 0.32; 39,232; 1,78
CWISEP J213930.45+042721.6	47.6 ± 6.7	.../T9	20.44 ± 0.10	20.53 ± 0.41	S	172; 122; 172; -, 172
HN Peg B	55.15 ± 0.03	.../T2.5	CY	16.91 ± 0.06	15.86 ± 0.03	15.40 ± 0.03	15.12 ± 0.03	16.60 ± 0.18	D	154; 89; 154; 154; 15,154
Wolf 940B	80.74 ± 0.05	.../T8.5	C	18.97 ± 0.03	18.16 ± 0.02	18.77 ± 0.03	18.85 ± 0.05	20.06 ± 0.03	S	43; 89; 43; -, 43
WISE J214706.78-102924.0	51.8 ± 2.4	.../T7.5	17.37 ± 0.02	17.73 ± 0.09	[17.86 ± 0.22]	18.43 ± 0.26	D	159; 122; 159; -, 1,14,121,169
2MASS J21481628+4003593	123.7 ± 0.4	L6/L6 FLD-G	...	15.52 ± 0.06	14.050 ± 0.010	12.86 ± 0.02	11.72 ± 0.02	15.48 ± 0.10	D	151; 89; 0,144; -, 15,78
2MASS J21522609+0937575	51.3 ± 3.4	L6;/...	B	...	15.09 ± 0.02	14.13 ± 0.03	13.32 ± 0.03	15.20 ± 0.17	D	193; 122; 194; 193; 14,15
2MASS J21543318+5942187	64.7 ± 1.5	.../T5	...	16.54 ± 0.09	15.44 ± 0.07	15.70 ± 0.09	15.70 ± 0.09	17.18 ± 0.19	D	150; 1; 150; -, 15
WISEPC J215751.38+265931.4	61.2 ± 2.0	.../T7	...	18.00 ± 0.05	17.04 ± 0.02	17.49 ± 0.04	17.35 ± 0.06	18.32 ± 0.19	D	117; 122; 117; -, 15,14
2MASS J21580457-1550098	43.1 ± 0.9	L4/L5	...	16.13 ± 0.05	14.84 ± 0.02	13.95 ± 0.04	13.16 ± 0.04	14.66 ± 0.12	D	115; 89; 0,164; -, 15,14
WISEA J220304.18+461923.4	75.1 ± 3.4	.../T8	18.57 ± 0.02	20.30 ± 0.14	S	168; 122; 168; -, 168
WISE J220905.73+271143.9	161.7 ± 2.0	.../Y0;	...	22.95 ± 0.07	22.86 ± 0.13	22.39 ± 0.15	...	22.29 ± 0.07	S	56; 122; 56; -, 202
2MASS J22092183-2711329	40.7 ± 3.9	.../T2.5	B	...	15.53 ± 0.02	15.20 ± 0.15	15.11 ± 0.15	16.19 ± 0.24	D	164; 14; 164; 77; 14,15
WISEPC J220922.10-273439.5	75.5 ± 3.6	.../T7	...	17.53 ± 0.05	16.55 ± 0.02	16.91 ± 0.05	17.31 ± 0.06	18.64 ± 0.20	D	117; 122; 117; -, 15,14
WISEPC J221354.69+091139.4	54.5 ± 2.5	.../T7	...	17.81 ± 0.05	16.76 ± 0.02	17.11 ± 0.05	17.12 ± 0.06	17.93 ± 0.20	D	117; 121; 117; -, 15,14
2MASS J22153705+2110554	57.6 ± 3.6	.../T1pec	15.90 ± 0.02	15.51 ± 0.06	15.17 ± 0.06	16.69 ± 0.20	D	109; 122; 109; -, 14,15
2MASSW J2224438-015852	86.2 ± 0.4	L4.5/L3; FLD-G	B	15.32 ± 0.06	13.89 ± 0.03	12.84 ± 0.03	11.98 ± 0.03	14.99 ± 0.10	D	114; 89; 0,145; 77; 73,123
WISEPC J222623.05+044003.9	54.4 ± 5.9	.../T8	...	18.04 ± 0.03	16.90 ± 0.02	17.45 ± 0.07	17.24 ± 0.09	18.02 ± 0.26	D	117; 121; 117; -, 126
CWISEP J223022.60+254907.5	62.2 ± 8.7	.../Y1 (or later)	21.85 ± 0.34	S	172; 122; 172; -, 0
WISE J223617.59+510551.9	102.8 ± 1.9	.../T5	...	15.655 ± 0.014	14.457 ± 0.011	14.61 ± 0.02	14.57 ± 0.05	17.09 ± 0.18	D	159; 14; 12; -, 15,12
2MASS J2238074+435317	44.2 ± 0.2	L1.5/L0.6	B	14.64 ± 0.06	13.81 ± 0.03	13.12 ± 0.03	12.53 ± 0.03	14.01 ± 0.11	D	51; 89; 0.6; 11; 15
WISEPC J223937.55+161716.2	42.9 ± 3.0	.../T3	B	17.00 ± 0.05	15.96 ± 0.02	15.57 ± 0.05	15.37 ± 0.05	16.43 ± 0.20	D	117; 14; 117; 77; 15,14
2MASS J22425317+2542573	46.9 ± 0.5	L3/L1.5	...	16.03 ± 0.06	14.76 ± 0.04	13.82 ± 0.03	13.03 ± 0.03	14.72 ± 0.11	D	96; 89; 0.39; -, 15

Table 1 continued

Table 1 (continued)

Object	Parallax a (mas)	Spectral Type a, b (Optical/NIR)	Flag c	γ_{MKO} (mag)	δ_{MKO} (mag)	H_{MKO} (mag)	K_{MKO} (mag)	M_{bol} (mag)	Source d	References (Disc; ϖ ; SpT; Flag; Phot)
WISEA J224319.56-145857.3	68.3 ± 9.6	.../Y0	21.02 ± 0.37	S	171; 122; 171; -; 0
2MASS J2244316+204343	58.7 ± 0.9	L6.5/L6; VL-G	Y	17.53 ± 0.05	16.33 ± 0.03	15.06 ± 0.03	13.90 ± 0.03	15.91 ± 0.11	D	60; 145; 0, 3; 3; 73, 123
2MASS J22490917+3205489	43.1 ± 1.8	L5/...	15.54 ± 0.02	14.41 ± 0.05	13.57 ± 0.05	15.08 ± 0.14	D	53; 89; 53; -; 14, 15
DENIS-P J225210.73-173013.4	60.6 ± 0.6	.../L7.5	B	15.26 ± 0.03	14.20 ± 0.03	13.41 ± 0.03	12.90 ± 0.02	15.14 ± 0.10	D	111; 89; 111; 192; 73
WISEA J225404.16-265257.5	63.0 ± 8.8	.../T9.5	20.08 ± 0.18	20.63 ± 0.40	S	171; 122; 171; -; 122
2MASS J2254188+312349	72.0 ± 3.0	T5/T4	...	[16.23 ± 0.05]	15.000 ± 0.010	[14.84 ± 0.05]	[14.84 ± 0.05]	16.78 ± 0.19	D	24; 162; 0, 32; -; 1, 78
CWISEP J225628.97+400227.3	101.8 ± 11.2	.../Y1 (or later)	21.70 ± 0.41	22.42 ± 0.24	S	172; 122; 122; -; 172
WISE J230133.32+021635.0	54.1 ± 2.5	.../T6.5	...	17.62 ± 0.02	16.358 ± 0.010	16.70 ± 0.03	16.87 ± 0.05	17.73 ± 0.19	D	159; 122; 159; -; 126
WISEA J230329.45+315022.7	46.5 ± 3.3	.../T2 (blue)	15.92 ± 0.02	15.53 ± 0.16	15.52 ± 0.16	16.62 ± 0.22	D	203; 14; 203; -; 14, 15
2MASS J23185497-1301106	66.5 ± 3.2	.../T5	15.30 ± 0.02	15.30 ± 0.13	15.13 ± 0.13	16.85 ± 0.20	D	164; 14; 164; -; 14, 15
WISEPC J231939.13-184404.3	80.9 ± 2.7	.../T7.5	...	18.56 ± 0.06	17.56 ± 0.02	17.95 ± 0.05	18.27 ± 0.08	19.91 ± 0.14	K	117; 122; 117; -; 15, 117
ULAS J232035.28+144829.8	47.0 ± 4.0	.../T5	...	18.14 ± 0.02	16.79 ± 0.02	17.14 ± 0.02	17.40 ± 0.02	17.90 ± 0.23	D	205; 162; 44; -; 44
ULAS J232123.79+135454.9	82.8 ± 2.1	.../T7.5	...	17.92 ± 0.03	16.72 ± 0.03	17.15 ± 0.03	17.160 ± 0.010	18.68 ± 0.18	D	205; 122; 44; -; 44
2MASS J23254530+4251488	69.2 ± 1.5	L8/L7.5:	...	16.58 ± 0.05	15.42 ± 0.02	14.53 ± 0.05	13.76 ± 0.05	16.06 ± 0.11	D	53; 89; 0, 39; -; 15, 14
ULAS J232600.40+020139.2	45.6 ± 3.1	.../T8	...	19.40 ± 0.08	17.98 ± 0.04	18.46 ± 0.12	18.41 ± 0.20	18.64 ± 0.25	D	47; 122; 47; -; 126
WISEPC J232728.75-273056.5	46.8 ± 5.5	.../L9	...	17.58 ± 0.05	16.47 ± 0.02	15.55 ± 0.05	14.87 ± 0.05	16.23 ± 0.24	D	117; 122; 117; -; 15, 14
WISE J233527.07+451140.9	44.0 ± 1.4	.../L7pec	...	18.02 ± 0.06	16.83 ± 0.03	15.63 ± 0.02	14.65 ± 0.06	16.00 ± 0.12	D	218; 145; 145; -; 15, 13
2MASS J2339101+135230	51.2 ± 4.2	.../T5	...	16.955 ± 0.014	15.846 ± 0.010	16.06 ± 0.02	16.20 ± 0.04	17.17 ± 0.21	D	24; 122; 32; -; 126
WISEPC J234026.62-074507.2	47.8 ± 3.1	T7/T7	...	17.20 ± 0.06	16.08 ± 0.03	16.41 ± 0.04	16.51 ± 0.06	17.28 ± 0.20	D	117; 121; 0, 117; -; 15
WISEPC J234446.25+103415.8	68.0 ± 2.6	.../T9	...	19.88 ± 0.12	18.78 ± 0.06	19.07 ± 0.11	...	20.16 ± 0.12	S	117; 122; 117; -; 126, 117
WISEPC J234841.10-102844.4	58.4 ± 3.5	.../T7	...	17.69 ± 0.05	16.62 ± 0.02	16.99 ± 0.05	16.84 ± 0.06	17.83 ± 0.21	D	117; 121; 117; -; 15, 14
2MASS J23512200+3010540	41.2 ± 1.4	L5.5/L5; FLD-G	Y	17.05 ± 0.11	15.76 ± 0.10	14.64 ± 0.06	13.99 ± 0.06	15.38 ± 0.13	D	116; 145; 0, 145; 116, 84, 145; 15
WISEA J235402.79+024014.1	130.6 ± 3.3	.../Y1	23.07 ± 0.20	22.88 ± 0.30	...	22.13 ± 0.08	S	202; 122; 202; -; 202
CWISEP J235547.99+380438.9	49.3 ± 6.9	.../Y0	20.28 ± 0.10	20.90 ± 0.38	S	172; 122; 172; -; 172
2MASS J2356547-155310	69.0 ± 3.4	.../T5.5	...	16.64 ± 0.06	15.48 ± 0.03	15.70 ± 0.03	15.73 ± 0.03	17.29 ± 0.19	D	24; 225; 32; -; 73, 123
WISE J235716.49+122741.8	61.9 ± 3.0	.../...	...	17.34 ± 0.02	16.100 ± 0.010	16.49 ± 0.03	16.52 ± 0.04	17.68 ± 0.19	D	159; 122; -; 126

Table 1 continued

Table 1 (*continued*)

Object	Parallax a (mas)	Spectral Type a, b (Optical/NIR)	Flag c	Y_{MKO} (mag)	J_{MKO} (mag)	H_{MKO} (mag)	K_{MKO} (mag)	M_{bol} (mag)	Source d	References (Disc; π ; SpT; Flag; Phot)
--------	-----------------------	---------------------------------------	----------	---------------------------	---------------------------	---------------------------	---------------------------	---------------------------	------------	---

NOTE—This table updates the volume-limited sample of Paper I. This table lists all spectroscopically confirmed L0–Y2 dwarfs having declinations between -30° and $+60^\circ$ and parallax-determined distances less than 25 pc. Objects with photometric spectral types and/or distances from K21 that meet the other criteria are also included. Y_{MKO} , J_{MKO} , H_{MKO} , and K_{MKO} photometry enclosed in single brackets indicates synthetic photometry (Paper I); double brackets indicates photometry converted from 2MASS into the MKO system using $M_{K_s, 2\text{MASS}}$ and the polynomials of Dupuy & Liu (2017).

a Parallaxes and spectral types enclosed in curly braces were determined photometrically.

b β , γ , and δ indicate classes of increasingly low gravity based on optical (Kirkpatrick 2005; Cruz et al. 2009) or near-infrared (Gagné et al. 2015b; Cruz et al. 2018) spectra. FLD-G indicates near-infrared spectral signatures of field-age gravity, INT-G indicates intermediate gravity, and VL-G indicates very low gravity (Allers & Liu 2013).

c B = binary (presented here as a single unresolved source); C = resolved companion to a star or brown dwarf; Y = young ($\lesssim 200$ Myr); S = subdwarf.

d M_{bol} for unresolved binaries (see Flag column) should be treated with caution.

d Source of the M_{bol} value (Section 3.4). D = conversion from $M_{K_{\text{MKO}}}$ using the polynomial from Dupuy & Liu (2017); J = J_{MKO} bolometric correction from Liu et al. (2010); K = K_{MKO} bolometric correction from Liu et al. (2010); S = Super-magnitude (DK13; Appendix A).

References—(1) This work, (2) Albert et al. (2011), (3) Allers & Liu (2013), (4) Artigau et al. (2006), (5) Artigau et al. (2011), (6)

Bardalez Gagliuffi et al. (2014), (7) Bardalez Gagliuffi et al. (2019), (8) Bardalez Gagliuffi et al. (2020), (9) Beamin et al. (2013), (10) Beichman et al. (2014), (11) Bernat et al. (2010), (12) Best et al. (2013), (13) Best et al. (2015), (14) Best et al. (2020), (15) Best et al. (2021), (16) W. Best et al. (in prep), (17) Bihain et al. (2013), (18) Bouy et al. (2003), (19) Bouy et al. (2005), (20) Bowler et al. (2010), (21) Burgasser et al. (1999), (22) Burgasser et al. (2000a), (23) Burgasser et al. (2000b), (24) Burgasser et al. (2002), (25) Burgasser et al. (2003a), (26) Burgasser et al. (2003c), (27) Burgasser et al. (2003b), (28) Burgasser et al. (2003d), (29) Burgasser et al. (2004), (30) Burgasser et al. (2005b), (31) Burgasser et al. (2005a), (32) Burgasser et al. (2006a), (33) Burgasser et al. (2006b), (34) Burgasser & McElwain (2006), (35) Burgasser et al. (2008a), (36) Burgasser et al. (2008b), (37) Burgasser et al. (2008c), (38) Burgasser et al. (2010b), (39) Burgasser et al. (2010a), (40) Burgasser et al. (2011), (41) Burgasser et al. (2016), (42) Burningham et al. (2008), (43) Burningham et al. (2009), (44) Burningham et al. (2010a), (45) Burningham et al. (2010b), (46) Burningham et al. (2011), (47) Burningham et al. (2013), (48) Castro & Gizis (2012), (49) Castro et al. (2013), (50) Chiu et al. (2006), (51) Cruz et al. (2003), (52) Cruz et al. (2004), (53) Cruz et al. (2007), (54) Cruz et al. (2009), (55) Cushing et al. (2011), (56) Cushing et al. (2014), (57) Cushing et al. (2016), (58) Cushing et al. (2018), (59) Cutri et al. (2003), (60) Dahn et al. (2002), (61) Dahn et al. (2017), (62) Deacon et al. (2005), (63) Deacon et al. (2011), (64) Deacon et al. (2012a), (65) Deacon et al. (2012b), (66) Deacon et al. (2014), (67) Deacon et al. (2017a), (68) Deacon et al. (2017b), (69) Delfosse et al. (1997), (70) Delfosse et al. (1999), (71) Delorme et al. (2008), (72) Dupuy et al. (2009), (73) Dupuy & Liu (2012), (74) Dupuy & Kraus (2013), (75) Dupuy et al. (2015a), (76) Dupuy & Liu (2017), (77) T. Dupuy (private communication), (78) Dye et al. (2018), (79) Faherty et al. (2012), (80) Faherty et al. (2014), (81) Faherty et al. (2016), (82) Faherty et al. (2018), (83) Fan et al. (2000), (84) Gagné et al. (2014), (85) Gagné et al. (2015b), (86) Gagné et al. (2015a), (87) Gagné et al. (2017), (88) Gagné & Faherty (2018), (89) Gaia Collaboration et al. (2023), (90) Gauza et al. (2015), (91) Geballe et al. (2002), (92) Gelino et al. (2014), (93) Gizis et al. (2000), (94) Gizis et al. (2001), (95) Gizis (2002), (96) Gizis et al. (2003), (97) Gizis et al. (2011b), (98) Gizis et al. (2011a), (99) Gizis et al. (2013), (100) Gizis et al. (2015), (101) Goldman et al. (2010), (102) Gomes et al. (2013), (103) Goto et al. (2002), (104) Greco et al. (2019), (105) Hall (2002), (106) H. Harris (private communication), (107) Hawley et al. (2002), (108) Janson et al. (2011), (109) Kellogg et al. (2015), (110) Kellogg et al. (2017), (111) Kendall et al. (2004), (112) Kendall et al. (2007), (113) Kirkpatrick et al. (1999), (114) Kirkpatrick et al. (2000), (115) Kirkpatrick et al. (2008), (116) Kirkpatrick et al. (2010), (117) Kirkpatrick et al. (2011), (118) Kirkpatrick et al. (2012), (119) Kirkpatrick et al. (2014), (120) Kirkpatrick et al. (2016), (121) Kirkpatrick et al. (2019), (122) Kirkpatrick et al. (2021), (123) Knapp et al. (2004), (124) Koerner et al. (1999), (125) Lawrence et al. (2007), (126) Lawrence et al. (2012), (127) Leggett et al. (2000), (128) Leggett et al. (2002b), (129) Leggett et al. (2002a), (130) Leggett et al. (2009), (131) Leggett et al. (2010), (132) Leggett et al. (2012), (133) Leggett et al. (2013), (134) Leggett et al. (2015), (135) Leggett et al. (2016), (136) Leggett et al. (2017), (137) Lépine et al. (2002), (138) Liebert et al. (2003), (139) Liu et al. (2002), (140) Liu & Leggett (2005), (141) Liu et al. (2010), (142) Liu et al. (2011), (143) Liu et al. (2012), (144) Liu et al. (2013), (145) Liu et al. (2016), (146) M. Liu et al. (in prep), (147) Lodieu et al. (2005), (148) Lodieu et al. (2007b), (149) Lodieu et al. (2012), (150) Looper et al. (2007), (151) Looper et al. (2008), (152) Lucas et al. (2010), (153) Lucas et al. (2012), (154) Luhman et al. (2007), (155) Luhman et al. (2012), (156) Luhman (2014b), (157) Luhman & Sheppard (2014), (158) Luhman (2014a), (159) Mace et al. (2013a), (160) Mace et al. (2013b), (161) Mamajek et al. (2018), (162) Manjavacas et al. (2013), (163) Marocco et al. (2010), (164) Marocco et al. (2013), (165) Marocco et al. (2015), (166) Martin et al. (1999), (167) Martin et al. (2010), (168) Martin et al. (2018), (169) McMahon et al. (2013), (170) McMahon et al. (2021), (171) Meisner et al. (2020a), (172) Meisner et al. (2020b), (173) Metzhev et al. (2008), (174) Mugrauer et al. (2006), (175) Murray et al. (2011), (176) Muzic et al. (2012), (177) Nakajima et al. (1995), (178) Nilsson et al. (2017), (179) Peña Ramirez et al. (2015), (180) Phan-Bao et al. (2008), (181) Pineda et al. (2016), (182) Pinfield et al. (2008), (183) Pinfield et al. (2012), (184) Pinfield et al. (2014a), (185) Pinfield et al. (2014b), (186) Pope et al. (2013), (187) Potter et al. (2002), (188) Radigan et al. (2008), (189) Rebolo et al. (1998), (190) Reid et al. (2000), (191) Reid et al. (2001), (192) Reid et al. (2006b), (193) Reid et al. (2006a), (194) Reid et al. (2008), (195) Reylié (2018), (196) Ruiz et al. (1997), (197) Salim et al. (2003), (198) Schilbach et al. (2009), (199) Schmidt et al. (2010a), (200) Schmidt et al. (2010b), (201) Schneider et al. (2014), (202) Schneider et al. (2015), (203) Schneider et al. (2016), (204) Scholz & Menninger (2002), (205) Scholz (2010a), (206) Scholz (2010b), (207) Scholz et al. (2011), (208) Scholz et al. (2012), (209) Scholz et al. (2014), (210) Scholz & Bell (2018), (211) Scholz (2020), (212) Skrutskie et al. (2006), (213) Smart et al. (2018), (214) Smith et al. (2014), (215) Smith et al. (2018), (216) Strauss et al. (1999), (217) Thalmann et al. (2009), (218) Thompson et al. (2013), (219) Thorstensen & Kirkpatrick (2003), (220) Tinney et al. (2003), (221) Tinney et al. (2005), (222) Tinney et al. (2018), (223) Torres et al. (2019), (224) Tsvetanov et al. (2000), (225) Vrba et al. (2004), (226) Warren et al. (2007), (227) Wilson et al. (2001), (228) Wilson et al. (2003), (229) Wright et al. (2013), (230) Zhang et al. (2017), (231) Zhang et al. (2019), (232) Zhang et al. (2021), (233) van Leeuwen (2007).

2.2. New Parallaxes

We present new J -band parallax measurements for four members of the volume-limited sample, shown in Table 2 and also included in Table 1. The objects were observed with CFHT/WIRCam as part of the Hawaii Infrared Parallax Program (Dupuy & Liu 2012). The observation strategies, data reduction, and astrometric solutions are all as described in Dupuy & Liu (2012) and Dupuy & Liu (2017).

This is the first published parallax for CF-BDS J030135.11–161418.0. K21 published parallaxes for the other three objects, which are generally consistent with ours. We opted to use our measurements because they are more precise. Theissen (2018) also published a parallax for 2MASS J21543318+5942187 using astrometry from *WISE*. This parallax is formally consistent with ours, but has a much larger uncertainty.

3. DEMOGRAPHICS OF L, T, AND Y DWARFS

3.1. Lutz-Kelker Bias

Parallax measurements are not exact, so each object in a parallax-defined sample may in fact lie closer or farther than the distance obtained by inverting the parallax. At the boundary of a volume-limited sample, the volume of space just outside the sample is larger than the volume just inside, so typically there will be more objects with measured distances scattering inward than scattering outward, artificially inflating the number of objects in the sample. This is a manifestation of the bias that Eddington (1913) identified for data near the boundaries of sample bins. Lutz & Kelker (1973) realized that the same concept applies to parallax-defined samples: on average, objects are slightly farther away than measured, and their luminosities are slightly underestimated by the parallaxes. In the Lutz-Kelker formulation, the size of the bias depends on the parallax uncertainty as a fraction of the parallax. The mean fractional uncertainty of our sample is 5%, and the corresponding Lutz-Kelker correction implies that our parallaxes probe a volume of space $\approx 3\%$ larger than their nominal distances indicate. Since we achieve an uncertainty of $\approx 10\%$ for our space density calculation (Section 3.3), Lutz-Kelker bias is not a significant source of uncertainty, but we nevertheless account for this bias in our analysis.

Lutz & Kelker (1973) determined that the distribution of the true parallax ϖ about the measured parallax ϖ_0 is

$$P(\varpi|\varpi_0) \propto \left(\frac{\varpi}{\varpi_0}\right)^4 \exp\left(-\frac{(\varpi - \varpi_0)^2}{2\sigma^2}\right) \quad (1)$$

where σ is the standard deviation of ϖ_0 (i.e., the measurement error). The expected value of ϖ from this

distribution is

$$\varpi = \frac{\varpi_0 + \sqrt{(\varpi_0^2 - 16\sigma^2)}}{2} \quad (2)$$

We corrected the parallaxes in our list to their expected values using Equation (2); the median correction was 0.4 mas. We stress that as the Lutz-Kelker correction is a statistical correction for samples of objects, we used these corrected parallaxes only for analysis of our volume-limited sample as a whole and do not quote them for individual objects. The effect of the correction was to reduce the membership of our volume-limited sample by $\approx 3\%$, confirming that this bias is not significant relative to our $\approx 10\%$ uncertainty on the overall space density.

3.2. Completeness

We estimated the completeness of our volume-limited sample using the V/V_{\max} statistic (Schmidt 1968), employed by both K21 and our Paper I. Briefly, V is the volume of space with radius equal to the distance from the Sun of a given sample member, and V_{\max} is the volume of space with radius equal to the outer limit of the sample (for our full sample, this is 25 pc). Each object in the sample thus has a V/V_{\max} value between 0 and 1. If a sample has uniform spatial distribution — a valid assumption for our sample which sits near the Galactic midplane — the expectation value will be $\langle V/V_{\max} \rangle = 0.5$. Our volume-limited sample is centered on the Sun, so we would expect any incompleteness to be in the more distant portions of our sample where objects appear more faint.

Figure 1 shows $\langle V/V_{\max} \rangle$ as a function of limiting distance for our volume-limited sample, for distances 8–25 pc. In addition, we show $\langle V/V_{\max} \rangle$ as a function of distance for five spectral type bins. Uncertainties for $\langle V/V_{\max} \rangle$ were determined using the method described in Paper I; briefly, we used Monte Carlo trials to incorporate the parallax uncertainties and statistical fluctuations (drawn from the binomial distribution) due to our limited sample size. Figure 1 makes clear that our volume-limited sample is close to completeness ($\approx 92\%$ at 25 pc) for spectral types L0–T4. Our sample is less complete for cooler spectral types, for which $\langle V/V_{\max} \rangle$ steadily decreases at larger distances and is well below 0.5 at 25 pc. The full sample has $\langle V/V_{\max} \rangle = 0.50 \pm 0.04$ at 14 pc (143 objects). $\langle V/V_{\max} \rangle$ declines beyond this distance to $\langle V/V_{\max} \rangle = 0.39 \pm 0.02$ at 25 pc, indicating $\approx 78\%$ completeness for the full sample. This is lower than in Paper I because of the inclusion of T8.5 and later objects, which are prohibitively faint and difficult to observe beyond ≈ 15 pc. Overall, the completeness of

Table 2. New Parallaxes and Proper Motions

Object	α_{J2000} (deg)	δ_{J2000} (deg)	Epoch (MJD)	Relative			Absolute			N_{ep}	Δt (yr)	χ^2/dof
				ϖ_{rel} (mas)	$\mu_{\alpha, \text{rel}} \cos \delta$ (mas yr $^{-1}$)	$\mu_{\delta, \text{rel}}$ (mas yr $^{-1}$)	ϖ_{abs} (mas)	$\mu_{\alpha, \text{abs}} \cos \delta$ (mas yr $^{-1}$)	$\mu_{\delta, \text{abs}}$ (mas yr $^{-1}$)			
CFBDS J030135.11-161418.0	045.3965467	-16.2382606	54436.31	48.0 ± 3.8	297.8 ± 3.0	126.1 ± 3.1	49.1 ± 3.8	301.9 ± 3.2	124.4 ± 3.4	8	8.06	10.3/11
2MASS J0512063-294954	078.0269272	-29.8311129	57317.60	48.8 ± 2.8	-1.0 ± 1.6	78.8 ± 2.0	49.6 ± 2.8	0.6 ± 1.8	79.9 ± 2.3	7	2.12	10.3/9
WISE J064205.58+410155.5	100.5233880	+41.0318223	56585.62	63.2 ± 1.2	-0.5 ± 1.2	-374.8 ± 1.2	64.1 ± 1.1	-2.0 ± 1.4	-377.4 ± 1.5	7	2.17	10.7/9
2MASS J21543318+5942187	328.6376414	+59.7040555	55050.45	63.3 ± 1.5	-160.1 ± 0.5	-463.8 ± 0.7	64.7 ± 1.5	-166.0 ± 1.1	-469.6 ± 0.9	6	5.16	9.3/7

NOTE—(α_{J2000} , δ_{J2000} , Epoch): coordinates and epoch for our first observation of that target.

our sample is very similar to that of Paper I, except for the impact of adding the late-T and Y dwarfs from K21.

3.3. Space Density

To accurately calculate the space density of L, T, and Y dwarfs in the solar neighborhood, we needed to correct for incompleteness in our sample. We also needed to account for the uncertainties on the parallax measurements, which affect whether objects observed near the 25 pc boundary are actually inside the sample. To address these issues, we used the UltracoolSheet to compile a list of 1119 L0–Y2 dwarfs from the literature that met the same criteria as for our volume-limited sample (Section 2) but at any distance. We refer to this as the “full parallax list”. It is effectively our volume-limited sample augmented by L0–Y2 dwarfs with parallax measurements placing them beyond 25 pc. Using this list allowed us to incorporate the impact on our space density measurements of objects appearing to lie beyond 25 pc but whose uncertainties allowed a significant possibility of membership in our sample.

From this full parallax list we drew new 25 pc volume-limited samples in a Monte Carlo fashion, perturbing the Lutz-Kelker-corrected parallaxes according to their uncertainties (assumed to be normally distributed) and rejecting objects with parallaxes < 40 mas. These perturbations sometimes moved objects with parallaxes measured near 40 mas from outside to inside the 25 pc distance limit and vice versa, so the membership varied at the outer edges of the Monte Carlo samples.

We then needed to correct each Monte Carlo sample for incompleteness. In Paper I, we obtained a rough correction by dividing the number of objects in a sample by twice its $\langle V/V_{\max} \rangle$ value (Section 3.2). However, this approach provides only an estimate because $\langle V/V_{\max} \rangle$ varies with different spatial positions of objects within a sample even when the number of objects in the sample is fixed. We therefore developed a new method to correct for incompleteness that accounts for the distribution of objects within the sample and also gives a statistical estimate of uncertainty. For each Monte Carlo trial, we calculated $\langle V/V_{\max} \rangle$ at multiple distances from 2 to 25 pc (analogous to Figure 1), i.e., for a distance d , we identified the subsample of objects with distances less than d and calculated $\langle V/V_{\max} \rangle$ for that volume-limited subsample. We used steps of 0.1 pc, and identified the largest distance (d_{lim}) at which a trial subsample had $\langle V/V_{\max} \rangle \geq 0.5$. We treated the Monte Carlo sample as complete at that distance, and calculated the space density for the sample using the number of objects N_{lim} enclosed in the volume defined by d_{lim} . Finally, we calculated d_{lim} , N_{lim} , and the space density for our volume-

limited sample as the median and 68.3% confidence limits from all of the Monte Carlo trials.

Table 3 presents our final space density results and $\langle V/V_{\max} \rangle$ for the entire sample, as well as separately for L, T, and Y dwarfs, for five spectral type bins spanning the sample, for individual spectral types, and for single objects, binaries/triples, companions, and young objects. For the space density, we report two sets of confidence limits that include noise from the binomial and Poisson distributions, respectively. The calculation and purposes of these confidence limits are described in detail in Paper I. Briefly, the binomial uncertainties (σ_{binomial}) reflect the uncertainty in our measurement of the space densities within 25 pc of the Sun, given that our sample only covers 68% of the associated volume. The Poisson uncertainties (σ_{Poisson}) reflect the uncertainty in our measurement of the space densities more broadly in our region of our Galaxy, of which our solar neighborhood is a small part. As in Paper I, we adopt the Poisson uncertainties in order to describe the space density of brown dwarfs in general and to enable direct comparison with previous estimates. We note that the uncertainties for our measurements in Table 3 have increased from Paper I in most categories, with our new values better reflecting the uncertainty in the completeness of our sample and its subsets.

For our full 25 pc sample of L0–Y2 dwarfs, we find $d_{\text{lim}} = 14.3^{+0.5}_{-1.4}$ pc, $N_{\text{lim}} = 154^{+20}_{-39}$ objects, and a space density of $(1.83^{+0.16}_{-0.15}) \times 10^{-2}$ pc $^{-3}$. However, proceeding through our sample toward colder spectral types, d_{lim} drops steadily beyond T3, while the number objects per spectral type peaks at T8 and then drops rapidly. It is unclear to what extent this latter decline is due to an actually smaller number of T9 and Y dwarfs in the solar neighborhood, but the decreasing d_{lim} and $\langle V/V_{\max} \rangle$ imply that our sample is significantly incomplete and our space density estimates may be less accurate for these cold, faint spectral types. Table 3 therefore includes several sub-samples with spectral types down to only T8 (not including T8.5) to facilitate comparison with our Paper I sample, and also to emphasize that our results for sub-samples including T8.5 and later-type dwarfs should be used with caution.

For L0–T8 dwarfs, our space density estimate of $(1.25 \pm 0.10) \times 10^{-2}$ pc $^{-3}$ has increased by 27% from Paper I, more than the 13% increase in the number of objects with these spectral types. Inspecting the sub-samples in Table 3, we note that for sub-samples for which d_{lim} is close to 25 pc (implying completeness), we obtain space densities consistent with Paper I when accounting for the larger number of members of our updated sample. Where d_{lim} is significantly less than 25 pc,

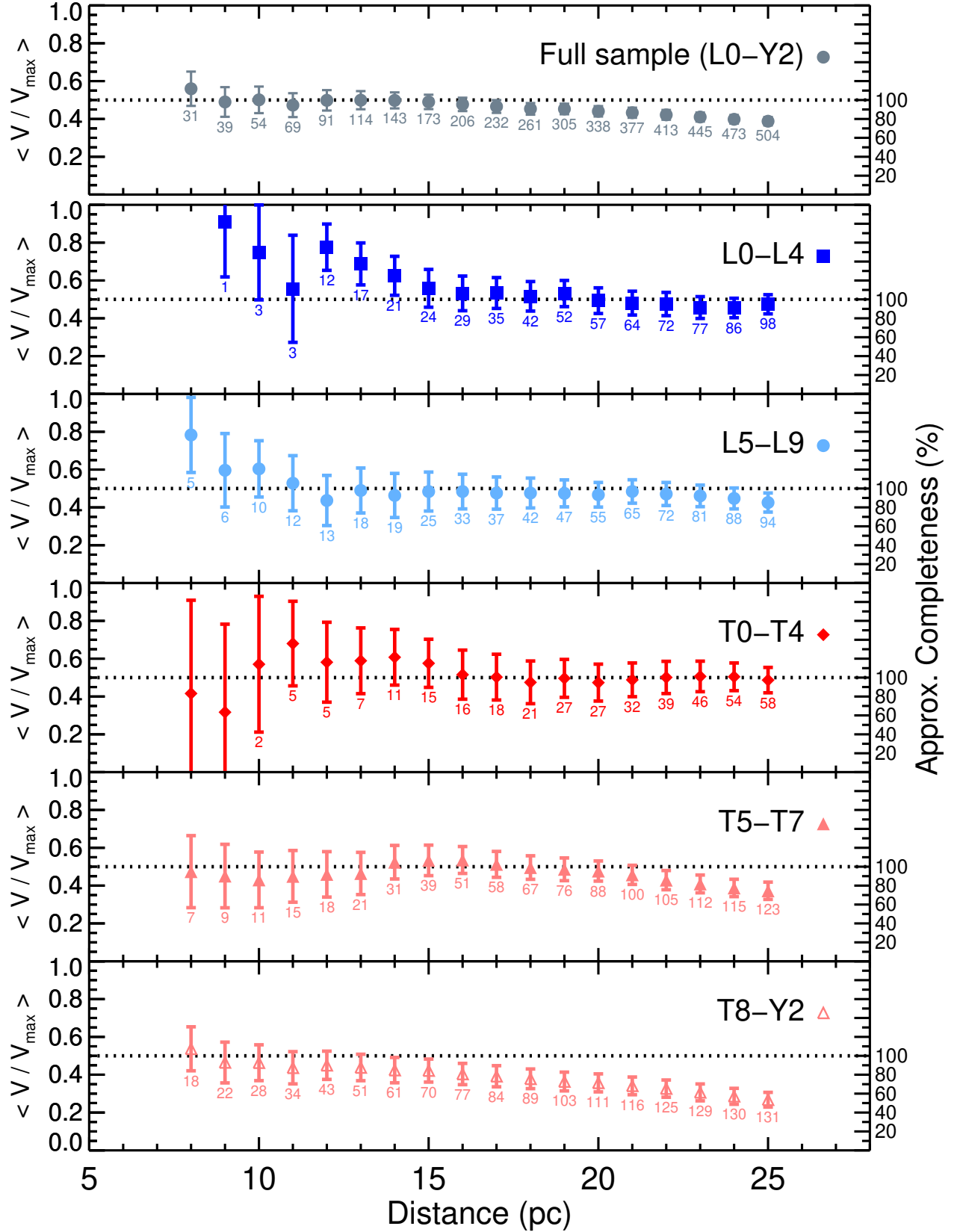


Figure 1. $\langle V/V_{\max} \rangle$ as a function of distance for our entire volume-limited sample (spectral types L0–Y2, top panel) and for five spectral type bins (other panels). (This plot updates Figure 3 in Paper I.) The right-hand axes indicate approximate completeness values corresponding to $\langle V/V_{\max} \rangle$ values less than 0.5, estimated as twice the $\langle V/V_{\max} \rangle$ value. Our full sample has $\langle V/V_{\max} \rangle \approx 0.5$ to within its uncertainty at 16 pc, consistent with completeness, with the declining trend of $\langle V/V_{\max} \rangle$ implying incompleteness beyond this distance. Most of the incompleteness in our full sample is for spectral types T5 and later, which is unsurprising given their faintness. Our sample is $\approx 92\%$ complete for L0–T4.5 dwarfs.

Table 3. Space Density and $\langle V/V_{\max} \rangle$ for Our 25 pc Sample of L0–Y2 Dwarfs

Objects	$N_{25\text{pc}}$	$\langle V/V_{\max} \rangle_{25\text{pc}}^a$	d_{lim}	N_{lim}	Space Density (10^{-3} objects pc^{-3})		
					Value	σ_{binomial}	σ_{Poisson}
L0 ≤ SpT < L1	16	0.49 ± 0.13	24.9 ^{+0.1} _{-3.2}	16 ⁺³ ₋₄	0.36	±0.05	±0.10
L1 ≤ SpT < L2	28	0.50 ± 0.10	25.0 ^{+0.0} _{-4.4}	28 ⁺³ ₋₉	0.63	+0.07 -0.09	+0.15 -0.13
L2 ≤ SpT < L3	19	0.46 ± 0.11	23.7 ^{+0.4} _{-0.6}	18 ⁺³ ₋₂	0.48	±0.06	+0.12 -0.11
L3 ≤ SpT < L4	14	0.39 ± 0.13	15.2 ^{+1.0} _{-0.1}	6 ⁺² ₋₁	0.60	+0.14 -0.10	+0.29 -0.21
L4 ≤ SpT < L5	21	0.48 ± 0.11	24.5 ^{+0.2} _{-0.9}	21 ⁺³ ₋₄	0.50	±0.06	+0.13 -0.11
L5 ≤ SpT < L6	28	0.45 ± 0.10	22.3 ^{+1.1} _{-0.8}	23 ⁺⁴ ₋₃	0.72	+0.08 -0.09	+0.16 -0.14
L6 ≤ SpT < L7	15	0.42 ± 0.13	20.2 ^{+1.8} _{-1.0}	11 ⁺³ ₋₂	0.44	±0.08	+0.15 -0.13
L7 ≤ SpT < L8	17	0.46 ± 0.13	23.8 ^{+0.7} _{-9.1}	16 ⁺³ ₋₈	0.41	+0.22 -0.07	+0.20 -0.12
L8 ≤ SpT < L9	17	0.40 ± 0.12	22.5 ± 0.5	16 ⁺² ₋₃	0.49	±0.07	+0.13 -0.12
L9 ≤ SpT < T0	17	0.40 ± 0.13	20.7 ^{+1.1} _{-1.2}	12 ± 2	0.46	±0.08	+0.15 -0.13
T0 ≤ SpT < T1	9	0.48 ± 0.18	24.6 ^{+0.4} _{-1.1}	8 ± 2	0.20	±0.04	+0.09 -0.07
T1 ≤ SpT < T2	9	0.50 ± 0.19	25.0 ^{+0.0} _{-1.5}	8 ⁺² ₋₃	0.18	±0.04	±0.07
T2 ≤ SpT < T3	15	0.43 ± 0.14	21.1 ^{+2.6} _{-6.5}	11 ⁺⁴ ₋₆	0.41	+0.13 -0.08	+0.19 -0.13
T3 ≤ SpT < T4	11	0.64 ± 0.16	25.0 ± 0.0	9 ⁺² ₋₃	0.20	+0.04 -0.07	±0.07
T4 ≤ SpT < T5	14	0.44 ± 0.14	20.6 ^{+3.7} _{-1.6}	10 ⁺⁴ ₋₃	0.40	±0.08	+0.14 -0.12
T5 ≤ SpT < T6	40	0.41 ± 0.08	21.2 ^{+0.8} _{-0.5}	29 ⁺⁴ ₋₃	1.06	±0.12	+0.21 -0.19
T6 ≤ SpT < T7	34	0.35 ± 0.09	17.7 ^{+1.5} _{-1.0}	21 ⁺⁵ ₋₄	1.28	±0.17	+0.30 -0.28
T7 ≤ SpT < T8	49	0.35 ± 0.07	14.9 ^{+1.3} _{-0.6}	19 ⁺⁵ ₋₃	1.98	+0.26 -0.27	+0.49 -0.43
T8 ≤ SpT < T9	67	0.32 ± 0.06	14.5 ^{+0.7} _{-0.5}	29 ⁺⁴ ₋₅	3.35	+0.39 -0.36	+0.63 -0.61
T9 ≤ SpT < Y0	35	0.31 ± 0.08	14.3 ^{+1.5} _{-1.8}	15 ⁺⁶ ₋₄	1.81	+0.32 -0.29	+0.57 -0.46
Y0 ≤ SpT < Y1	16	0.19 ± 0.11	9.3 ^{+0.2} _{-0.1}	8 ± 2	3.45	+0.73 -0.62	+1.35 -1.03
Y1 ≤ SpT < Y2	11	0.17 ± 0.12	11.6 ^{+2.2} _{-1.1}	6 ± 2	1.31	+0.41 -0.35	+0.69 -0.51
SpT = Y2	2	0.03 ± 0.13	2.8 ^{+7.2} _{-0.0}	1 ± 1	15.92	+14.91 -1.02	+30.05 -1.80
L0 ≤ SpT < L5	98	0.47 ± 0.05	20.1 ± 0.4	58 ± 5	2.51	+0.19 -0.18	+0.36 -0.33
L5 ≤ SpT < T0	94	0.43 ± 0.05	18.6 ± 2.7	48 ⁺²¹ ₋₁₇	2.63	+0.29 -0.22	+0.44 -0.37
T0 ≤ SpT < T5	58	0.49 ± 0.07	24.6 ^{+0.4} _{-1.2}	53 ⁺⁶ ₋₈	1.25	±0.11	+0.20 -0.17
T5 ≤ SpT ≤ T8	168	0.37 ± 0.05	16.4 ^{+0.5} _{-0.4}	77 ± 8	6.08	+0.40 -0.41	±0.71
T8.5 ≤ SpT ≤ Y2	86	0.28 ± 0.04	10.4 ± 0.2	27 ⁺³ ₋₅	8.23	+0.96 -0.98	+1.66 -1.57
L0 ≤ SpT < T0	192	0.45 ± 0.04	19.0 ^{+0.5} _{-0.3}	101 ⁺¹² ₋₈	5.10	±0.29	+0.53 -0.50
T0 ≤ SpT ≤ T8	226	0.40 ± 0.04	16.4 ± 0.4	93 ⁺⁹ ₋₈	7.39	+0.44 -0.45	+0.78 -0.75
T0 ≤ SpT < Y0	283	0.37 ± 0.03	15.8 ^{+0.4} _{-0.6}	116 ⁺¹¹ ₋₁₃	10.15	+0.55 -0.58	+0.98 -0.96
Y0 ≤ SpT ≤ Y2	29	0.17 ± 0.07	9.3 ^{+0.8} _{-1.0}	13 ⁺³ ₋₄	5.57	+0.95 -0.97	+1.73 -1.52
Single	429	0.39 ± 0.02	14.7 ^{+0.6} _{-1.0}	143 ⁺¹⁹ ₋₂₇	15.77	+0.81 -0.79	+1.42 -1.33
Binary/triple ^b	48	0.48 ± 0.08	24.5 ^{+0.4} _{-1.3}	45 ⁺⁵ ₋₆	1.09	+0.09 -0.10	+0.17 -0.16
Companion ^c	30	0.35 ± 0.09	18.7 ^{+0.4} _{-0.0}	20 ⁺³ ₋₂	1.07	+0.13 -0.15	+0.27 -0.21
Young	20	0.41 ± 0.11	23.2 ^{+0.2} _{-0.5}	20 ⁺² ₋₃	0.56	+0.07 -0.08	+0.13 -0.12
All L0 ≤ SpT ≤ T8	418	0.42 ± 0.03	16.4 ^{+0.7} _{-0.3}	161 ⁺²⁰ ₋₁₄	12.46	+0.56 -0.57	+0.99 -1.01
All	504	0.39 ± 0.02	14.3 ^{+0.5} _{-1.4}	154 ⁺²⁰ ₋₃₉	18.33	+0.91 -0.92	+1.62 -1.53

NOTE— This table expands Table 2 from Paper I by adding spectral types T8.5–Y2, and adopts a new correction for incompleteness (Section 3.2). $N_{25\text{pc}}$: Number of objects in our full volume-limited sample. $\langle V/V_{\max} \rangle_{25\text{pc}}$: Calculated for our full volume-limited sample. A sample with uniform spatial distribution will have $\langle V/V_{\max} \rangle = 0.5$. d_{lim} : Median and 68% confidence limits for the largest distance at which $\langle V/V_{\max} \rangle \geq 0.5$ (implying a complete sample) from our Monte Carlo trials. N_{lim} : Median and 68% confidence limits for the number of objects in the sample out to d_{lim} . *Space Density*: Median and 68% confidence limits for N_{lim} divided by the volume of the sample at d_{lim} from our Monte Carlo trials. σ_{binomial} describes how precisely our space density measurements represent the full 25 pc volume around the Sun. σ_{Poisson} describes how precisely our space density measurements represent brown dwarfs in our general neighborhood of the Galaxy. The calculation of σ_{binomial} and σ_{Poisson} is described in Appendix B of Paper I.

^a Mean and standard deviation from Monte Carlo trials that resample the parallaxes from their errors and incorporate binomial uncertainties to account for statistical fluctuations in our sample.

^b Close binaries and triples are counted as single objects with unresolved spectral types.

^c Three companions are themselves binaries (see Paper I for details) and are also included in the binary/triple bin.

we systematically find larger space densities than in Paper I, which indicates that the method we used to correct for incompleteness in Paper I failed to account for the spatial distribution of objects within the sub-samples and underestimated the space densities of incomplete sub-samples.

Our updated $(5.10_{-0.50}^{+0.53}) \times 10^{-3} \text{ pc}^{-3}$ space density for L dwarfs, as well as our values for the L dwarf subclasses, are systematically $\approx 20\text{--}80\%$ larger than many previous estimates (Cruz et al. 2007; Reyl e et al. 2010; Marocco et al. 2015), although they are formally different only at the $\sim 1\text{--}2\sigma$ level due to large uncertainties. Bardalez Gagliuffi et al. (2019) have also recently published space densities for M7–L5 dwarfs that are larger than previous estimates, but our early-L measurements are $\approx 70\%$ smaller than theirs. We addressed this discrepancy in Paper I. Our L dwarf space density is consistent with the recent measurements of K21 based on their 20 pc all-sky volume-limited sample, which is somewhat surprising given that they treat the binary components as separate objects whereas we do not (Section 3.5); however, assuming a $\approx 15\%$ binary fraction for our sample, our space densities would differ by $\approx 10\%$, i.e., consistent within uncertainties. For T0–T8 dwarfs, a similar trend is clear: our updated $(7.39_{-0.75}^{+0.78}) \times 10^{-3} \text{ pc}^{-3}$ space density is larger than some previous estimates (Burningham et al. 2013; Marocco et al. 2015) but consistent with those of Metchev et al. (2008), Reyl e et al. (2010), and K21.

3.4. Bolometric Magnitudes

Bolometric luminosities (L_{bol}) are fundamental, observable physical quantities of ultracool dwarfs that can be directly compared to evolutionary models, providing constraints on ages and masses. To determine these constraints for L, T, and Y dwarfs in the solar neighborhood, we calculated the bolometric luminosity (L_{bol}) of each member of our volume-limited sample. We used the $\log(L_{\text{bol}}/L_{\odot})$ vs. $M_{K_{\text{MKO}}}$ polynomial of Dupuy & Liu (2017), derived from L_{bol} calculated by Filippazzo et al. (2015), for objects with $9.1 \leq M_{K_{\text{MKO}}} \leq 17.8$ mag, the magnitude range over which this polynomial is valid. This range included the brightest objects in our sample and provided L_{bol} for 370 objects, but did not include 133 objects with $M_{K_{\text{MKO}}} > 17.8$ mag or which lacked K -band photometry.

For the remaining objects (mostly having spectral types $\geq T8$), we created an updated version of the “super-magnitude” method developed by Dupuy & Kraus (2013), applicable to objects with spectral types L4 and later. Our updated method is described in detail in Appendix A. Briefly, we used the Sonora-Bobcat

model atmospheres (Marley et al. 2021) to define polynomials that convert the combined absolute flux in several bands (usually J_{MKO} , H_{MKO} , and *Spitzer*/IRAC [3.6] and [4.5], or J_{MKO} , H_{MKO} , and AllWISE $W1$ and $W2$) into L_{bol} . The Sonora-Bobcat models cover T_{eff} down to 200 K, below the coldest objects in our sample, so using this super-magnitude method we were able to calculate L_{bol} for 105 of the remaining 133 objects, many of which had no previous determination of L_{bol} .

We used the K_{MKO} (when possible) or J_{MKO} bolometric corrections of Liu et al. (2010) to determine L_{bol} for 26 of the remaining objects, leaving two for which we could not determine a value of L_{bol} because they lack the photometry needed for all of the above methods. These two objects, ULAS J074502.79+233240.3 and GJ 758B, were therefore not included in our volume-limited sample.

We converted L_{bol} to bolometric magnitude (M_{bol}) using $M_{\text{bol},\odot} = 4.74$ mag. For the super-magnitude-derived L_{bol} , we propagated the uncertainties from the objects’ parallaxes and photometry through Monte Carlo trials to obtain uncertainties for the M_{bol} . We present our M_{bol} results in Table 1. We caution that for unresolved binaries our M_{bol} calculation should be treated as less reliable, particularly for pairs in which the secondary component contributes a significant amount of the total flux.

3.5. Luminosity Function for Single Objects

As discussed at length in Paper I, there is evidence suggesting that the components of binaries and companions to high-mass primaries may have different mass distributions and formation histories from single objects, e.g., the spectral type distribution of wide companions notably favors T dwarfs more than in the rest of our volume-limited sample. The numbers of binaries and companions in our volume-limited sample may also be impacted by different selection effects. These related but distinct populations therefore need to be treated as such. In addition, a proper analysis of binaries needs L_{bol} to be calculated separately for each component, requiring resolved absolute photometry which is often not available, in particular in the mid-infrared *Spitzer*/IRAC and WISE bands. We therefore focus our remaining analysis on the single objects in our volume-limited sample.

We used The UltracoolSheet and our own high-angular resolution imaging survey (W. Best et al., in preparation, described briefly in Paper I) to identify 48 binaries and multiples and 30 wide companions (separations typically $> 10''$) to main-sequence primaries in our sample, which we removed to create a volume-limited sample of 429 single objects. Similarly, we re-

moved binaries and wide companions from the full parallax list to create a list of single L0–Y2 dwarfs in our volume-limited sample and beyond. Using this list, we determined the bolometric luminosity function of the single objects in our volume-limited sample, correcting for incompleteness and incorporating Poisson uncertainties in the manner described in Section 3.3. We used bins of 1 mag in M_{bol} and Monte Carlo trials to calculate uncertainties. The mean effect of our Lutz-Kelker correction (Section 3.1) on our luminosity bins was $-0.03 \times 10^{-3} \text{ pc}^{-3}$ per bin. This is less than the uncertainties on the space densities in those bins, confirming that our luminosity function was not significantly impacted by the correction.

We present our completeness-corrected luminosity function in Table 4, and plot it in Figure 2. This is the first bolometric luminosity function calculated for single brown dwarfs in the solar neighborhood. The function spans $13 \leq M_{\text{bol}} \leq 24$ mag, and appears consistent with a flat distribution for $M_{\text{bol}} \geq 15$ mag, although there is a suggestion of gradual increase in space density toward fainter luminosities. The brightest bin ($M_{\text{bol}} = 13\text{--}14$ mag) corresponds to \approx M8–L1 dwarfs (Zhang et al. 2020) and is thus significantly incomplete due to our exclusion of M dwarfs from our sample, so we do not include this bin in our subsequent population synthesis analysis. On the faint end, the three bins with $M_{\text{bol}} \geq 21$ mag have large uncertainties due to fewer objects and $d_{\text{lim}} < 10$ pc, so we likewise exclude these bins from our analysis.

4. POPULATION SYNTHESIS

4.1. Overview

To constrain the mass and age distributions underlying the observed luminosity function of ultracool dwarfs, we employed population synthesis, i.e., forward modeling of our volume-limited sample. Such modeling adopts parametrized distributions of masses and ages of objects, from which synthetic objects are drawn. Each synthetic object’s mass and age can then be used to derive L_{bol} , T_{eff} , and other physical properties using evolutionary models. We can then compare luminosity functions for our synthetic populations to that of our volume-limited sample to constrain the underlying age and mass parameters. This comparison enables us to simultaneously constrain the mass and age distributions of nearby brown dwarfs.

4.2. Initial Mass Function

Studies of the stellar IMF typically adopt a power law with form $\xi(M) \equiv dN/d(\log M) \propto M^{-\Gamma}$, where M is stellar mass and N is the occurrence rate. This is

the form used in the seminal work by Salpeter (1955), who determined that occurrence decreases toward larger masses, with $\Gamma = 1.35$ for stars with masses $\geq 1M_{\odot}$ in nearby clusters. Previous work on ultracool dwarfs has commonly used the alternate power-law form (Kroupa 2001)

$$\Psi(M) \equiv \frac{dN}{dM} \propto M^{-\alpha} \quad (3)$$

with Ψ representing space density, so we also used this form, which is related to the Salpeter form by $\alpha = \Gamma + 1$ (so $\alpha = 2.35$ for $\geq 1M_{\odot}$ stars). Figure 3 shows three examples of the brown dwarf mass distributions drawn from different choices of α , where $\alpha = 0$ means a uniform distribution of masses. Chabrier (2003) has also shown that an IMF which takes the form of a power law above $1 M_{\odot}$ and a lognormal distribution below $1 M_{\odot}$ (defined by a peak mass and a characteristic width) is consistent with data available at the time.

4.3. Age Distribution

For age distributions, we used the exponential form

$$b(t) \propto e^{-\beta t} \quad (4)$$

where b is the birthrate and $t \in [0, 10]$ Gyr is the time since the formation of the Galaxy; hence, the present-day age of an object born at time t is $(10 - t)$ Gyr. This is the most commonly used form in previous work that does not simply assume a flat age distribution (e.g., Allen et al. 2005; Deacon & Hambly 2006; Day-Jones et al. 2013). Figure 3 shows three examples of age distributions resulting from different choices of β . Note that $\beta = 0$ is equivalent to a flat age distribution, which is consistent with many estimates for the formation history of nearby stars (e.g., Soderblom et al. 1991; Gizis et al. 2002) but has been called into question by more recent work (e.g., Mor et al. 2019; Fantin et al. 2019).

4.4. Evolutionary Models

We used two sets of evolutionary models to generate L_{bol} and T_{eff} for members of our synthetic ultracool dwarf populations (Section 4.5).

(1) The solar-metallicity “hybrid” evolutionary models of Saumon & Marley (2008, hereinafter SM08) have to date provided the best matches to measured masses and luminosities for L through mid-T dwarfs (Dupuy et al. 2015b; Dupuy & Liu 2017; Chen et al. 2022). The SM08 models assume a gradual loss of cloud opacity as objects cool through the L/T transition, coupling cloudy models at 1400 K with cloudless models at 1200 K by linearly interpolating the surface boundary condition in T_{eff} for each surface gravity in the model grid. The models are conjectural in that they do not derive from

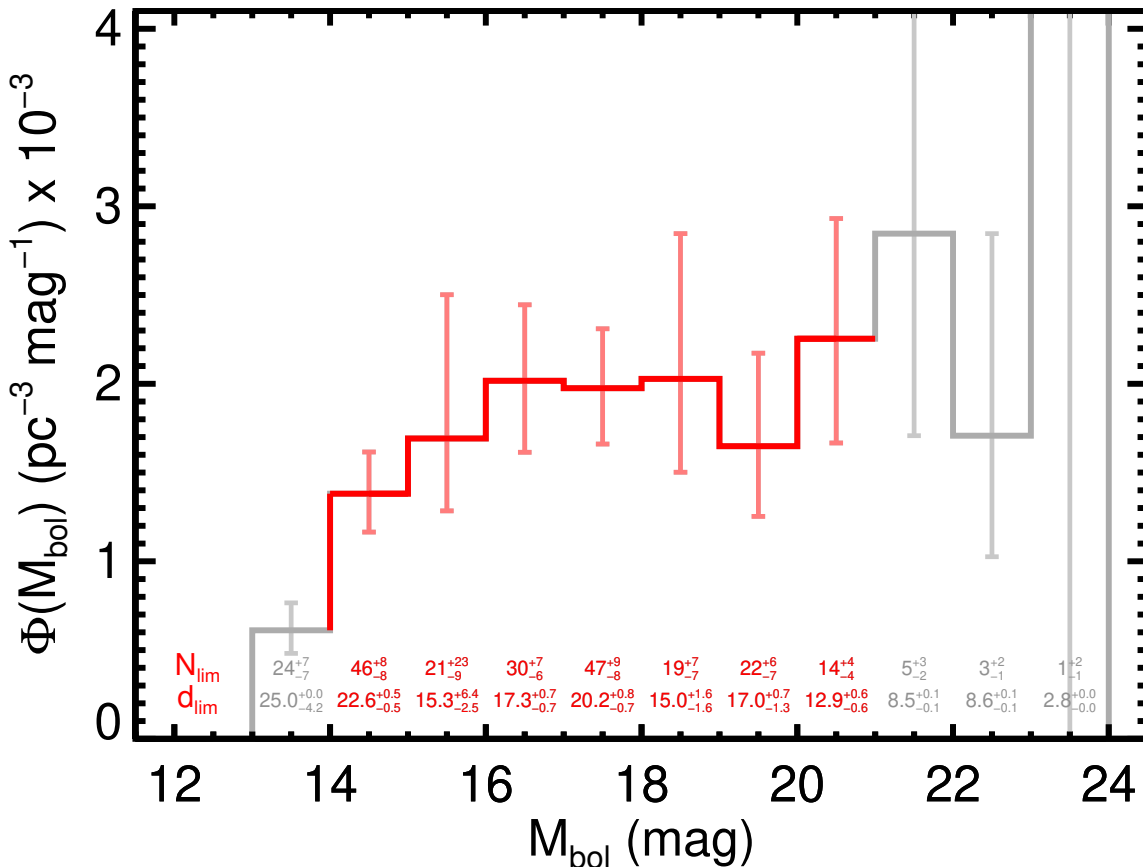


Figure 2. The bolometric luminosity function for single objects in our volume-limited sample, plotted as the space density of bins of 1 bolometric magnitude. Along the bottom we print the number of objects within the volume-complete distance (N_{lim}) and the volume-complete distance (d_{lim}) for each bin from Table 4; we use these numbers to calculate the space densities. Bins plotted in red have robustly-measured space densities, which we use to infer population parameters in Section 4. Bins excluded from our analysis are plotted in gray: the brightest bin (13–14 mag) is incomplete due to our exclusion of M dwarfs from our sample, while the three faintest bins contain fewer than 10 objects within their d_{lim} . The luminosity function is consistent with a flat distribution for $M_{\text{bol}} \geq 15$ mag, but the overall shape suggests an increase toward fainter magnitudes.

a physical explanation for the cloud-clearing, but they are coupled to the cooling of the brown dwarf interiors. The SM08 models span a mass range of $0.002 M_{\odot}$ to $0.085 M_{\odot}$ and an age range of 3 Myr to 10 Gyr, so these are the boundaries of our synthetic populations.

(2) The AMES-COND evolutionary models (Baraffe et al. 2003, hereinafter COND) underlie the widely-used BT-Settl model atmosphere grids (Allard et al. 2012). BT-Settl includes clouds for L dwarfs and a physical prescription for the transition to clear-photosphere T dwarfs, making these models well-suited for studying both L and T dwarf atmospheres as well as the L/T transition. However, the atmospheric component of the BT-Settl models is not coupled with the evolutionary component and does not impact the L_{bol} and T_{eff} in the model grid. The evolutionary components of the BT-

Settl models are thus identical to each other and to the original COND models, except that the BT-Settl versions have more densely sampled age grids and extend to higher masses (beyond the upper mass limit of our analysis). We therefore refer to this evolutionary model grid as simply COND, although we use the solar-metallicity grid published with BT-Settl. The COND models have a wider mass range of $0.0005 M_{\odot}$ to $0.1 M_{\odot}$ and age range of 1 Myr to 10 Gyr, but for consistency we limit our synthetic populations to the boundaries required by the SM08 models.

We note that more recent evolutionary models are available, but they sample less of the brown dwarf parameter space or do not incorporate clouds. BHAC15 (Baraffe et al. 2015) has a lower mass limit of $0.01 M_{\odot}$ and a lower T_{eff} limit of 1200 K, and thus excludes most

Table 4. Luminosity Function for Our 25 pc Volume-Limited Sample of Single L0–Y2 Dwarfs

Objects	$N_{25\text{pc}}$	$\langle V/V_{\text{max}} \rangle_{25\text{pc}}$	d_{lim}	N_{lim}	Space Density (10^{-3} objects pc^{-3})		
					Value	σ_{binomial}	σ_{Poisson}
$13.0 \leq M_{\text{bol}} < 14.0^a$	26	0.50 ± 0.10	$25.0^{+0.0}_{-4.2}$	25^{+4}_{-7}	0.60	$+0.11$ -0.09	$+0.15$ -0.13
$14.0 \leq M_{\text{bol}} < 15.0$	56	0.46 ± 0.07	22.6 ± 0.5	45 ± 5	1.37	$+0.15$ -0.14	$+0.23$ -0.22
$15.0 \leq M_{\text{bol}} < 16.0$	55	0.44 ± 0.07	$15.3^{+6.4}_{-2.5}$	19^{+23}_{-8}	1.82	$+0.65$ -0.34	$+0.81$ -0.41
$16.0 \leq M_{\text{bol}} < 17.0$	58	0.42 ± 0.07	17.3 ± 0.7	30 ± 5	1.99	± 0.27	$+0.43$ -0.40
$17.0 \leq M_{\text{bol}} < 18.0$	70	0.39 ± 0.07	$20.2^{+0.8}_{-0.7}$	47^{+6}_{-7}	1.96	± 0.21	$+0.33$ -0.31
$18.0 \leq M_{\text{bol}} < 19.0$	48	0.35 ± 0.08	15.0 ± 1.6	19^{+6}_{-7}	1.99	$+0.60$ -0.39	$+0.82$ -0.53
$19.0 \leq M_{\text{bol}} < 20.0$	44	0.31 ± 0.08	$17.0^{+0.7}_{-1.3}$	22^{+4}_{-6}	1.62	$+0.37$ -0.29	$+0.52$ -0.40
$20.0 \leq M_{\text{bol}} < 21.0$	41	0.15 ± 0.08	12.9 ± 0.6	14^{+3}_{-2}	2.22	$+0.43$ -0.39	$+0.68$ -0.59
$21.0 \leq M_{\text{bol}} < 22.0^b$	22	0.07 ± 0.09	8.5 ± 0.1	5 ± 1	2.85	$+0.57$ -0.65	$+1.71$ -1.14
$22.0 \leq M_{\text{bol}} < 23.0^b$	7	0.02 ± 0.08	8.6 ± 0.1	3 ± 1	1.65	± 0.53	$+1.14$ -0.68
$23.0 \leq M_{\text{bol}} < 24.0^b$	1	0.00 ± 0.02	2.8 ± 0.0	1^{+0}_{-1}	15.92	$+0.00$ -15.92	$+31.85$ -15.92

NOTE—The columns are the same as in Table 3, presented here for bins of 1 bolometric magnitude. d_{lim} , N_{lim} , and space densities were calculated and corrected for incompleteness using the same method as for the spectral type bins in Table 3. The space densities are plotted with Poisson uncertainties in Figure 2.

^aThis bin is incomplete due to our exclusion of M dwarfs from our sample. We do not use this M_{bol} bin in our comparison with synthetic populations (Section 4.5).

^bSpace density is based on $N_{\text{lim}} < 10$ and has large uncertainties. We do not use this M_{bol} bin in our comparison with synthetic populations (Section 4.5).

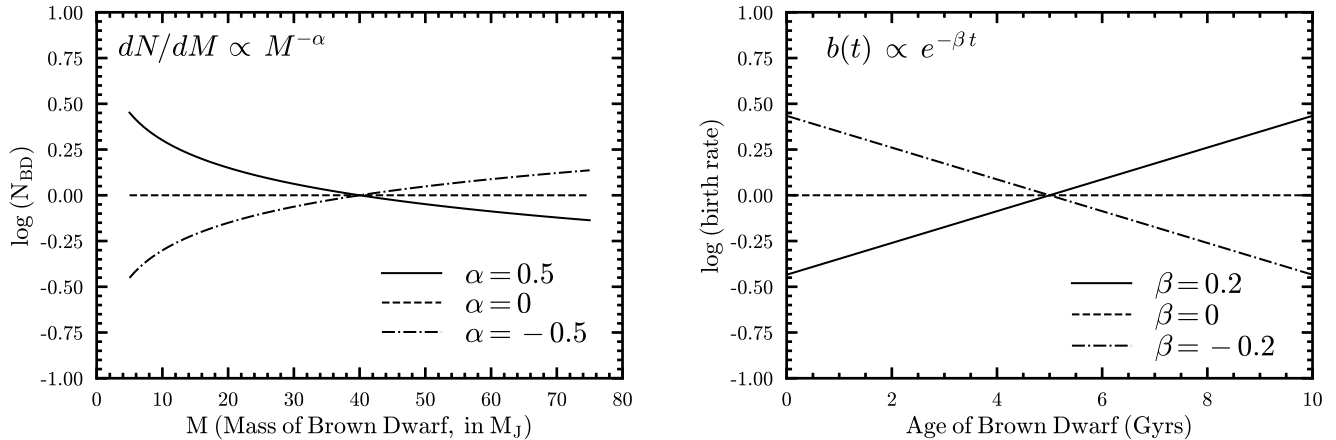


Figure 3. Left: Examples of mass distributions drawn from Kroupa’s power law form of the IMF for $\alpha = \{-0.5, 0, +0.5\}$. Right: Examples of exponential age distributions with $\beta = \{-0.2, 0, +0.2\}$. Both vertical axis scales are arbitrary. Previous ultracool dwarf studies have found estimates spanning $-1 \lesssim \alpha \lesssim 1$ with $\alpha = 0$ corresponding to a uniform mass function, and have typically assumed a uniform age distribution ($\beta = 0$).

T dwarfs and all Y dwarfs. ATMO2020 (Phillips et al. 2020) has an upper mass limit of $0.075 M_{\odot}$, and therefore does not include objects with $M_{\text{bol}} \leq 14$ mag at ages $\gtrsim 1$ Gyr, thus excluding synthetic analogs of the low-mass stars in our volume-limited sample. In addition, ATMO2020 does not incorporate the impact of atmospheric clouds on evolution. The Sonora Bobcat models (Marley et al. 2021) have masses spanning $0.0005 M_{\odot}$ to $0.1 M_{\odot}$ and age range of 0.01 Myr to 20 Gyr but do not incorporate clouds.

4.5. Construction and Comparison of Synthetic Luminosity Functions

We constructed synthetic populations with the same volume and space density as our corrected 25 pc sample (Table 4) of single objects, oversampled by a factor of 1000. We drew masses from the power-law distribution of Equation (3) and ages from the exponential distribution of Equation (4), and used the evolutionary models to interpolate L_{bol} and T_{eff} for each object. We converted the synthetic L_{bol} to M_{bol} and binned synthetic objects into the same 1 mag M_{bol} bins we used for our volume-limited sample (Table 4). Figure 4 shows examples of these synthetic luminosity functions and illustrates the impact of varying the mass distribution (α) on synthetic luminosity functions with the age distribution (β) held constant. Larger values of α generate populations with more low-luminosity objects, since larger α favors lower masses (Figure 3). Figure 5 shows the impact of varying β with α held constant: Larger β similarly results in populations with more low-luminosity objects, since those populations have larger numbers of older objects.

When comparing the synthetic luminosity functions to our volume-limited sample, we did not use the $13 \leq M_{\text{bol}} < 14$ mag bin, which is significantly incomplete in our volume-limited sample due to our exclusion of M dwarfs. We also did not use any objects with $M_{\text{bol}} \geq 21$ mag because our volume-limited sample contains fewer than 10 objects within the completeness distance (d_{lim}) in each of those faint magnitude bins, so the completeness-corrected space densities in those bins have very large uncertainties. The total space density of the seven bins spanning $14 \leq M_{\text{bol}} < 21$ mag is $(1.20^{+0.11}_{-0.10}) \times 10^{-2} \text{ pc}^{-3}$. We normalized the luminosity functions of our synthetic populations to match this.

The SM08 models include masses $0.002 M_{\odot}$ to $0.085 M_{\odot}$ and ages 3 Myr to 10 Gyr, so we could only assign masses and ages to our synthetic objects within these limits. We explored whether this impacted the distribution of $14 \leq M_{\text{bol}} < 21$ mag objects in our synthetic populations. The SM08 model grid includes objects with

$M_{\text{bol}} < 14$ mag at all ages, so the upper mass limit of the models does not encroach on the $M_{\text{bol}} \geq 14$ mag cutoff for our analysis. Objects with mass = $0.002 M_{\odot}$ have synthetic $M_{\text{bol}} \geq 21$ mag for ages ≥ 100 Myr, so the lower mass limit of the models only impacts the faint end of our analysis at young < 100 Myr ages. The COND models have wider mass and age ranges (Section 4.4), so for consistency with our SM08 population synthesis, we only draw masses and ages from the same ranges. Limitations in model parameter space are not a significant issue in our analysis given our wide M_{bol} range.

We constructed a grid of synthetic populations using $-2 \leq \alpha \leq 2$ in steps of 0.02 and $-5 \leq \beta \leq 1.5$ in steps of 0.02. We initially calculated χ^2 for the fit of our volume-limited sample’s luminosity function to that of each synthetic population using our mean and rms for each M_{bol} bin, and we identified a single χ^2 minimum at $(\alpha, \beta) = (-0.04, -0.06)$. However, we also noted significant asymmetry in some of the uncertainties on our volume-limited sample’s M_{bol} bins (Table 4; Figure 2). We therefore sought a method to quantitatively compare our synthetic luminosity functions that did not assume a Gaussian distribution of luminosities in each bin of our volume-limited sample, as is inherent to the χ^2 statistic.

For each bin of M_{bol} , we determined the space density histogram from our Monte Carlo trials (Section 3.5) in bins of 10^{-5} pc^{-3} , and we smoothed these histograms using a boxcar of width $2.5 \times 10^{-4} \text{ pc}^{-3}$ ($\approx 10\%$ of the extent of the 95% confidence intervals for the M_{bol} bins). We normalized each smoothed histogram to a total of 1 and treated these as probability distribution functions (PDFs) for the space densities of the M_{bol} bins in our volume-limited sample. To compare each synthetic luminosity function to our volume-limited sample, we assigned the probability from the corresponding PDF to the synthetic space density in each M_{bol} bin. We took the product of these probabilities for each synthetic luminosity function to be its overall likelihood.

Figure 6 shows the distribution of likelihoods over the (α, β) parameter grid for the synthetic populations based on the SM08 models. We identified a maximum likelihood at $(\alpha, \beta) = (0.16, -0.12)$ (similar to the χ^2 minimum), but also a large range of (α, β) having likelihoods near the maximum. For synthetic populations based on the COND models, we obtained a broadly similar distribution but with a maximum likelihood at $(\alpha, \beta) = (1.02, -1.52)$. The confidence limits for both sets of evolutionary models show that the mass function is constrained only to a broad $-1 \lesssim \alpha \lesssim 1$, which encompasses all previous literature estimates. β is constrained to $\lesssim 0.5$, but can extend to large negative values, implying that our volume-limited sample’s luminos-

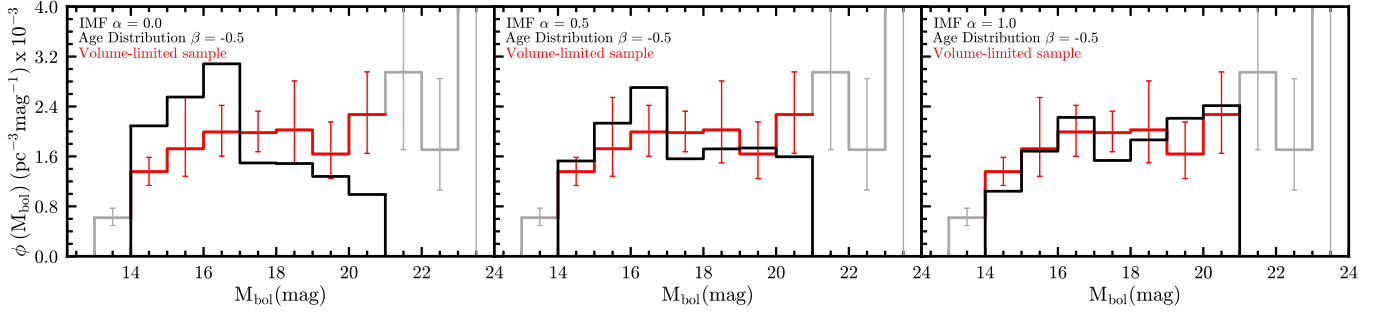


Figure 4. Synthetic bolometric luminosity functions based on power-law IMFs with three representative values of α (black) compared with our volume-limited sample’s luminosity function (red/gray, from Figure 2). The synthetic M_{bol} were derived from the SM08 models and assume an exponential age distribution with $\beta = -0.5$. Increasing α (left to right) leads to populations with more faint objects because larger α favors the creation of more low-mass objects.

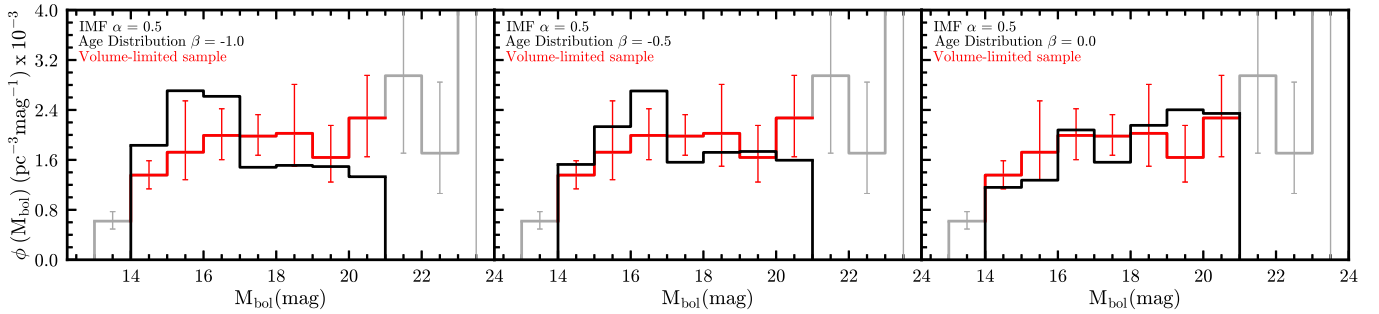


Figure 5. Synthetic bolometric luminosity functions based on exponential age distributions with three representative values of β (black) compared with the luminosity function for our volume-limited sample (red/gray, from Figure 2). The synthetic M_{bol} were derived from the SM08 models and assume a power-law IMF with $\alpha = 0.5$. Increasing β (left to right) leads to populations with more faint objects because larger β favors older objects which have cooled to fainter luminosities.

ity function is consistent with a wide range of age distributions, excluding only very old populations. Plausible fits to the volume-limited sample within the 95% confidence limits extend to $\beta < -5$ where populations have unrealistically young age distributions, i.e., $>40\%$ of objects in the volume-limited sample would have ages less than 200 Myr, and there would be no objects older than ≈ 2 Gyr. Such populations are clearly in conflict with even the limited age constraints from lithium depletion, binaries with measured dynamical masses, and kinematics (e.g., Kirkpatrick et al. 2008; Dupuy & Liu 2017; Hsu et al. 2021).

4.5.1. A Constraint from the Young L0–L7 Fraction

The lack of strong constraints on β from this luminosity function analysis indicates the need for another source of constraint on the age distribution of our volume-limited sample. In Paper I, we identified young objects based on spectroscopic indicators of youth or kinematic association with a young moving group of stars. Here, we focus specifically on L0–L7 dwarfs in our

sample, for which red-optical and near-IR spectroscopic indicators of low surface gravity are available for ages $\lesssim 200$ Myr (Cruz et al. 2009; Allers & Liu 2013; Gagné et al. 2015b; Liu et al. 2016). Our volume-limited sample contains 12 single L0–L7 dwarfs having such indicators of youth. After correcting for incompleteness and Lutz-Kelker bias, 12 young out of 127 single L0–L7 dwarfs represents a fraction of $9.2\%^{+3.0\%}_{-2.6\%}$ in our volume-limited sample. For our analysis, we adopt an age of 0–200 Myr for these objects as suggested by Allers & Liu (2013) and Liu et al. (2016), with the caveat that no well-calibrated age scale has been established for the spectroscopic low gravity indicators. (We discuss plausible age ranges for young L0–L7 dwarfs and their impact on our results in Section 5.2). We note that our young L0–L7 dwarf fraction is consistent with the $7.6\% \pm 1.6\%$ fraction of L dwarfs with ages < 100 Myr found by Kirkpatrick et al. (2008) based on the presence of lithium absorption.

We converted the T_{eff} values for our synthetic population members to spectral types by inverting the SpT–

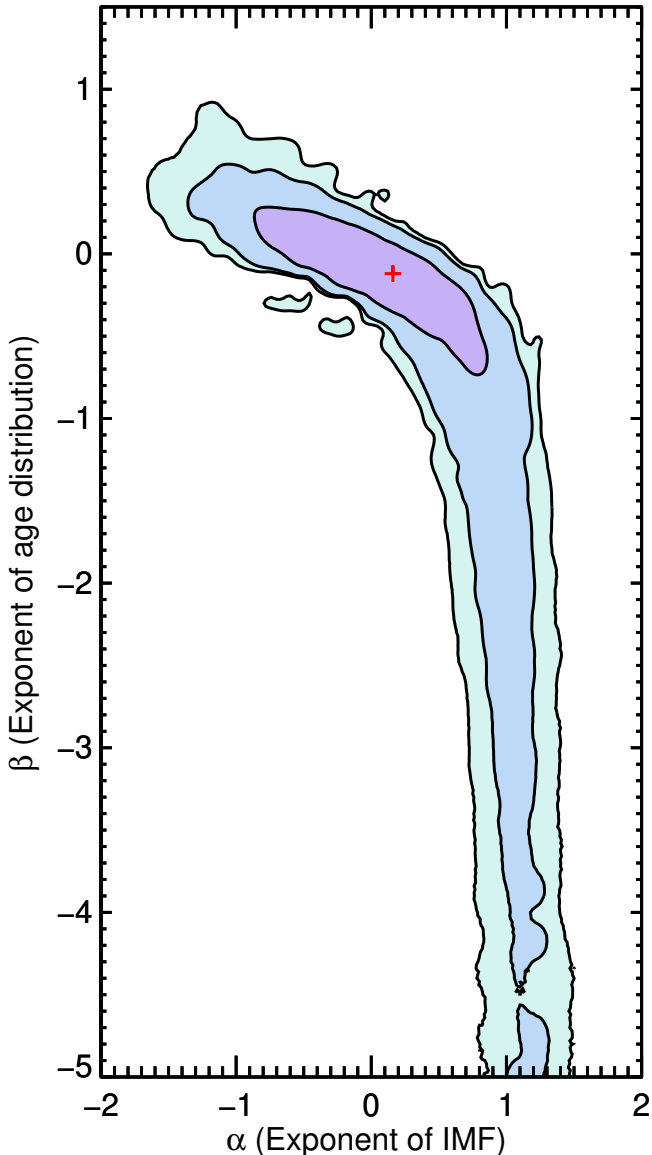


Figure 6. Contour plot (smoothed) of likelihoods for the fits of our volume-limited sample’s luminosity function to those from synthetic populations based on the α (IMF) and β (age distribution) parameters and the SM08 evolutionary models. The red cross at $\alpha = 0.16$ and $\beta = -0.12$ indicates the maximum likelihood. Contours trace the 68.3%, 95.5%, and 99.7% confidence limits. The mass function is constrained only to a broad $-1 \lesssim \alpha \lesssim 1$ range. β is only constrained toward negative values, and plausible (95.5% confidence) fits extend to $\beta < -5$ where populations are unrealistically young. Comparing our luminosity function to synthetic populations cannot by itself produce meaningful constraints for the mass and age distributions.

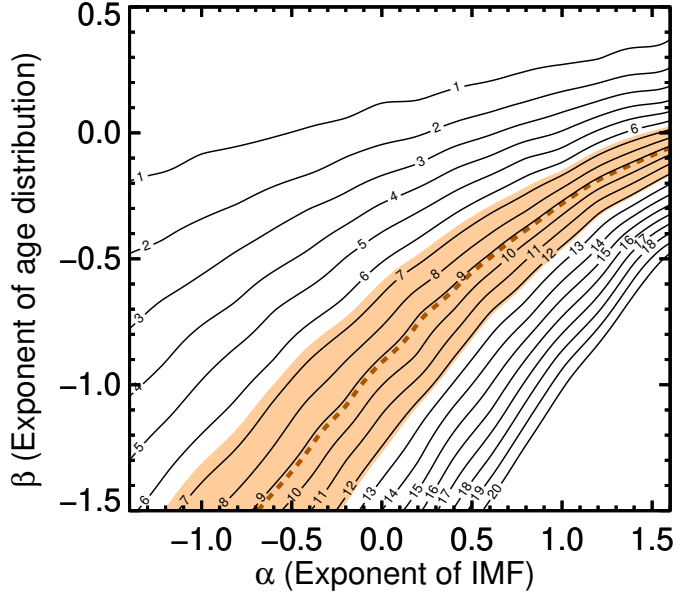


Figure 7. Smoothed contours showing the percentage of single L0–L7 dwarfs in our synthetic populations that are young (< 200 Myr), as a function of the α (mass function) and β (age distribution) parameters. Synthetic populations with a larger percentage of young L0–L7 dwarfs occur for higher α (more lower-mass objects) and lower β (more young objects). The brown dashed contour and shaded region indicate where $9.2\%^{+3.0\%}_{-2.6\%}$ of L0–L7 dwarfs in the synthetic populations are young, corresponding to the percentage measured in our volume-limited sample.

T_{eff} relation of [Stephens et al. \(2009\)](#), identifying objects with synthetic spectral types L0–L7 (specifically, later than M9.75 and earlier than L7.25). We then calculated the percentage of L0–L7 dwarfs with ages less than 200 Myr in each of our synthetic populations. Figure 7 shows these percentages as a contour plot in the same β vs. α space used in Figure 6, but for a narrower, more realistic range of α and β — in particular, setting $-1.5 \leq \beta \leq 0.5$ to exclude implausibly young age distributions. Within this more realistic range, synthetic populations with lower values of β have more young objects and thus naturally have a higher percentage of young L0–L7 dwarfs. Populations with higher values of α also have a higher percentage of young L0–L7 dwarfs because they have more low-mass objects which cool quickly to later spectral types, so the warmer L0–L7 dwarfs that are in the sample are more likely to be young. Figure 7 illustrates that the constraints in (α, β) from the young L0–L7 population are complementary to those from the luminosity function analysis (Figure 6).

Figure 8 combines the (α, β) constraints from the luminosity function analysis, recalculated for the grid used

in Figure 7, with the constraints from the percentage of young L0–L7 dwarfs in our volume-limited sample. The two sets of contours are roughly perpendicular in the (α, β) plane. We multiplied the probability grids from each analysis to combine these two constraints, obtaining the final (α, β) constraints shown in Figure 8. This combined analysis establishes strong constraints on both α and β , which were not possible based on either analysis separately. We then marginalized the combined probability distribution over the (α, β) grid for each parameter to obtain their median values and confidence limits.

5. MASS AND AGE DISTRIBUTION CONSTRAINTS

For the SM08 evolutionary models, we obtained $\alpha = 0.58_{-0.20}^{+0.16}$ and $\beta = -0.44 \pm 0.14$ (median values with 68% confidence limits) with nearly-symmetric posterior distributions (Figures 8 and 9). These are more precise statistical constraints on both parameters than from any previous analysis. The fit of the luminosity function for our volume-limited sample with that of the synthetic population generated using $\alpha = 0.58$ and $\beta = -0.44$ yields $\chi^2 = 10.8$ for 4 degrees of freedom.

Repeating the steps outlined in Section 4.5 but using the COND evolutionary models instead of SM08, we obtained $\alpha = 0.50 \pm 0.16$ and $\beta = -0.58 \pm 0.16$, again from near-symmetric posteriors (Figures 9 and 10). These values are consistent with those found using the SM08 models, with the corresponding synthetic luminosity function providing a fit with $\chi^2 = 7.2$ (4 degrees of freedom). The similarity in the α and β posteriors indicates that the choice of evolutionary model does not significantly impact our analysis, as the young L0–L7 fraction constraint exerts a strong influence.

Our sample includes 57 objects that have only photometric distances from K21 (no parallaxes; Section 2.1). We explored whether the bolometric luminosities we calculated for these objects could be systematically impacting our population synthesis results. We repeated our analysis using the SM08 models but excluding these objects, and obtained nearly identical contours, medians, and confidence limits for α and β . This perhaps surprising result is a consequence of our method of correcting for incompleteness (Section 3.3, which effectively discards objects beyond the largest distance at which a sample or subsample is complete (d_{lim}) from our population analysis. These 57 objects without parallaxes are almost all farther away than the completeness distances for their respective bolometric magnitude bins, so removing them from our sample had little impact on our calculations.

5.1. Best-fit Synthetic Luminosity Functions

Figure 11 shows the synthetic luminosity function based on the SM08 and COND models for our respective best-fit α and β . The SM08 luminosity function is reasonably consistent with that of our volume-limited sample, but we note one apparent difference. The models predict a peak in the luminosity function at $M_{\text{bol}} = 16$ –17 mag and a deficit at 17–18 mag. SM08 ascribe this feature to a release of entropy as brown dwarfs lose the clouds from their photospheres in the transition from L to T dwarfs, causing the objects to temporarily slow their rate of cooling at $M_{\text{bol}} \approx 16$ –17 mag followed by a more rapid decline. This scenario is supported by binaries with dynamically-determined masses, whose mass-luminosity relation is better matched to the SM08 “hybrid” models than to cloudless models (Dupuy et al. 2015b; Dupuy & Liu 2017). Our volume-limited sample’s luminosity function is essentially flat across $M_{\text{bol}} = 15$ –21 mag and does not appear to reflect this predicted slowdown in cooling, although the difference is not strongly significant; our M_{bol} bins differ from the SM08 luminosity function by 1.5σ and 1.4σ in the $M_{\text{bol}} = 16$ –17 mag and 17–18 mag bins, respectively. One possible explanation for the difference is that the transition from cloudy to cloudless objects occurs at lower temperatures in younger, lower-gravity brown dwarfs; this could wash out the luminosity peak seen in the SM08 models (e.g., Metchev & Hillenbrand 2006; Liu et al. 2016), in which the transition occurs over the same T_{eff} range for all objects.

The COND-based synthetic luminosity function (Figure 11) appears more closely matched to our volume-limited sample, especially over the $M_{\text{bol}} = 15$ –20 mag range, and does not show a peak/deficit or other feature that indicates an impact from the L/T transition cloud clearing on bolometric luminosity. This is expected from the cloudless COND models, but is more surprising in our volume-limited sample that contains many L/T transition objects which are expected to be in various stages of cloud-clearing. Future evolutionary models that provide a better accounting for the effects of clouds may shed more light on the impact of L/T transition cloud-clearing on the luminosity function. Alternatives to a single power-law mass function and/or an exponential age distribution may also better represent the local ultracool dwarf population.

For subsequent discussion, we adopt the values of α and β we obtained using the SM08 models because those models better represent the properties of our L0–Y2 sample due to the inclusion of clouds for L dwarfs.

5.2. Ages of Young L0–L7 Dwarfs

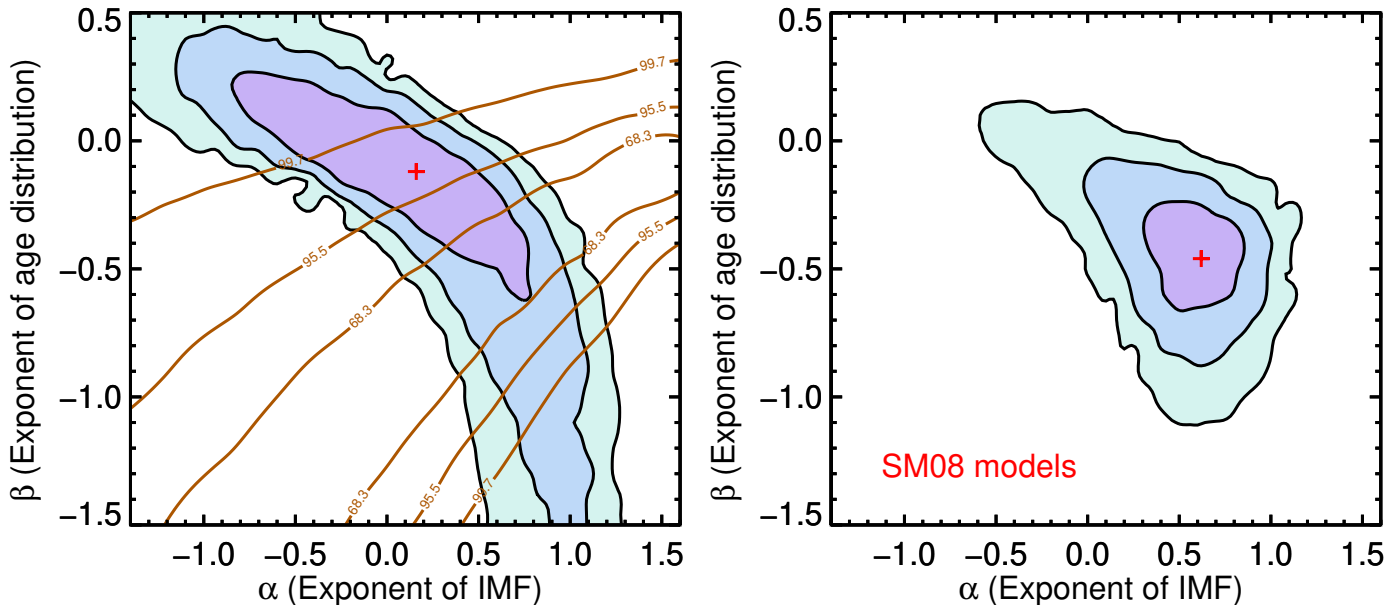


Figure 8. *Left:* Constraints on the α (mass function) and β (age distribution) parameters from our luminosity function analysis using the SM08 evolutionary models, calculated for the same (α, β) grid as in Figure 7. The red cross indicates the likelihood maximum. The overlaid brown 68.3% (1σ), 95.5% (2σ), and 99.7% (3σ) contours represent the $9.2^{+3.0}_{-2.6}\%$ fraction of single young L0–L7 dwarfs in our volume limited sample (shown in Figure 7). *Right:* Product of the probability distributions from the luminosity function and young L0–L7 fraction analyses, with contours showing the 68.3%, 95.5%, and 99.7% confidence limits, and a maximum likelihood at $\alpha = 0.58^{+0.16}_{-0.20}$ and $\beta = -0.44 \pm 0.14$. The intersection of the luminosity function and young L0–L7 fraction constraints provides a much stronger joint constraint on α and β than either analysis alone, thereby yielding the strongest statistical constraints to date on the mass and age distributions of nearby L0–Y2 dwarfs.

In our analysis, the choice of evolutionary models does not have a major impact on our results because the fraction of young L0–L7 dwarfs provides a powerful and complementary constraint for the mass and age distributions. However, the usefulness of the young L0–L7 dwarf fraction is determined by our ability to identify such objects in our volume-limited sample, estimate their ages, and understand the completeness of our young single L0–L7 dwarf sample. The objects in our sample have mostly been vetted for low-gravity spectroscopic signatures in the literature: Of the 127 single L0–L7 dwarfs (optical or NIR spectral types) in our volume-limited sample, 109 (86%) have an optical or NIR spectroscopic surface gravity classification. None of the remaining 18 have other indications of youth, e.g., kinematic association with a young moving group, so our young single L0–L7 dwarf sample is likely to be complete. We assume these 18 objects are not young, so our $9.2^{+3.0}_{-2.6}\%$ young single L0–L7 dwarf fraction (Section 4.5.1) is technically a lower limit. The identification of more young single L0–L7 dwarfs in our sample would lead to our population analysis finding a more positive α and more negative β , further reinforcing the major trends of our results.

However, the ages corresponding to such low-gravity signatures are not well established⁴. The $\lesssim 200$ Myr age limit for objects with low-gravity signatures quoted by Allers & Liu (2013) and Liu et al. (2016) derives from the ages of young moving groups, which have significant uncertainties at the older end where low-gravity signatures are weak and fewer such groups have been identified (e.g., Gagné et al. 2018). We explored the uncertainty in this 200 Myr limit by considering the ages of moving groups whose members have weaker low-gravity features. For example, the majority of members of the AB Doradus Moving Group (ABDMG; Zuckerman et al. 2004) with spectroscopic gravity classifications have intermediate INT-G spectra (e.g., Liu et al. 2016), and the 149^{+51}_{-19} Myr age of ABDMG (Bell et al. 2015) has 3σ limits spanning ≈ 100 –300 Myr. The Carina-Near Moving Group (CARN; Zuckerman et al. 2006), age

⁴ We note also that two objects we identify as young in our volume-limited sample, 2MASS J00332386–1521309 and 2MASS J10224821+5825453, have optical gravity class β indicating moderately low gravity (Cruz et al. 2009) but kinematics indicating possible membership in the Galactic thick disk (Gonzales et al. 2019), which suggests a much older age.

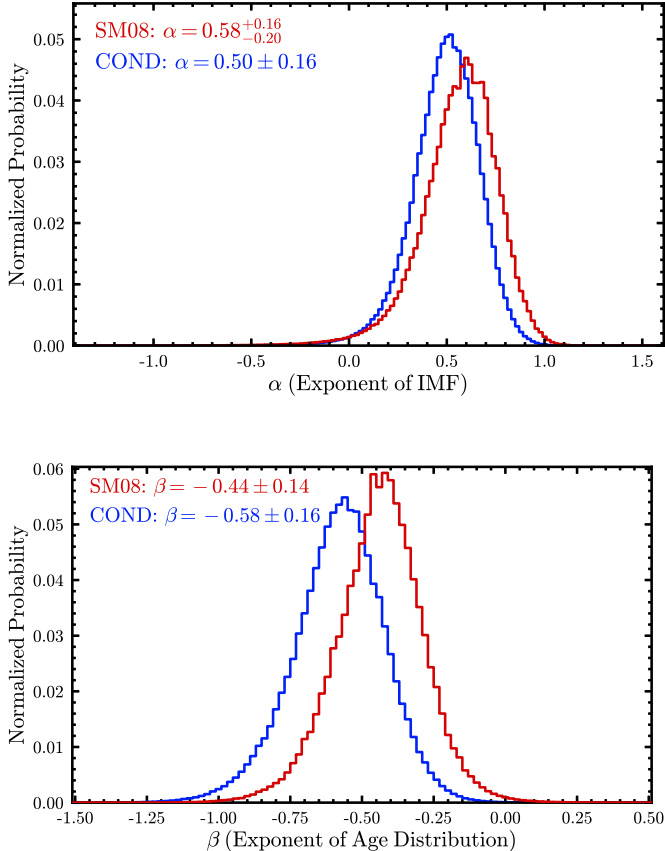


Figure 9. Probability distribution functions (PDFs) for the α (mass function, *top*) and β (age distribution, *bottom*) parameters marginalized from the combined probability distributions shown in Figures 8 and 10, using the SM08 (red) and COND (blue) evolutionary models, respectively. The median and 68% confidence limits are shown at upper left in both plots. Both parameters are well constrained, and the significant overlap in the PDFs for each parameter confirm that the choice of evolutionary model does not significantly impact our results.

200 ± 50 Myr, has L0–L7 dwarfs with both INT-G and FLD-G (field-age gravity) but no VL-G (very low-gravity) classifications (UltracoolSheet, version 2.0.0, in preparation), and its 2σ age range spans 100–300 Myr.

We therefore re-ran our analysis using age limits spanning 100–300 Myr for the young L0–L7 dwarfs. This yielded parameters in the ranges $0.36 \leq \alpha \leq 0.88$ for the mass function and $-0.98 \leq \beta \leq -0.26$ for the age distribution, with younger age limits corresponding to higher values of α and lower values of β , i.e., lower-mass and younger populations. These ranges are somewhat broader than the 68% confidence limits for the 200 Myr young L0–L7 age limit, but they extend the plausible intervals almost exclusively toward higher values of α and

lower values of β . This firmly reinforces that α is positive and β is negative, pointing to a young and low-mass brown dwarf population in the Solar neighborhood.

5.3. The Apparent Peak of the Mass Function

Many studies of the stellar IMF have found that it reaches a single maximum at ≈ 0.2 – $0.3 M_{\odot}$ (Bastian et al. 2010, and references therein). Our finding of a positive value for α , indicating an increase in numbers toward lower masses over the 0.002 – $0.085 M_{\odot}$ range of our analysis, may appear to be inconsistent with the oft-cited stellar IMF peak. We clarify that this peak is seen using log-normal forms of the mass function, or broken power law forms that parameterize the distribution of $\log(\text{mass})$. Our analysis, and all analyses of the substellar mass function that use the form in Equation 3, parameterize the mass distribution in linear space, in which masses above the substellar regime are far more spread out. A mass function with $\alpha < 1$ would appear in $\log(\text{mass})$ space to decline toward lower masses, even though it rises in linear mass space. Our result is therefore not inconsistent with the log-normal IMF peak at low stellar masses. In the linear-mass power-law parameterization of Equation 3, the peak of the mass function may in fact be at its extreme low-mass cutoff, which we discuss in Section 6.2.1.

6. COMPARISON WITH PREVIOUS WORK

6.1. Nearby Ultracool Dwarfs

Previous modeling of the local ultracool population has produced relatively loose constraints on the IMF (Table 5). Our $\alpha = 0.58^{+0.16}_{-0.20}$ is consistent with the estimates from the pioneering works of Kroupa (2001, $\alpha = 0.3 \pm 0.7$) and Allen et al. (2005, $\alpha = 0.3 \pm 0.6$), although neither of these works constrain the age distribution. Our α is notably higher (indicating an IMF with more lower-mass objects) than the $\alpha \approx 0$ estimate of Metchev et al. (2008), based on T dwarf space density measurements that are consistent with ours but derived from a less complete sample, in particular for later-T dwarfs. Our α disagrees even more strongly with several studies that estimated $-1 < \alpha < 0$ by visually comparing modeled space densities or luminosity functions to the space densities of late-M to late-T dwarfs or subsets thereof (Pinfield et al. 2008; Reylé et al. 2010; Kirkpatrick et al. 2012; Day-Jones et al. 2013; Burningham et al. 2013). These studies relied on smaller and usually magnitude-limited samples which produced larger uncertainties on their space densities and luminosity functions than we have obtained with our 25 pc parallax-based sample, and did not fit for the age distribution of sample members. All of these previous results are

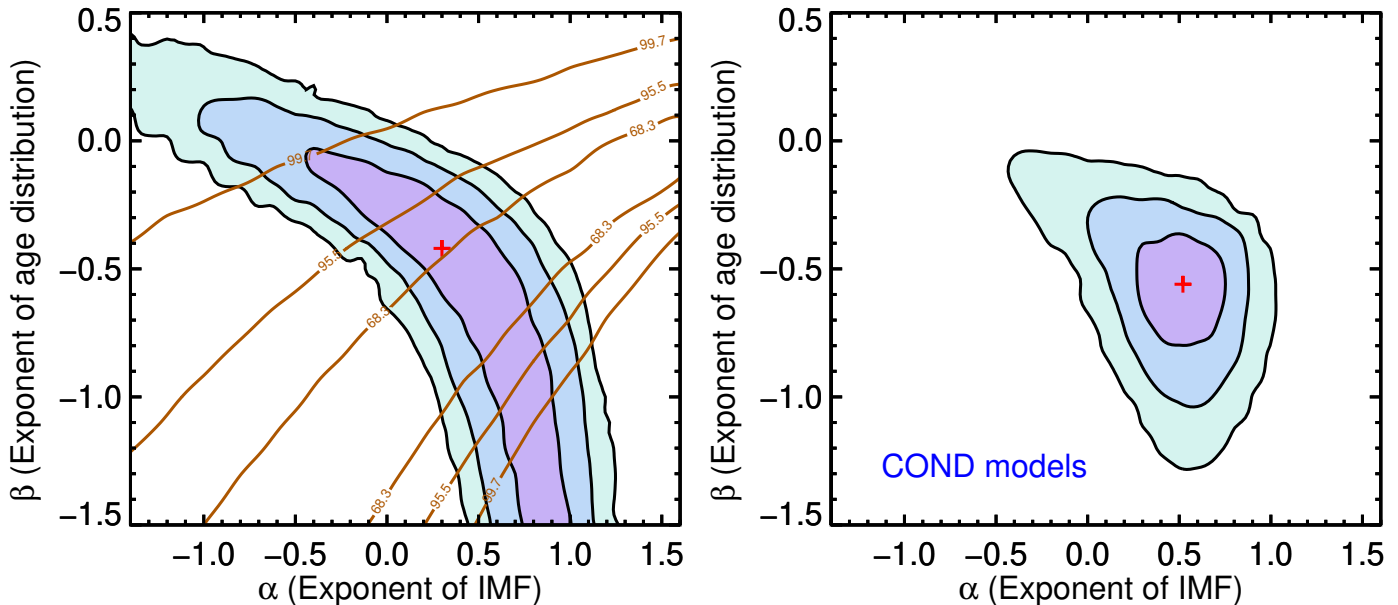


Figure 10. Same as Figure 8, but using the COND evolutionary models, resulting in constraints of $\alpha = 0.50 \pm 0.16$ and $\beta = -0.58 \pm 0.16$. The contours and median parameter values are consistent with those found using the SM08 models, indicating that the choice of evolutionary model does not significantly impact our analysis.

consistent with the broad α distribution we found using only the luminosity function of our volume-limited sample (Figure 6); the inclusion of the young L0–L7 dwarf fraction in our analysis is key to constraining the mass distribution to positive values of α (Figures 8 and 10). We note that if we impose a flat age distribution (i.e., $\beta = 0$) on our analysis, as do two of the above studies, we find a maximum likelihood of $\alpha = -0.06_{-0.28}^{+0.26}$, which is consistent with all of the above results for α . However, the flat age distribution is clearly disfavored by our analysis (Figure 9).

Previous efforts have produced very few constraints on the age distribution of ultracool dwarfs (Table 5), with some of those works simply assuming that brown dwarfs have been forming at a constant rate since the birth of the Galaxy ~ 10 Gyr ago. Allen et al. (2005) demonstrated that evolutionary models predict systematic differences in the age distributions of ultracool spectral types, with late-L dwarfs being the youngest group overall, but found that their observed luminosity function was unable to sufficiently distinguish between increasing, constant, and decreasing birthrates for nearby ultracool dwarfs. Day-Jones et al. (2013) and Marocco et al. (2015) were able to exclude age distributions strongly favoring old objects using L0–T8 magnitude-limited samples, but did not directly fit for β or a similar parameter. The only previous study that calculated an age distribution, using the same exponential model

that we use, found $\beta = -0.13 \pm 0.17$ for masses between 0.072 and 0.1 M_{\odot} (early-L and late-M dwarfs; Deacon & Hambly 2006), based on a sample of 55 objects. Our value of $\beta = -0.44 \pm 0.14$, based on our much larger volume-limited sample and — crucially — including constraints from the fraction of young L0–L7 dwarfs, implies a clearly younger population of L and T dwarfs. Figure 12 demonstrates the inconsistency of our result with a uniform age distribution.

6.1.1. Galactic Dynamics

We note that our age distribution is qualitatively consistent with the age distribution found by Dupuy & Liu (2017) based on dynamical masses of late-M to mid-T binaries (Figure 12). That distribution also skews toward younger objects: They found a median age of 1.3 Gyr, with a 90% confidence interval of 0.4–4.2 Gyr. They highlight the fact that galactic dynamics excite objects out of the Galactic midplane over time (e.g., Robin et al. 2003; Mackereth et al. 2019) and thereby deplete the solar neighborhood of older objects. The skew towards young objects in our volume-limited ultracool sample may therefore be as much a reflection of this dynamical heating as it is the underlying birth history of the L and T dwarfs in the sample.

We note also that as dynamical heating removes objects from the Galactic midplane, the remaining mass distribution may be impacted as well, a scenario that has not been addressed to date. Further modeling of ul-

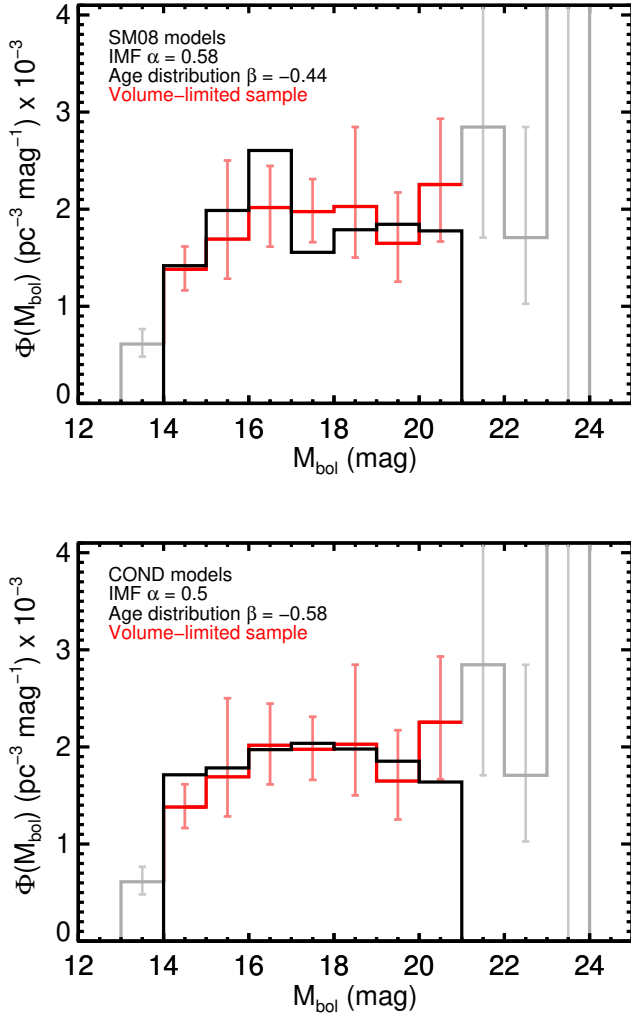


Figure 11. *Top:* Our 25 pc luminosity function (red/gray) overlaid with the best-fit luminosity function (black) from a synthetic population based on the SM08 hybrid models with IMF $dN/dM \propto M^{0.58}$ and age distribution $b(t) \propto e^{-0.44t}$. The bins with $M_{\text{bol}} < 14$ mag and $M_{\text{bol}} > 21$ mag (gray) were not used in our analysis. *Bottom:* Same as top, but showing the best-fit luminosity function from a synthetic population based on the COND models, with IMF $dN/dM \propto M^{0.50}$ and age distribution $b(t) \propto e^{-0.58t}$. The COND-based synthetic luminosity functions match that of our volume-limited sample better overall, in particular across the L/T transition ($M_{\text{bol}} \approx 15\text{--}17$ mag).

tracool dwarfs in the Galactic thin disk, thick disk and halo populations (e.g., [Aganze et al. 2022](#)) is needed to establish whether dynamical heating has altered the ultracool mass distribution of the solar neighborhood.

6.2. [Kirkpatrick et al. \(2021\)](#)

K21 published the most recent effort to determine the mass function of ultracool dwarfs in the solar neighbor-

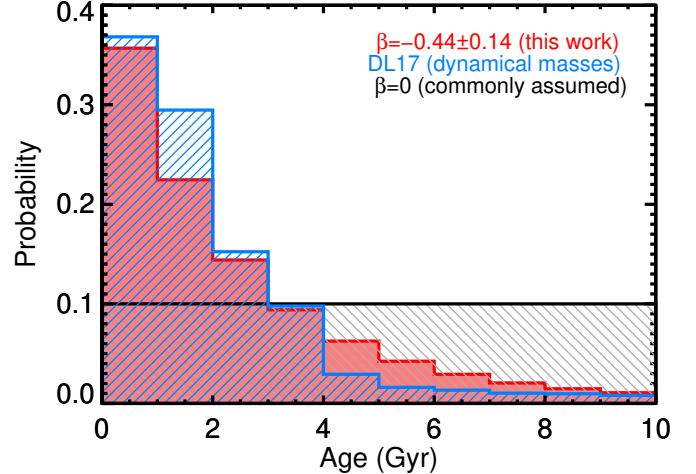


Figure 12. Distribution of ages for our best-fit exponential age distribution $\beta = -0.44 \pm 0.14$ (red), marginalized over the uncertainty on β . Our age distribution is clearly inconsistent with the uniform age distribution (black) assumed by many previous works, including the recent analysis by K21. Our result is more consistent with the age distribution found by [Dupuy & Liu \(2017\)](#) using dynamical masses of late-M to mid-T binaries.

hood. They based their analysis on a volume-limited sample of L, T, and Y dwarfs that they describe as complete for $T_{\text{eff}} \geq 600$ K (spectral types $\lesssim T8$), drawing upon the same set of parallaxes as our sample. K21 arrived at $\alpha = 0.6 \pm 0.1$, so in many ways our works appear to be similar. However, the K21 sample construction and analysis differ from ours in several important ways. We describe these differences in detail.

- The K21 sample covers the full sky but is volume-limited at 20 pc, making theirs a wider but shallower survey that encompasses a 25% smaller volume of space than ours. In contrast, our sample extends to 25 pc but only includes declinations $-30^\circ \leq \delta \leq +60^\circ$ (68% of the sky). We chose these declination boundaries because this is the part of the sky that has been thoroughly searched for all spectral types $\leq T8$. In particular, the optical PS1 survey proved to be essential for constructing complete samples of L/T transition dwarfs ([Best et al. 2015, 2020](#)), and PS1 has a southern limit of $\delta = -30^\circ$. There has been no complete survey for L/T transition objects outside of the PS1 footprint because the JHK bands of NIR surveys such as 2MASS cannot distinguish L/T transition dwarfs from background M dwarfs (e.g., [Reid et al. 2008](#)), and the $YJHK$ UKIDSS survey ([Lawrence et al. 2007](#)) and optical SDSS survey

Table 5. Previous Estimates of Mass Function Exponent α and Age Distribution Exponent β

Source	Region	Range	Mass Function	Age Distribution
Alves de Oliveira et al. (2013)	ρ Ophiuchus	Mass: 5–80 M_{Jup}	$\alpha = 0.7 \pm 0.3$	≈ 1 Myr
Da Rio et al. (2012)	Orion Nebula Cluster	Mass: 0.03–0.29 M_{\odot}	$\alpha = 0.6 \pm 0.33$	≈ 1 –3 Myr
Gennaro & Robberto (2020)	Orion Nebula Cluster	Mass: 0.005–0.16 M_{\odot}	$\alpha = 0.58 \pm 0.06$	≈ 1 –3 Myr
Alves de Oliveira et al. (2013)	IC 348	Mass: 13–80 M_{Jup}	$\alpha = 1.0 \pm 0.3$	≈ 3 Myr
Peña Ramírez et al. (2012)	σ Orionis	Mass: 0.006–0.35 M_{\odot}	$\alpha = 0.6 \pm 0.2$	≈ 3 Myr
Damian et al. (2023)	σ Orionis	Mass: 0.004–0.19 M_{\odot}	$\alpha = 0.18 \pm 0.19$	≈ 2 –4 Myr
Lodieu et al. (2007a)	Upper Scorpius	Mass: 0.01–0.3 M_{\odot}	$\alpha = 0.6 \pm 0.1$	≈ 5 Myr
Casewell et al. (2007)	Pleiades	Mass: ≈ 0.015 –0.065 M_{\odot}	$\alpha = 0.62 \pm 0.14$	≈ 120 Myr
Kroupa (2001)	Solar neighborhood	Mass: 0.01–0.08 M_{\odot}	$\alpha = 0.3 \pm 0.7$	no constraint
Allen et al. (2005)	Solar neighborhood	Mass: 0.04–0.1 M_{\odot}	$\alpha = 0.3 \pm 0.6$	no constraint
Deacon & Hambly (2006)	Solar neighborhood	Mass: 0.072–0.1 M_{\odot}	$\alpha = 0.95 \pm 1.17$	$\beta = -0.13 \pm 0.17$
Pinfield et al. (2008)	Solar neighborhood	SpT: T4–T8.5	$-1 < \alpha < -0.5$	no constraint
Metchev et al. (2008)	Solar neighborhood	SpT: T0–T8	$\alpha \approx 0$	no constraint
Reylé et al. (2010)	Solar neighborhood	SpT: L5–T8	$\alpha \lesssim 0$	no constraint
Kirkpatrick et al. (2012)	Solar neighborhood	SpT: T6–Y1	$-0.5 < \alpha < 0$	assumed $\beta = 0$
Day-Jones et al. (2013)	Solar neighborhood	SpT: L4–T4.5	$-1 < \alpha < 0$	$\beta \lesssim 0.5$
Burningham et al. (2013)	Solar neighborhood	SpT: T6–T8.5	$-1 < \alpha < -0.5$	assumed $\beta = 0$
K21	Solar neighborhood	SpT: L0–Y2	$\alpha = 0.6 \pm 0.1^a$	assumed $\beta = 0$
This work (SM08 models) ^b	Solar neighborhood	SpT: L0–Y2	$\alpha = 0.58^{+0.16}_{-0.20}$	$\beta = -0.44 \pm 0.14$
This work (COND models)	Solar neighborhood	SpT: L0–Y2	$\alpha = 0.50 \pm 0.16$	$\beta = -0.58 \pm 0.16$

NOTE—This table lists representative constraints on the exponent α of a power-law IMF ($\Psi(M) \propto M^{-\alpha}$) and the exponent β of an exponential age distribution ($b(t) \propto e^{-\beta t}$) from the literature, along with our results at the bottom. The results from nearby clusters listed at the top show a selection with representative values of α from studies that used a power-law IMF. For solar neighborhood studies, only Deacon & Hambly (2006) and this work obtain a measurement for the age distribution; other work assumes a flat age distribution or obtains no significant constraint.

^aUncertainty is an estimate based on the similarity of χ^2 for $\alpha = \{0.5, 0.6, 0.7\}$ from a comparison of their T_{eff} function to synthetic populations.

^bWe adopt these constraints on the mass and age distribution for our discussion in Section 6.

only observed a subset of the PS1 footprint. If the spatial distribution of ultracool dwarfs within 25 pc of the Sun is significantly non-uniform (contrary to our assumption), our space density measurements could be impacted since our sample does not cover the whole sky, but no confirmed evidence of this has been found to date (Kirkpatrick et al. 2019, Paper I).

- K21 included the resolved components of known binaries as distinct objects in their sample, whereas we excluded binaries in order to avoid mixing the potentially different mass distributions and formation histories of binaries with those of single ultracool dwarfs (Section 3.5). The K21 sample therefore contains more objects (525) even though it encompasses a 25% smaller volume of space than our 25 pc sample (504 objects).

- K21 demonstrated that 150 K wide T_{eff} bins of their sample are statistically consistent with completeness for $T_{\text{eff}} \geq 600$ K. However, the $\langle V/V_{\text{max}} \rangle$ statistic indicates that their sample taken as a whole is $\approx 90\%$ complete for such objects, and only $\approx 80\%$ complete south of declination -30° , where fewer searches and follow-up observations have occurred. K21 also apply 5–13% corrections for incompleteness in the Galactic plane when calculating space densities. In contrast, we have calculated space densities only from volumes within our sample that are confirmed to be complete by the $\langle V/V_{\text{max}} \rangle$ statistic (Section 3.3). Our space densities are therefore based on smaller but more robustly complete samples.
- K21 constrain the mass function underlying their volume-limited sample using a population synthe-

sis approach that is similar to ours, but with a few key differences. Notably, K21 draw ages for their synthetic populations from a uniform 0–10 Gyr distribution. This has been common practice in ultracool population studies, but we show it is inconsistent with the space density of young L dwarfs in the solar neighborhood (Section 4.5.1; Figure 7) and our subsequent finding that the overall age distribution clearly favors younger objects (Section 5; Figure 12).

- Rather than using a luminosity function as we do, K21 conduct their analysis using the T_{eff} function of their sample, with temperatures derived mostly from literature studies and H -band photometry, and compare this to synthetic populations to constrain the IMF. They argue that determination of the bolometric luminosities for their sample should wait until more objects have broad spectral energy distribution measurements, in particular for the late-T and Y dwarfs. However, the T_{eff} vs. M_H relation from Filippazzo et al. (2015, hereinafter F15) used by K21 for most objects with spectral types $\leq T8$ is itself based on L_{bol} values calculated by F15. The F15 T_{eff} values were also derived from averaging T_{eff} at ages 0.5 and 10 Gyr for all objects except those identified as members of young moving groups and clusters, reinforcing K21’s assumption of a flat age distribution⁵. In the end, both K21’s and our analyses use polynomial relations based on F15’s bolometric luminosities for most of the objects in our samples to constrain the population properties. Our choice to use bolometric luminosities provides a less biased representation of the sample because they do not require an age assumption. In addition, our M_{bol} uncertainties are small (≈ 0.1 – 0.2 mag) relative to the 1 mag bin size of our luminosity function, whereas the K21 T_{eff} uncertainties (mostly 79 K or 88 K) are usually $>50\%$ of their 150 K bin size. We also recognize that both studies use several alternative methods to determine L_{bol} or T_{eff} for the small minority of sources that do not have the data necessary to use relations based on F15’s L_{bol} , which could create inhomogeneities in the L_{bol} and T_{eff} distributions used in population synthesis. This can best be ad-

ressed by more direct measurements of L_{bol} and T_{eff} .

- K21 allow the space density of their synthetic populations to be a free parameter when fitting their synthetic T_{eff} functions to their volume-limited sample, whereas we fix our synthetic population space density to the value measured from our volume-limited sample. K21’s fits therefore have an additional degree of freedom, but their best-match synthetic population may have a space density that is inconsistent with their volume-limited sample.

Despite these differences in our sample construction and analyses, K21 derive space densities for spectral subtype bins with similar precision to ours, and obtain a similar constraint on the exponent of a power-law IMF: $\alpha = 0.6 \pm 0.1$, with their quoted uncertainty representing that the χ^2 for their T_{eff} function fit differs little for $\alpha \in \{0.5, 0.6, 0.7\}$. However, the apparent agreement of our $\alpha = 0.58^{+0.16}_{-0.20}$ with K21’s result is in fact misleading given the clear disagreement in our age distributions. Formally, the constant age distribution (i.e., $\beta = 0$) assumed by K21 is 3.1σ different from our result. If we were to also assume $\beta = 0$, we would find $\alpha = -0.06^{+0.26}_{-0.28}$ to be most likely, but this is 2.4σ different from the $\alpha = 0.58^{+0.16}_{-0.20}$ and $\beta = -0.44 \pm 0.14$ we find in our full analysis (Figure 8), and 2.4σ different from the K21 value. It is not clear what difference(s) between our analyses could lead to such similar values for α despite the discrepant age distributions. No one difference is an obvious culprit, so it may be a combination of multiple factors.

K21 favor the SM08 hybrid models over the COND models, largely because they find an excellent match between their T_{eff} distribution and that of SM08, in particular at the pile-up in T_{eff} in the L/T transition which we do not see reflected in our luminosity function. This discrepancy would suggest that the SM08 models have correctly predicted a T_{eff} pile-up but incorrectly predicted an L_{bol} pile-up in the L/T transition. However, such a situation is physically contradictory for objects in which cloud-clearing is releasing trapped entropy. If these objects experience slower declines in T_{eff} , causing the pile-up, then we should also see slower declines in L_{bol} .

6.2.1. The Low-Mass Cutoff

K21 explore one feature of their sample that we do not: the low-mass cutoff of the local brown dwarf population. K21 model this as a sharp cutoff at three possible masses: 10, 5, and 1 M_{Jup} , but are unable

⁵ Formally, this is different from the 0–10 Gyr distribution used by K21 for their synthetic populations, so their analysis is not internally consistent, with the largest difference for objects younger than 0.5 Gyr.

to obtain a constraint, finding that the best fits to their T_{eff} function do not depend strongly on the cutoff value. They note that more accurate measurements of the space density in their lowest two T_{eff} bins (spanning 150–450 K) will enable a constraint on the low-mass cutoff. The IMF constraint that we have found, like that found by K21, predicts an increase in the number of objects as mass decreases, so a cutoff is needed to avoid generating populations dominated by extremely low-mass objects. In our analysis, the minimum mass was implicitly set by the lowest mass in the SM08 model grid ($0.002 M_{\odot}$). However, since objects at the faint end of the luminosity range we used for our population synthesis ($M_{\text{bol}} = 21$ mag) have higher masses at ages ≥ 100 Myr — as much as $0.026 M_{\odot}$ at 10 Gyr — our analysis is not sensitive to the low-mass cutoff. At present, the best available constraint is that the minimum brown dwarf mass cannot be greater than the $\approx 5 M_{\text{Jup}}$ of the known free-floating planetary-mass brown dwarfs in nearby star-forming regions (e.g., Luhman et al. 2009; Best et al. 2017; Zhang et al. 2021; Damian et al. 2023).

6.3. Star-forming Regions

Studies of star-forming regions and young clusters that estimate power-law IMFs have mostly found $0 < \alpha < 1$, with constraints tending toward the higher end of that range (Table 5; see also, e.g., Moraux et al. 2003; Scholz et al. 2013; Gennaro & Robberto 2020). Our $\alpha = 0.58^{+0.16}_{-0.20}$ therefore generally agrees with the IMF of nearby star-forming regions. This is consistent with a low-mass IMF that has not changed appreciably over the history of our Galaxy, and with galactic dynamics that have not significantly altered the ultracool mass function of the Solar neighborhood.

7. SUMMARY

We have updated the volume-limited sample of L and T dwarfs from Best et al. (2021, Paper I), expanding it to include L0–Y2 dwarfs and adding recent discoveries and parallax measurements. The sample now contains 504 members, covers 68.3% of the sky ($\delta = -30^{\circ}$ to $+60^{\circ}$), extends to 25 pc, and is defined by parallaxes for 85% of the sample, the exception being objects (mostly late-T and Y dwarfs) identified by K21 as brown dwarfs having photometric distances within 25 pc. Our sample is $\approx 78\%$ complete overall but is $\approx 92\%$ complete for spectral types L0–T4, indicating near-completeness through the L/T transition out to 25 pc. We corrected for incompleteness using the $\langle V/V_{\text{max}} \rangle$ statistic to identify the maximum distance at which our sample is statistically complete. We included an additional correction

for Lutz-Kelker bias, although we found it did not significantly impact our results. We calculated a space density of $(1.83^{+0.16}_{-0.15}) \times 10^{-2} \text{ pc}^{-3}$ for our volume-limited sample of L0–Y2 dwarfs, ≈ 20 – 80% larger than many previous estimates but consistent with that of K21.

We calculated bolometric luminosities and present a completeness-corrected luminosity function for single objects in our volume-limited sample. We used our luminosity function in combination with the fraction of young single L0–L7 dwarfs in our sample and synthetic populations based on SM08 and COND evolutionary models to simultaneously constrain the mass and age distributions of single brown dwarfs in the solar neighborhood. The luminosity function and young L0–L7 dwarf fraction offered complementary constraints in our analysis, the latter being essential for obtaining a meaningful age distribution constraint. For a power-law mass function ($\Psi(M) \propto M^{-\alpha}$) and exponential age distribution ($b(t) \propto e^{-\beta t}$), we find $\alpha = 0.58^{+0.16}_{-0.20}$ and $\beta = -0.44 \pm 0.14$ using the SM08 models, and we find $\alpha = 0.50 \pm 0.16$ and $\beta = -0.58 \pm 0.16$ using the COND models.

Our analysis used an age of 0–200 Myr for the young L0–L7 dwarfs, based on spectroscopic low-gravity features and membership in young moving groups, whose maximum ages are not precisely known. Alternate analyses using a wide range of 100 to 300 Myr for the maximum young L0–L7 dwarf age resulted in parameters spanning $0.36 \leq \alpha \leq 0.88$ for the mass function and $-0.98 \leq \beta \leq -0.26$ for the age distribution, somewhat broader than our 68% confidence intervals for a 0–200 Myr age range but clearly confirming that α is positive and β is negative.

Although the SM08 models have been shown to provide a better representation of individual brown dwarf luminosities due to their inclusion of clouds for L dwarfs and subsequent cloud depletion in the transition to T dwarfs, we find that synthetic populations from the COND models provide a better match to our volume-limited sample’s luminosity function. However, the consistency of the constraints on the mass and age distributions that we find using the SM08 and COND models indicate that the choice of evolutionary model is not significant in our analysis, and we adopt the SM08-based constraints for α and β . These represent the most precise statistical constraints on both parameters to date, and the first calculation of the age distribution of brown dwarfs in the solar neighborhood based on a volume-limited sample.

Our mass distribution indicates an increase in space density toward lower brown dwarf masses, in tension with many previous estimates for the solar neighbor-

hood (which favored fewer low-mass objects) but consistent with recent findings in nearby star-forming regions. Our age distribution clearly favors younger ultracool dwarfs rather than the commonly-assumed uniform age distribution, which may be as much a result of galactic dynamics systematically removing objects from the midplane over time as it is a result of the historical birth rate.

We thank the anonymous referee for a careful review and helpful comments. W. Best acknowledges support from grant HST-GO-15238 provided by STScI and AURA. We acknowledge the grant provided under the John W. Cox Endowment for Advanced Studies in Astronomy by the Department of Astronomy at The University of Texas at Austin that supported A. Sanghi for the duration of Summer 2020. This research was funded in part by the Gordon and Betty Moore Foundation through grant GBMF8550 to M. Liu. T. Dupuy acknowledges support from UKRI STFC AGP grant ST/W001209/1. This work has benefitted from The UltracoolSheet, maintained by Will Best, Trent Dupuy,

Michael Liu, Aniket Sanghi, Rob Siverd, and Zhoujian Zhang, and developed from compilations by Dupuy & Liu (2012), Dupuy & Kraus (2013), Liu et al. (2016), Best et al. (2018), Best et al. (2021), Sanghi et al. (2023), and Schneider et al. (2023). This research has benefitted from the SpeX Prism Library [and the SpeX Prism Library Analysis Toolkit], maintained by Adam Burgasser at <http://www.browndwarfs.org/spexprism>. This work has made use of data from the European Space Agency (ESA) mission *Gaia* (<http://www.cosmos.esa.int/gaia>), processed by the *Gaia* Data Processing and Analysis Consortium (DPAC, <http://www.cosmos.esa.int/web/gaia/dpac/consortium>). Funding for the DPAC has been provided by national institutions, in particular the institutions participating in the *Gaia* Multilateral Agreement. This research has made use of NASA’s Astrophysical Data System and the SIMBAD and VizieR databases operated at CDS, Strasbourg, France. For the purpose of open access, the author has applied a Creative Commons Attribution (CC BY) license to any Author Accepted Manuscript version arising from this submission.

APPENDIX

A. AN UPDATED “SUPER-MAGNITUDE” METHOD FOR CALCULATING BOLOMETRIC LUMINOSITIES

The standard method for determining the bolometric luminosity of a source is to integrate its spectral energy distribution (SED) as a function of wavelength or frequency. Ideally this means integrating a broad spectrum or multi-band photometry spanning most of the SED (e.g., F15; Sanghi et al. 2023). For cold brown dwarfs, however, this method is currently not useful as most of the flux emerges in the mid-infrared where spectra and broad-band photometry are difficult to obtain from the ground, especially for fainter objects, and *JWST* has not yet observed a large sample of brown dwarfs in the mid-infrared. Empirical relations in the literature mapping ultracool dwarf spectral types and broadband photometry to bolometric luminosities (e.g., Liu et al. 2010; Dupuy & Liu 2017, F15) are not valid for spectral types \gtrsim T8 due to the lack of such cold objects with independently-determined bolometric luminosities.

To overcome this barrier, Dupuy & Kraus (2013, hereinafter DK13) added the absolute fluxes in several broad-band NIR and MIR bandpasses to obtain a “super-magnitude” for each object. They used the J_{MKO} , H_{MKO} , and *Spitzer*/IRAC [3.6] and [4.5] bands to define the m_{JH12} super-magnitude whenever such photometry was available in all four bands for an object, since these bands capture \gtrsim 50% of the total flux for late-T and Y dwarfs. When those four bands were not all available, they used super-magnitude from other combinations of bandpasses to match the available photometry. DK13 then calculated the super-magnitudes using the same bandpasses for model spectra (Morley et al. 2012) spanning appropriate ranges of temperature, surface gravity, and cloud thickness. They used the mean super-magnitudes and the corresponding model bolometric luminosities to derive bolometric corrections for the super-magnitudes, enabling bolometric magnitude determinations for T8 and later-type dwarfs.

We have updated this method in several ways:

1. We now use the flux tables for the Sonora-Bobcat cloudless atmosphere models (Marley et al. 2021) to calculate model super-magnitudes using combinations of the J_{MKO} , H_{MKO} , [3.6], [4.5], and AllWISE $W1$ and $W2$ bands. The zero-points we used to convert J , H , [3.6], [4.5], $W1$, $W2$ fluxes into Vega magnitudes were, respectively, 9.31, 8.52, 2.13, 1.26, 4.94, $1.90 \times 10^{-11} \text{ W m}^{-2} \text{ s}^{-1}$. We calculated these by direct integration of the high-resolution

model Vega spectrum from SpeXtool (Cushing et al. 2004) over each bandpass. The zero-points for our super-magnitudes are the sum of the relevant zero-point fluxes, e.g., for m_{JH12} the zero-point is $2.12 \times 10^{-10} \text{ W m}^{-2} \text{ s}^{-1}$.

2. Rather than limiting our super-magnitude calculations to ranges of T_{eff} and surface gravity appropriate only for late-T and Y dwarfs, we have calculated super-magnitudes using all of the Sonora-Bobcat models ($200 \leq T_{\text{eff}} \leq 2400 \text{ K}$ and $3.0 \leq \log g \leq 5.5$).
3. Using the super-magnitudes and luminosities from the Sonora-Bobcat models, we fit 5th-order polynomials to convert the super-magnitudes directly into bolometric luminosities, eliminating the intermediate calculation of bolometric corrections. This change means that the polynomials require *absolute* super-magnitudes to accurately determine the bolometric luminosities.
4. As the Sonora-Bobcat models are computed for three metallicities, $[\text{Fe}/\text{H}] = \{-0.5, 0.0, 0.5\}$, we derived separate polynomials for these three metallicities.

The polynomials converting super-magnitudes to bolometric luminosities are presented in Table 6, along with the RMS of the residuals from the polynomial fits in super-magnitude bins. The residuals for the polynomial fits are shown in Figure 13. The residuals for each super-magnitude show little variation over the full range of metallicities. The polynomials give exceptionally tight relations ($\sigma < 0.02 \text{ dex}$) between m_{JH12} and L_{bol} for $m_{JH12} < 17$, corresponding to $T_{\text{eff}} \gtrsim 400 \text{ K}$. At lower T_{eff} there is an expanding envelope of uncertainty about the polynomial relation. The residuals for the m_{JHW1W2} polynomials (replacing the *Spitzer*/IRAC [3.6] and [4.5] bands with the comparable WISE *W1* and *W2* bands) are very similar. For objects lacking photometry in the near-infrared *J* and *H* bands (which is the case for some known Y dwarfs), the m_{12} and m_{W1W2} super-magnitude polynomials have residuals with a spread of $\approx 0.10 \text{ mag}$, tightening down to $\approx 0.03 \text{ mag}$ at $m_{12} \approx 15 \text{ mag}$ and $m_{W1W2} \approx 16 \text{ mag}$ ($T_{\text{eff}} \sim 500 \text{ K}$).

Figure 14 compares our bolometric magnitudes derived from super-magnitudes to the M_{bol} from other sources and methods in the literature, presented as a function of $M_{K_{\text{MKO}}}$ and of spectral type for all L0–Y2 dwarfs with parallaxes and appropriate photometry. All underlying data (photometry and spectral types) used to compute the M_{bol} were taken from the UltracoolSheet. We show one set of M_{bol} derived from the m_{JH12} super-magnitude, using m_{12} in cases where J_{MKO} or H_{MKO} were unavailable; and a second set derived from m_{JHW1W2} and m_{W1W2} . Literature sources include the L_{bol} computed from low-resolution spectra and broadband photometry by F15, the spectral-type based J_{MKO} and K_{MKO} bolometric corrections of Liu et al. (2010), and the $\log(L_{\text{bol}}/L_{\odot})$ vs. $M_{K_{\text{MKO}}}$ polynomial of Dupuy & Liu (2017).

In general all methods for computing M_{bol} agree well for most of the L, T, and Y dwarf regime. The M_{bol} derived from m_{JHW1W2} and m_{W1W2} diverges sharply from other methods for $M_{K_{\text{MKO}}} < 11.5$ and spectral types earlier than L4. (Insufficient [3.6] and [4.5] photometry exists for such objects to corroborate this trend using m_{JH12} and m_{12} .) The super-magnitude-based M_{bol} are $\approx 0.3 \text{ mag}$ fainter for $M_{K_{\text{MKO}}} \approx 15 - 17 \text{ mag}$ (mid-T spectral types), suggesting that the atmosphere models are under-predicting the bolometric luminosities relative to the flux in passbands used in our super-magnitudes for these objects. The super-magnitudes clearly extend the M_{bol} sequence to fainter and cooler objects than previous methods are able to reach. The steady decline of bolometric luminosity as a function of $M_{K_{\text{MKO}}}$ appears to flatten significantly at $M_{K_{\text{MKO}}} \gtrsim 19 \text{ mag}$, suggesting a more rapid decline in *K*-band flux as these cool objects become colder. Empirical calibration for these objects must await mid-infrared spectra from the James Webb Space Telescope. Until then, we present our updated super-magnitude method as the best way to determine bolometric luminosities for objects with $M_{K_{\text{MKO}}} \gtrsim 18$ or spectral types T8 and later. For warmer objects, we note that the spectral type-based K_{MKO} bolometric corrections from Liu et al. (2010) and the $M_{K_{\text{MKO}}}$ polynomial of Dupuy & Liu (2017) give very similar results, and are both consistent with the calculations of F15. If direct calculation of M_{bol} from spectra and/or broadband photometry is not available or feasible, these methods or other similar conversions from the literature (e.g., F15; Faherty et al. 2016) should be sufficient.

REFERENCES

- Aganze, C., Burgasser, A. J., Malkan, M., et al. 2022, ApJ, Albert, L., Artigau, E., Delorme, P., et al. 2011, AJ, 141,

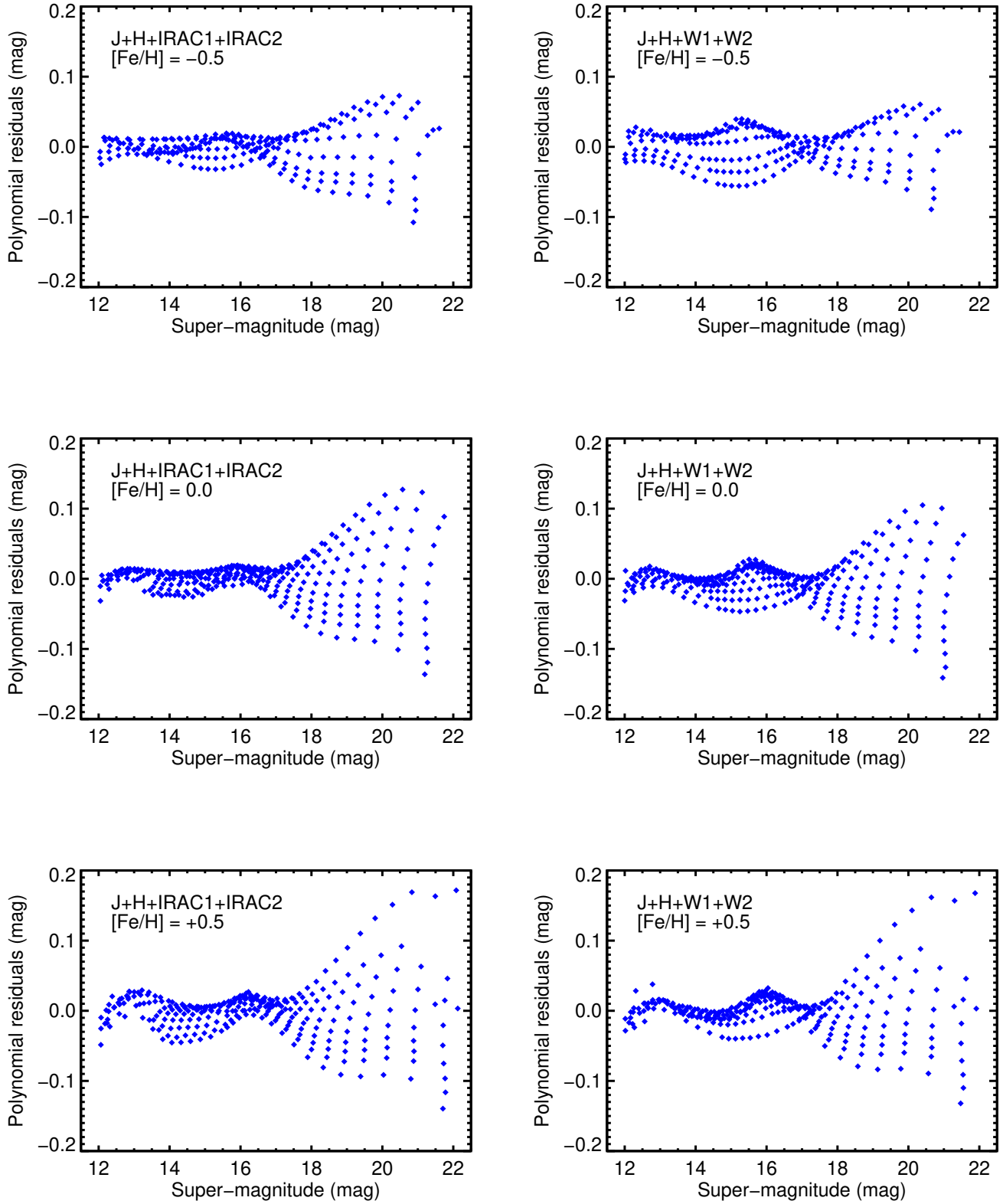


Figure 13. Residuals for the 5th-order polynomial fits converting super-magnitudes to bolometric luminosities, using Sonora-Bobcat cloudless atmosphere models.

Table 6. Polynomials Converting Super-magnitude to M_{bol}

Super-magnitude	c_0	c_1	c_2	c_3	c_4	c_5	Valid M range (mag)
[Fe/H] = -0.5							
M_{JH12}	-6.4398e+00	-1.4027e-01	2.3226e-01	-3.0873e-02	1.4257e-03	-2.2589e-05	12 - 22
M_{JHW1W2}	-2.7293e+01	6.0786e+00	-4.9259e-01	1.0392e-02	2.7620e-04	-1.0041e-05	12 - 22
M_{12}	-1.5231e+02	5.0524e+01	-6.5969e+00	4.1605e-01	-1.2839e-02	1.5571e-04	12 - 20
M_{W1W2}	-1.5505e+02	4.9420e+01	-6.2087e+00	3.7708e-01	-1.1211e-02	1.3099e-04	12 - 20
[Fe/H] = 0.0							
M_{JH12}	-2.7157e-01	-2.6723e+00	6.1027e-01	-5.7324e-02	2.3075e-03	-3.3885e-05	12 - 22
M_{JHW1W2}	-1.0493e+01	5.6039e-02	3.3836e-01	-4.5086e-02	2.0762e-03	-3.2808e-05	12 - 22
M_{12}	-2.4219e+02	7.7727e+01	-9.8550e+00	6.0935e-01	-1.8529e-02	2.2228e-04	12 - 20
M_{W1W2}	-2.8736e+02	8.9031e+01	-1.0910e+01	6.5390e-01	-1.9305e-02	2.2513e-04	12 - 20
[Fe/H] = +0.5							
M_{JH12}	-1.9805e+00	-2.6266e+00	6.5022e-01	-6.1584e-02	2.4614e-03	-3.5652e-05	12 - 22
M_{JHW1W2}	-2.3089e+01	3.4414e+00	-2.6539e-02	-2.5080e-02	1.5099e-03	-2.6089e-05	12 - 22
M_{12}	-3.6928e+02	1.1681e+02	-1.4623e+01	8.9825e-01	-2.7232e-02	3.2676e-04	12 - 20
M_{W1W2}	-2.7307e+02	8.3427e+01	-1.0076e+01	5.9445e-01	-1.7261e-02	1.9793e-04	12 - 21

Super-magnitude	RMS of polynomial over magnitude bins									
	12-13 (mag)	13-14 (mag)	14-15 (mag)	15-16 (mag)	16-17 (mag)	17-18 (mag)	18-19 (mag)	19-20 (mag)	20-21 (mag)	21-22 (mag)
[Fe/H] = -0.5										
M_{JH12}	0.011	0.009	0.012	0.016	0.012	0.025	0.038	0.049	0.065	0.026
M_{JHW1W2}	0.017	0.019	0.026	0.033	0.017	0.015	0.026	0.040	0.052	0.003
M_{12}	0.080	0.069	0.030	0.020	0.036	0.049	0.065	0.028
M_{W1W2}	0.086	0.082	0.060	0.022	0.018	0.031	0.042	0.052
[Fe/H] = 0.0										
M_{JH12}	0.010	0.012	0.012	0.010	0.010	0.027	0.046	0.062	0.073	0.086
M_{JHW1W2}	0.012	0.010	0.013	0.022	0.014	0.017	0.040	0.055	0.078	0.069
M_{12}	0.068	0.063	0.033	0.019	0.043	0.062	0.073	0.089
M_{W1W2}	0.071	0.075	0.058	0.026	0.023	0.046	0.063	0.081
[Fe/H] = +0.5										
M_{JH12}	0.019	0.020	0.018	0.014	0.011	0.022	0.045	0.064	0.080	0.094
M_{JHW1W2}	0.015	0.007	0.010	0.018	0.014	0.017	0.042	0.063	0.075	0.095
M_{12}	0.059	0.067	0.042	0.016	0.040	0.063	0.080	0.098
M_{W1W2}	0.068	0.074	0.066	0.030	0.023	0.050	0.068	0.085	0.097	...

NOTE— The polynomials are defined as $\log(L_{\text{bol}}/L_{\odot}) = \sum_{i=0}^5 c_i M^i$, where M is the absolute super-magnitude of the object. The rightmost column in the top section gives the valid range for the absolute super-magnitude (not bolometric magnitude). The super-magnitudes used to derive these polynomials were calculated from Sonora-Bobcat cloudless atmospheric models.

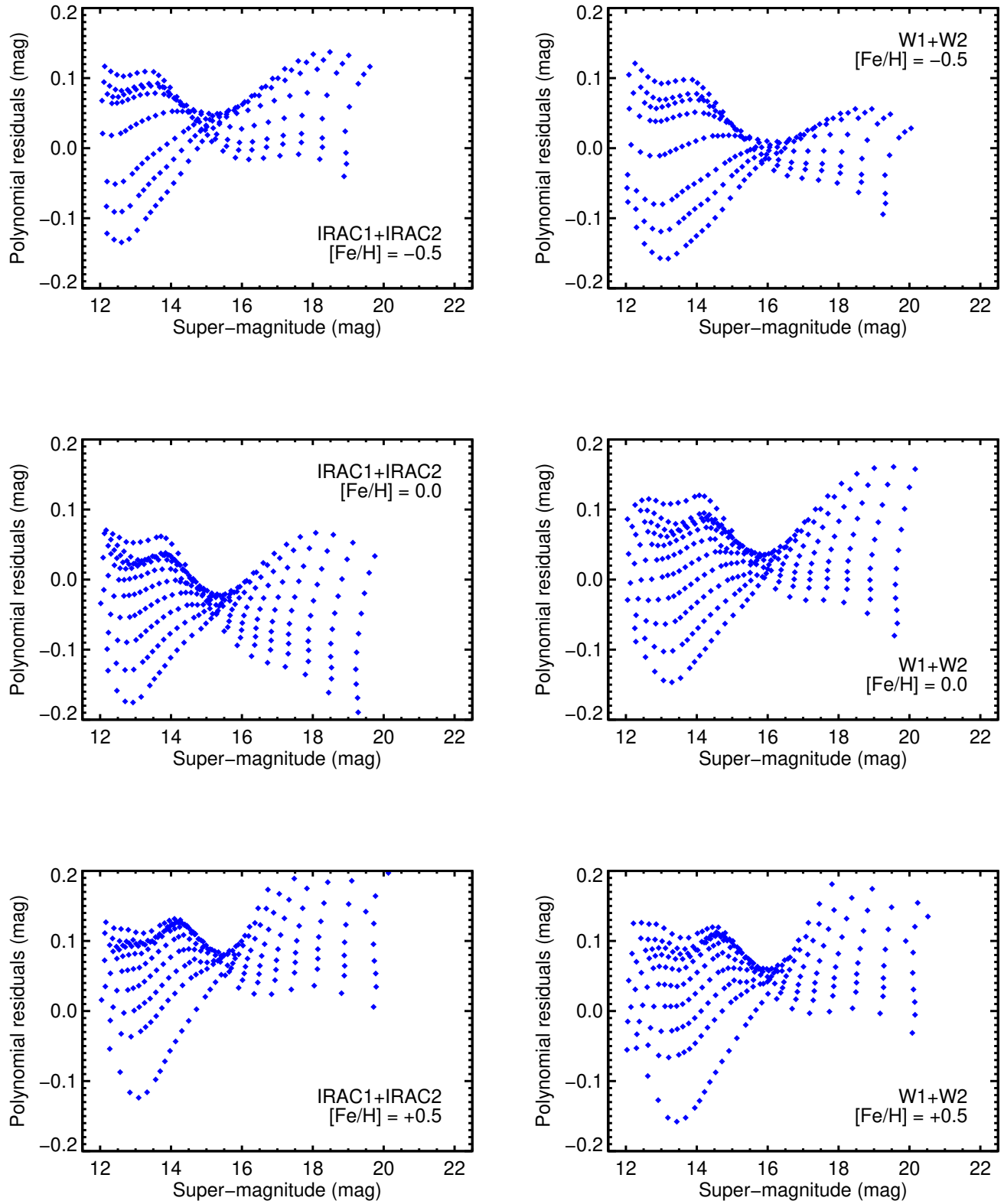


Figure 13. Continued.

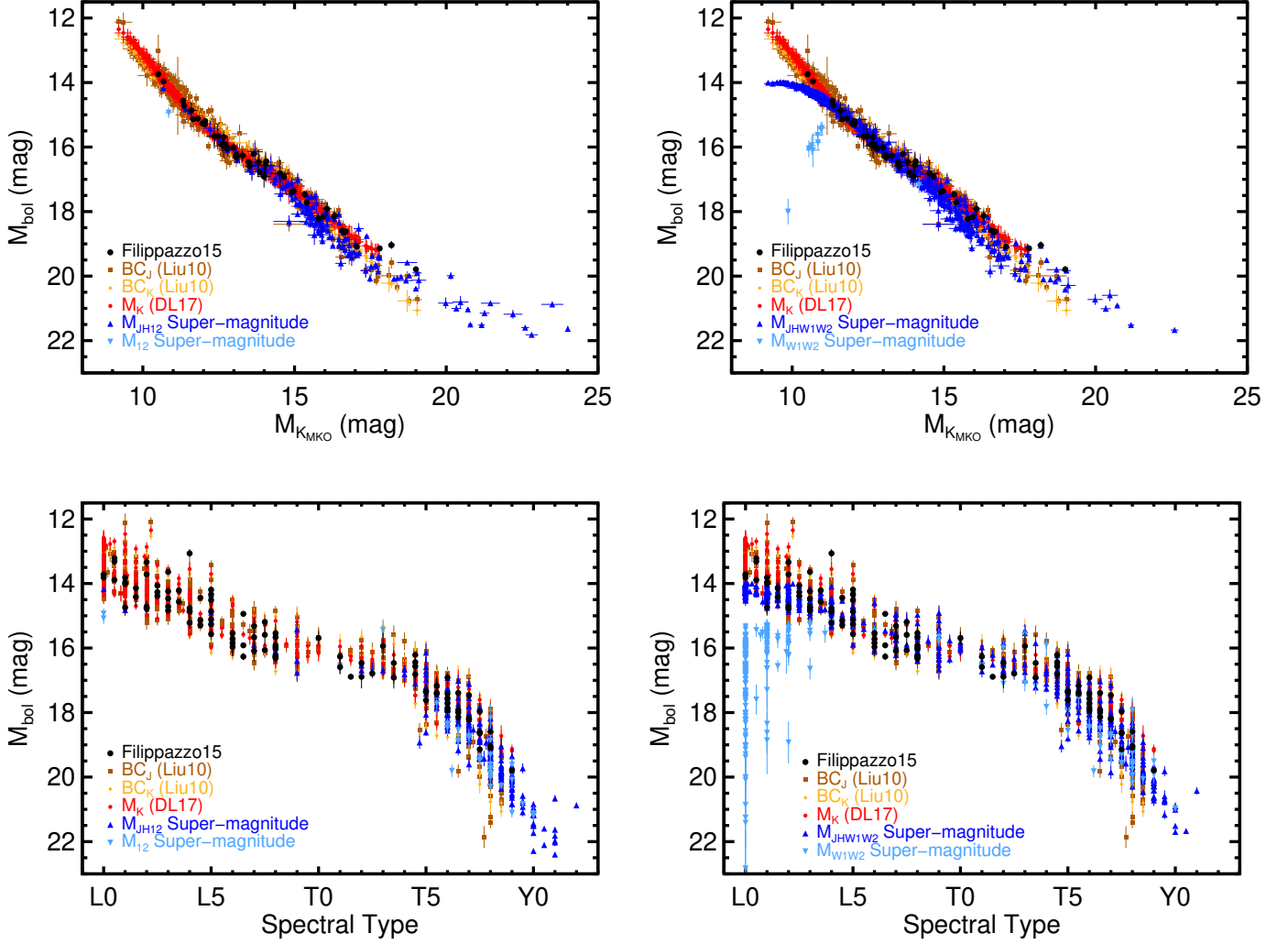


Figure 14. *Left:* Bolometric magnitudes calculated with our updated super-magnitude method for L0–Y2 dwarfs, using m_{JH12} (dark blue) or m_{I12} (light blue, when J_{MKO} or H_{MKO} photometry were not available), shown as a function of $M_{K_{MKO}}$ (top) and of spectral type (bottom). Included for comparison are bolometric magnitudes determined (F15; black circles), or calculated using the J_{MKO} and K_{MKO} bolometric corrections of Liu et al. (2010, brown squares and orange diamonds, respectively), or the $\log(L_{bol}/L_{\odot})$ vs. $M_{K_{MKO}}$ polynomial of Dupuy & Liu (2017, red circles). *Right:* Same plots but showing M_{bol} calculated using the m_{JHW1W2} (dark blue) or m_{W1W2} super-magnitudes. All methods generally agree, but the super-magnitude-based M_{bol} are ≈ 0.3 mag fainter for $M_{K_{MKO}} \approx 15 - 17$ mag (mid-T spectral types) and diverge sharply from other methods at spectral types earlier than $\approx L4$. The super-magnitude method extends the M_{bol} sequence to fainter and cooler objects than previous methods are able to reach and should be used to determine M_{bol} for spectral types $\approx T8$ and later.

- Allard, F., Homeier, D., & Freytag, B. 2012, *Philosophical Transactions of the Royal Society A: Mathematical*, 370, 2765
- Allen, P. R., Koerner, D. W., Reid, I. N., & Trilling, D. E. 2005, *ApJ*, 625, 385
- Allers, K. N., & Liu, M. C. 2013, *ApJ*, 772, 79
- Alves de Oliveira, C., Moraux, E., Bouvier, J., et al. 2013, *A&A*, 549, 123
- Artigau, E., Doyon, R., Lafreniere, D., et al. 2006, *ApJL*, 651, L57
- Artigau, E., Lafreniere, D., Doyon, R., et al. 2011, *ApJ*, 739, 48
- Baraffe, I., Chabrier, G., Barman, T. S., Allard, F., & Hauschildt, P. H. 2003, *A&A*, 402, 701
- Baraffe, I., Homeier, D., Allard, F., & Chabrier, G. 2015, *A&A*, 577, A42
- Bardalez Gagliuffi, D. C., Burgasser, A. J., Gelino, C. R., et al. 2014, *ApJ*, 794, 143
- Bardalez Gagliuffi, D. C., Burgasser, A. J., Schmidt, S. J., et al. 2019, *ApJ*, 883, 205
- Bardalez Gagliuffi, D. C., Faherty, J. K., Schneider, A. C., et al. 2020, *ApJ*, 895, 145
- Bastian, N., Covey, K. R., & Meyer, M. R. 2010, *ARA&A*, 48, 339
- Beamín, J. C., Minniti, D., Gromadzki, M., et al. 2013, *A&A*, 557, L8
- Beichman, C., Gelino, C. R., Kirkpatrick, J. D., et al. 2014, *ApJ*, 783, 68
- Bell, C. P. M., Mamajek, E. E., & Naylor, T. 2015, *MNRAS*, 454, 593
- Bernat, D., Bouchez, A. H., Ireland, M., et al. 2010, *ApJ*, 715, 724
- Best, W. M. J., Liu, M. C., Magnier, E. A., & Dupuy, T. J. 2020, *AJ*, 159, 257
- . 2021, *AJ*, 161, 42
- Best, W. M. J., Liu, M. C., Magnier, E. A., et al. 2013, *ApJ*, 777, 84
- . 2015, *ApJ*, 814, 118
- . 2017, *ApJ*, 837, 95
- Best, W. M. J., Magnier, E. A., Liu, M. C., et al. 2018, *ApJS*, 234, 1
- Bihain, G., Scholz, R.-D., Storm, J., & Schnurr, O. 2013, *A&A*, 557, 43
- Boss, A. P. 1997, *Science*, 276, 1836
- Bouy, H., Brandner, W., Martín, E. L., et al. 2003, *AJ*, 126, 1526
- Bouy, H., Martín, E. L., Brandner, W., & Bouvier, J. 2005, *AJ*, 129, 511
- Bowler, B. P., Liu, M. C., & Dupuy, T. J. 2010, *ApJ*, 710, 45
- Burgasser, A. J. 2004, *ApJS*, 155, 191
- Burgasser, A. J., Blake, C. H., Gelino, C. R., Sahlmann, J., & Bardalez Gagliuffi, D. C. 2016, *ApJ*, 827, 25
- Burgasser, A. J., Cruz, K. L., Cushing, M. C., et al. 2010a, *ApJ*, 710, 1142
- Burgasser, A. J., Geballe, T. R., Leggett, S. K., Kirkpatrick, J. D., & Golimowski, D. A. 2006a, *ApJ*, 637, 1067
- Burgasser, A. J., Kirkpatrick, J. D., Cruz, K. L., et al. 2006b, *ApJS*, 166, 585
- Burgasser, A. J., Kirkpatrick, J. D., Liebert, J., & Burrows, A. S. 2003a, *ApJ*, 594, 510
- Burgasser, A. J., Kirkpatrick, J. D., & Lowrance, P. J. 2005a, *AJ*, 129, 2849
- Burgasser, A. J., Kirkpatrick, J. D., McElwain, M. W., et al. 2003b, *AJ*, 125, 850
- Burgasser, A. J., Kirkpatrick, J. D., Reid, I. N., et al. 2003c, *ApJ*, 586, 512
- Burgasser, A. J., Liu, M. C., Ireland, M. J., Cruz, K. L., & Dupuy, T. J. 2008a, *ApJ*, 681, 579
- Burgasser, A. J.,Looper, D. L., Kirkpatrick, J. D., Cruz, K. L., & Swift, B. J. 2008b, *ApJ*, 674, 451
- Burgasser, A. J.,Looper, D. L., & Rayner, J. T. 2010b, *AJ*, 139, 2448
- Burgasser, A. J., & McElwain, M. W. 2006, *AJ*, 131, 1007
- Burgasser, A. J., McElwain, M. W., & Kirkpatrick, J. D. 2003d, *AJ*, 126, 2487
- Burgasser, A. J., McElwain, M. W., Kirkpatrick, J. D., et al. 2004, *AJ*, 127, 2856
- Burgasser, A. J., Reid, I. N., Leggett, S. K., et al. 2005b, *ApJL*, 634, L177
- Burgasser, A. J., Sitarski, B. N., Gelino, C. R., Logsdon, S. E., & Perrin, M. D. 2011, *ApJ*, 739, 49
- Burgasser, A. J., Tinney, C. G., Cushing, M. C., et al. 2008c, *ApJL*, 689, L53
- Burgasser, A. J., Kirkpatrick, J. D., Brown, M. E., et al. 1999, *ApJ*, 522, L65
- Burgasser, A. J., Kirkpatrick, J. D., Cutri, R. M., et al. 2000a, *ApJ*, 531, L57
- Burgasser, A. J., Wilson, J. C., Kirkpatrick, J. D., et al. 2000b, *AJ*, 120, 1100
- Burgasser, A. J., Kirkpatrick, J. D., Brown, M. E., et al. 2002, *ApJ*, 564, 421
- Burningham, B., Pinfield, D. J., Leggett, S. K., et al. 2008, *MNRAS*, 391, 320
- . 2009, *MNRAS*, 395, 1237
- Burningham, B., Pinfield, D. J., Lucas, P. W., et al. 2010a, *MNRAS*, 406, 1885
- Burningham, B., Leggett, S. K., Lucas, P. W., et al. 2010b, *MNRAS*, 404, 1952

- Burningham, B., Lucas, P. W., Leggett, S. K., et al. 2011, *MNRASL*, 414, L90
- Burningham, B., Cardoso, C. V., Smith, L., et al. 2013, *MNRAS*, 433, 457
- Burrows, A. S., Marley, M. S., Hubbard, W. B., et al. 1997, *ApJ*, 491, 856
- Casewell, S. L., Dobbie, P. D., Hodgkin, S. T., et al. 2007, *MNRAS*, 378, 1131
- Castro, P. J., & Gizis, J. E. 2012, *ApJ*, 746, 3
- Castro, P. J., Gizis, J. E., Harris, H. C., et al. 2013, *ApJ*, 776, 126
- Chabrier, G. 2003, *PASP*, 115, 763
- Chabrier, G., Johansen, A., Janson, M., & Rafikov, R. 2014, in *Protostars and Planets VI*, ed. H. Beuther, R. Klessen, C. P. Dullemond, & T. Henning, University of Arizona Press, Tucson, 619–642
- Chambers, K. C., Magnier, E. A., Metcalfe, N., et al. 2020, *ApJS*, in press, arXiv:1612.05560
- Chen, M., Li, Y., Brandt, T. D., et al. 2022, *AJ*, 163, 288
- Chiu, K., Fan, X., Leggett, S. K., et al. 2006, *AJ*, 131, 2722
- Cruz, K. L., Burgasser, A. J., Reid, I. N., & Liebert, J. 2004, *ApJL*, 604, L61
- Cruz, K. L., Kirkpatrick, J. D., & Burgasser, A. J. 2009, *AJ*, 137, 3345
- Cruz, K. L., Núñez, A., Burgasser, A. J., et al. 2018, *AJ*, 155, 34
- Cruz, K. L., Reid, I. N., Liebert, J., Kirkpatrick, J. D., & Lowrance, P. J. 2003, *AJ*, 126, 2421
- Cruz, K. L., Reid, I. N., Kirkpatrick, J. D., et al. 2007, *AJ*, 133, 439
- Cushing, M. C., Kirkpatrick, J. D., Gelino, C. R., et al. 2014, *AJ*, 147, 113
- Cushing, M. C., Moskovitz, N., & Gustafsson, A. 2018, *RNAAS*, 2, 50
- Cushing, M. C., Vacca, W. D., & Rayner, J. T. 2004, *PASP*, 116, 362
- Cushing, M. C., Kirkpatrick, J. D., Gelino, C. R., et al. 2011, *ApJ*, 743, 50
- Cushing, M. C., Hardegree-Ullman, K. K., Trucks, J. L., et al. 2016, *ApJ*, 823, 152
- Cutri, R. M., Skrutskie, M. F., Van Dyk, S., et al. 2003, *yCat*, II/246, 0
- Da Rio, N., Robberto, M., Hillenbrand, L. A., Henning, T., & Stassun, K. G. 2012, *ApJ*, 748, 14
- Dahn, C. C., Harris, H. C., Vrba, F. J., et al. 2002, *AJ*, 124, 1170
- Dahn, C. C., Harris, H. C., Subasavage, J. P., et al. 2017, *AJ*, 154, 147
- Damian, B., Jose, J., Biller, B. A., et al. 2023, arXiv.org
- Day-Jones, A. C., Marocco, F., Pinfield, D. J., et al. 2013, *MNRAS*, 430, 1171
- Deacon, N. R., & Hambly, N. C. 2006, *MNRAS*, 371, 1722
- Deacon, N. R., Hambly, N. C., & Cooke, J. A. 2005, *A&A*, 435, 363
- Deacon, N. R., Liu, M. C., Magnier, E. A., et al. 2011, *AJ*, 142, 77
- . 2012a, *ApJ*, 755, 94
- . 2012b, *ApJ*, 757, 100
- . 2014, *ApJ*, 792, 119
- Deacon, N. R., Magnier, E. A., Best, W. M. J., et al. 2017a, *MNRAS*, 468, 3499
- Deacon, N. R., Magnier, E. A., Liu, M. C., et al. 2017b, *MNRAS*, 467, 1126
- Delfosse, X., Tinney, C. G., Forveille, T., et al. 1999, *A&AS*, 135, 41
- . 1997, *A&A*, 327, L25
- Delorme, P., Delfosse, X., Albert, L., et al. 2008, *A&A*, 482, 961
- Dupuy, T. J., & Kraus, A. L. 2013, *Science*, 341, 1492
- Dupuy, T. J., & Liu, M. C. 2012, *ApJS*, 201, 19
- . 2017, *ApJS*, 231, 15
- Dupuy, T. J., Liu, M. C., & Ireland, M. J. 2009, *ApJ*, 692, 729
- Dupuy, T. J., Liu, M. C., & Leggett, S. K. 2015a, *ApJ*, 803, 102
- Dupuy, T. J., Liu, M. C., Leggett, S. K., et al. 2015b, *ApJ*, 805, 56
- Dye, S., Lawrence, A., Read, M. A., et al. 2018, *MNRAS*, 473, 5113
- Eddington, A. S. 1913, *MNRAS*, 73, 359
- Faherty, J. K., Burgasser, A. J., Cruz, K. L., et al. 2009, *AJ*, 137, 1
- Faherty, J. K., Gagné, J., Burgasser, A. J., et al. 2018, *ApJ*, 868, 44
- Faherty, J. K., Tinney, C. G., Skemer, A., & Monson, A. J. 2014, *ApJL*, 793, L16
- Faherty, J. K., Burgasser, A. J., Walter, F. M., et al. 2012, *ApJ*, 752, 56
- Faherty, J. K., Riedel, A. R., Cruz, K. L., et al. 2016, *ApJS*, 225, 10
- Fan, X., Knapp, G. R., Strauss, M. A., et al. 2000, *AJ*, 119, 928
- Fantin, N. J., Côté, P., McConnachie, A. W., et al. 2019, *ApJ*, 887, 148
- Filippazzo, J. C., Rice, E. L., Faherty, J., et al. 2015, *ApJ*, 810, 158
- Gagné, J., Burgasser, A. J., Faherty, J. K., et al. 2015a, *ApJL*, 808, L20
- Gagné, J., & Faherty, J. K. 2018, *ApJ*, 862, 138

- Gagné, J., Lafreniere, D., Doyon, R., Malo, L., & Artigau, E. 2014, *ApJ*, 783, 121
- Gagné, J., Faherty, J. K., Cruz, K. L., et al. 2015b, *ApJS*, 219, 33
- Gagné, J., Faherty, J. K., Burgasser, A. J., et al. 2017, *ApJL*, 841, L1
- Gagné, J., Mamajek, E. E., Malo, L., et al. 2018, *ApJ*, 856, 23
- Gaia Collaboration, Vallenari, A., Brown, A. G. A., et al. 2023, *A&A*, 674, A1, doi: [10.1051/0004-6361/202243940](https://doi.org/10.1051/0004-6361/202243940)
- Gauza, B., Bejar, V. J. S., Pérez Garrido, A., et al. 2015, *ApJ*, 804, 96
- Geballe, T. R., Knapp, G. R., Leggett, S. K., et al. 2002, *ApJ*, 564, 466
- Gelino, C. R., Smart, R. L., Marocco, F., et al. 2014, *AJ*, 148, 6
- Gennaro, M., & Robberto, M. 2020, *ApJ*, 896, 80
- Gizis, J. E. 2002, *ApJ*, 575, 484
- Gizis, J. E., Burgasser, A. J., Berger, E., et al. 2013, *ApJ*, 779, 172
- Gizis, J. E., Burgasser, A. J., Faherty, J. K., Castro, P. J., & Shara, M. M. 2011a, *AJ*, 142, 171
- Gizis, J. E., Burgasser, A. J., & Vrba, F. J. 2015, *AJ*, 150, 179
- Gizis, J. E., Kirkpatrick, J. D., & Wilson, J. C. 2001, *AJ*, 121, 2185
- Gizis, J. E., Monet, D. G., Reid, I. N., et al. 2000, *AJ*, 120, 1085
- Gizis, J. E., Reid, I. N., & Hawley, S. L. 2002, *AJ*, 123, 3356
- Gizis, J. E., Reid, I. N., Knapp, G. R., et al. 2003, *AJ*, 125, 3302
- Gizis, J. E., Troup, N. W., & Burgasser, A. J. 2011b, *ApJL*, 736, L34
- Goldman, B., Marsat, S., Henning, T., Clemens, C., & Greiner, J. 2010, *MNRAS*, 405, 1140
- Gomes, J. I., Pinfield, D. J., Marocco, F., et al. 2013, *MNRAS*, 431, 2745
- Gonzales, E. C., Faherty, J. K., Gagné, J., et al. 2019, *ApJ*, 886, 131
- Goto, M., Kobayashi, N., Terada, H., et al. 2002, *ApJL*, 567, L59
- Greco, J. J., Schneider, A. C., Cushing, M. C., Kirkpatrick, J. D., & Burgasser, A. J. 2019, *AJ*, 158, 182
- Hall, P. B. 2002, *ApJL*, 564, L89
- Hawley, S. L., Covey, K. R., Knapp, G. R., et al. 2002, *AJ*, 123, 3409
- Hsu, C.-C., Burgasser, A. J., Theissen, C. A., et al. 2021, *ApJS*, 257, 45
- Janson, M., Carson, J., Thalmann, C., et al. 2011, *ApJ*, 728, 85
- Kellogg, K., Metchev, S. A., Geißler, K., et al. 2015, *AJ*, 150, 182
- Kellogg, K., Metchev, S. A., Miles-Páez, P. A., & Tannock, M. E. 2017, *AJ*, 154, 112
- Kendall, T. R., Delfosse, X., Martín, E. L., & Forveille, T. 2004, *A&A*, 416, L17
- Kendall, T. R., Jones, H. R. A., Pinfield, D. J., et al. 2007, *MNRAS*, 374, 445
- Kirkpatrick, J. D. 2005, *ARA&A*, 43, 195
- Kirkpatrick, J. D., Reid, I. N., Liebert, J., et al. 1999, *ApJ*, 519, 802
- . 2000, *AJ*, 120, 447
- Kirkpatrick, J. D., Cruz, K. L., Barman, T. S., et al. 2008, *ApJ*, 689, 1295
- Kirkpatrick, J. D., Looper, D. L., Burgasser, A. J., et al. 2010, *ApJS*, 190, 100
- Kirkpatrick, J. D., Cushing, M. C., Gelino, C. R., et al. 2011, *ApJS*, 197, 19
- Kirkpatrick, J. D., Gelino, C. R., Cushing, M. C., et al. 2012, *ApJ*, 753, 156
- Kirkpatrick, J. D., Schneider, A. C., Fajardo-Acosta, S., et al. 2014, *ApJ*, 783, 122
- Kirkpatrick, J. D., Kellogg, K., Schneider, A. C., et al. 2016, *ApJS*, 224, 36
- Kirkpatrick, J. D., Martin, E. C., Smart, R. L., et al. 2019, *ApJS*, 240, 19
- Kirkpatrick, J. D., Gelino, C. R., Faherty, J. K., et al. 2021, *ApJS*, 253, 7
- Knapp, G. R., Leggett, S. K., Fan, X., et al. 2004, *AJ*, 127, 3553
- Koerner, D. W., Kirkpatrick, J. D., McElwain, M. W., & Bonaventura, N. R. 1999, *ApJL*, 526, L25
- Kroupa, P. 2001, *MNRAS*, 322, 231
- Lawrence, A., Warren, S. J., Almaini, O., et al. 2007, *MNRAS*, 379, 1599
- . 2012, *yCat*, II/314, 0
- Leggett, S. K., Hauschildt, P. H., Allard, F., Geballe, T. R., & Baron, E. 2002a, *MNRAS*, 332, 78
- Leggett, S. K., Morley, C. V., Marley, M. S., & Saumon, D. 2015, *ApJ*, 799, 37
- Leggett, S. K., Morley, C. V., Marley, M. S., et al. 2013, *ApJ*, 763, 130
- Leggett, S. K., Tremblin, P., Esplin, T. L., Luhman, K. L., & Morley, C. V. 2017, *ApJ*, 842, 118
- Leggett, S. K., Tremblin, P., Saumon, D., et al. 2016, *ApJ*, 824, 2
- Leggett, S. K., Geballe, T. R., Fan, X., et al. 2000, *ApJL*, 536, L35
- Leggett, S. K., Golimowski, D. A., Fan, X., et al. 2002b, *ApJ*, 564, 452

- Leggett, S. K., Cushing, M. C., Saumon, D., et al. 2009, *ApJ*, 695, 1517
- Leggett, S. K., Burningham, B., Saumon, D., et al. 2010, *ApJ*, 710, 1627
- Leggett, S. K., Saumon, D., Marley, M. S., et al. 2012, *ApJ*, 748, 74
- Lépine, S., Rich, R. M., Neill, J. D., Caulet, A., & Shara, M. M. 2002, *ApJL*, 581, L47
- Liebert, J., Kirkpatrick, J. D., Cruz, K. L., et al. 2003, *AJ*, 125, 343
- Liu, M. C., Dupuy, T. J., & Allers, K. N. 2016, *ApJ*, 833, 96
- Liu, M. C., Dupuy, T. J., Bowler, B. P., Leggett, S. K., & Best, W. M. J. 2012, *ApJ*, 758, 57
- Liu, M. C., Dupuy, T. J., & Leggett, S. K. 2010, *ApJ*, 722, 311
- Liu, M. C., Fischer, D. A., Graham, J. R., et al. 2002, *ApJ*, 571, 519
- Liu, M. C., & Leggett, S. K. 2005, *ApJ*, 634, 616
- Liu, M. C., Deacon, N. R., Magnier, E. A., et al. 2011, *ApJL*, 740, L32
- Liu, M. C., Magnier, E. A., Deacon, N. R., et al. 2013, *ApJL*, 777, L20
- Lodieu, N., Hambly, N. C., Jameson, R. F., et al. 2007a, *MNRAS*, 374, 372
- Lodieu, N., Scholz, R.-D., McCaughrean, M. J., et al. 2005, *A&A*, 440, 1061
- Lodieu, N., Pinfield, D. J., Leggett, S. K., et al. 2007b, *MNRAS*, 379, 1423
- Lodieu, N., Burningham, B., Day-Jones, A. C., et al. 2012, *A&A*, 548, 53
- Looper, D. L., Kirkpatrick, J. D., & Burgasser, A. J. 2007, *AJ*, 134, 1162
- Looper, D. L., Kirkpatrick, J. D., Cutri, R. M., et al. 2008, *ApJ*, 686, 528
- Lucas, P. W., Tinney, C. G., Burningham, B., et al. 2010, *MNRASL*, 408, L56
- Lucas, P. W., Hoare, M. G., Longmore, A., et al. 2012, *yCat*, II/316, 0
- Luhman, K. L. 2012, *ARA&A*, 50, 65
- . 2014a, *ApJL*, 786, L18
- . 2014b, *ApJ*, 781, 4
- Luhman, K. L., Mamajek, E. E., Allen, P. R., & Cruz, K. L. 2009, *ApJ*, 703, 399
- Luhman, K. L., & Sheppard, S. S. 2014, *ApJ*, 787, 126
- Luhman, K. L., Patten, B. M., Marengo, M., et al. 2007, *ApJ*, 654, 570
- Luhman, K. L., Loutrel, N. P., McCurdy, N. S., et al. 2012, *ApJ*, 760, 152
- Lutz, T. E., & Kelker, D. H. 1973, *PASP*, 85, 573
- Mace, G. N., Kirkpatrick, J. D., Cushing, M. C., et al. 2013a, *ApJS*, 205, 6
- . 2013b, *ApJ*, 777, 36
- Mackereth, J. T., Bovy, J., Leung, H. W., et al. 2019, *MNRAS*, 489, 176
- Mamajek, E. E., Marocco, F., Rees, J. M., et al. 2018, *RNAAS*, 2, 205
- Manjavacas, E., Goldman, B., Reffert, S., & Henning, T. 2013, *A&A*, 560, 52
- Marley, M. S., Saumon, D., Visscher, C., et al. 2021, *ApJ*, 920, 85
- Marocco, F., Smart, R. L., Jones, H. R. A., et al. 2010, *A&A*, 524, 38
- Marocco, F., Andrei, A. H., Smart, R. L., et al. 2013, *AJ*, 146, 161
- Marocco, F., Jones, H. R. A., Day-Jones, A. C., et al. 2015, *MNRAS*, 449, 3651
- Martin, E. C., Kirkpatrick, J. D., Beichman, C. A., et al. 2018, *ApJ*, 867, 109
- Martín, E. L., Brandner, W., & Basri, G. S. 1999, *Science*, 283, 1718
- Martín, E. L., Phan-Bao, N., Bessell, M., et al. 2010, *A&A*, 517, 53
- McMahon, R. G., Banerji, M., Gonzalez, E., et al. 2013, *The Messenger*, 154, 35
- . 2021, *yCat*, 2367
- Meisner, A. M., Faherty, J. K., Kirkpatrick, J. D., et al. 2020a, *ApJ*, 899, 123
- Meisner, A. M., Caselden, D., Kirkpatrick, J. D., et al. 2020b, *ApJ*, 889, 74
- Metchev, S. A., & Hillenbrand, L. A. 2006, *ApJ*, 651, 1166
- Metchev, S. A., Kirkpatrick, J. D., Berriman, G. B., & Looper, D. L. 2008, *ApJ*, 676, 1281
- Mor, R., Robin, A. C., Figueras, F., Roca-Fàbrega, S., & Luri, X. 2019, *A&A*, 624, L1
- Morau, E., Bouvier, J., Stauffer, J. R., & Cuillandre, J. C. 2003, *A&A*, 400, 891
- Morley, C. V., Fortney, J. J., Marley, M. S., et al. 2012, *ApJ*, 756, 172
- Mugrauer, M., Seifahrt, A., Neuhäuser, R., & Mazeh, T. 2006, *MNRASL*, 373, L31
- Murray, D. N., Burningham, B., Jones, H. R. A., et al. 2011, *MNRAS*, 414, 575
- Muzic, K., Radigan, J., Jayawardhana, R., et al. 2012, *AJ*, 144, 180
- Nakajima, T., Oppenheimer, B. R., Kulkarni, S. R., et al. 1995, *Nature*, 378, 463
- Nilsson, R., Veicht, A., Giorla Godfrey, P. A., et al. 2017, *ApJ*, 838, 64

- Peña Ramírez, K., Béjar, V. J. S., Zapatero Osorio, M. R., Petr-Gotzens, M. G., & Martín, E. L. 2012, *ApJ*, 754, 30
- Peña Ramírez, K., Zapatero Osorio, M. R., & Béjar, V. J. S. 2015, *A&A*, 574, A118
- Phan-Bao, N., Bessell, M. S., Martín, E. L., et al. 2008, *MNRAS*, 383, 831
- Phillips, M. W., Tremblin, P., Baraffe, I., et al. 2020, *A&A*, 637, A38
- Pineda, J. S., Hallinan, G., Kirkpatrick, J. D., et al. 2016, *ApJ*, 826, 73
- Pinfield, D. J., Burningham, B., Tamura, M., et al. 2008, *MNRAS*, 390, 304
- Pinfield, D. J., Burningham, B., Lodieu, N., et al. 2012, *MNRAS*, 422, 1922
- Pinfield, D. J., Gomes, J., Day-Jones, A. C., et al. 2014a, *MNRAS*, 437, 1009
- Pinfield, D. J., Gromadzki, M., Leggett, S. K., et al. 2014b, *MNRAS*, 444, 1931
- Pope, B., Martinache, F., & Tuthill, P. 2013, *ApJ*, 767, 110
- Potter, D., Martín, E. L., Cushing, M. C., et al. 2002, *ApJL*, 567, L133
- Radigan, J., Lafreniere, D., Jayawardhana, R., & Doyon, R. 2008, *ApJ*, 689, 471
- Rebolo, R., Zapatero Osorio, M. R., Madrugá, S., et al. 1998, *Science*, 282, 1309
- Reid, I. N., Cruz, K. L., Kirkpatrick, J. D., et al. 2008, *AJ*, 136, 1290
- Reid, I. N., Gizis, J. E., Kirkpatrick, J. D., & Koerner, D. W. 2001, *AJ*, 121, 489
- Reid, I. N., Kirkpatrick, J. D., Gizis, J. E., et al. 2000, *AJ*, 119, 369
- Reid, I. N., Lewitus, E., Allen, P. R., Cruz, K. L., & Burgasser, A. J. 2006a, *AJ*, 132, 891
- Reid, I. N., Lewitus, E., Burgasser, A. J., & Cruz, K. L. 2006b, *ApJ*, 639, 1114
- Reipurth, B., & Clarke, C. 2001, *AJ*, 122, 432
- Reylé, C. 2018, *A&A*, 619, L8
- Reylé, C., Delorme, P., Willott, C. J., et al. 2010, *A&A*, 522, A112
- Robin, A. C., Reylé, C., Derrière, S., & Picaud, S. 2003, *A&A*, 409, 523
- Ruiz, M. T., Leggett, S. K., & Allard, F. 1997, *ApJL*, 491, L107
- Salim, S., Lépine, S., Rich, R. M., & Shara, M. M. 2003, *ApJL*, 586, L149
- Salpeter, E. E. 1955, *ApJ*, 121, 161
- Sanghi, A., Liu, M. C., Best, W. M., et al. 2023, *ApJ*, 959, 63
- Saumon, D., & Marley, M. S. 2008, *ApJ*, 689, 1327
- Schilbach, E., Röser, S., & Scholz, R.-D. 2009, *A&A*, 493, L27
- Schmidt, M. 1968, *ApJ*, 151, 393
- Schmidt, S. J., West, A. A., Burgasser, A. J., Bochanski, J. J., & Hawley, S. L. 2010a, *AJ*, 139, 1045
- Schmidt, S. J., West, A. A., Hawley, S. L., & Pineda, J. S. 2010b, *AJ*, 139, 1808
- Schneider, A. C., Cushing, M. C., Kirkpatrick, J. D., et al. 2014, *AJ*, 147, 34
- Schneider, A. C., Greco, J., Cushing, M. C., et al. 2016, *ApJ*, 817, 112
- Schneider, A. C., Munn, J. A., Vrba, F. J., et al. 2023, *AJ*, 166, 103, doi: [10.3847/1538-3881/ace9bf](https://doi.org/10.3847/1538-3881/ace9bf)
- Schneider, A. C., Cushing, M. C., Kirkpatrick, J. D., et al. 2015, *ApJ*, 804, 92
- Scholz, A., Geers, V., Clark, P., Jayawardhana, R., & Muzic, K. 2013, *ApJ*, 775, 138
- Scholz, R.-D. 2010a, *A&A*, 515, 92
- . 2010b, *A&A*, 510, L8
- . 2020, *A&A*, 637, A45
- Scholz, R.-D., & Bell, C. P. M. 2018, *RNAAS*, 2, 33
- Scholz, R.-D., Bihain, G., Schnurr, O., & Storm, J. 2011, *A&A*, 532, L5
- . 2012, *A&A*, 541, 163
- Scholz, R.-D., Bihain, G., & Storm, J. 2014, *A&A*, 567, A43
- Scholz, R.-D., & Meusinger, H. 2002, *MNRAS*, 336, L49
- Skrutskie, M. F., Cutri, R. M., Stiening, R., et al. 2006, *AJ*, 131, 1163
- Smart, R. L., Bucciarelli, B., Jones, H. R. A., et al. 2018, *MNRAS*, 481, 3548
- Smith, L., Lucas, P. W., Bunce, R., et al. 2014, *MNRAS*, 443, 2327
- Smith, L. C., Lucas, P. W., Kurtev, R., et al. 2018, *MNRAS*, 474, 1826
- Soderblom, D. R., Duncan, D. K., & Johnson, D. R. H. 1991, *ApJ*, 375, 722
- Stephens, D. C., Leggett, S. K., Cushing, M. C., et al. 2009, *ApJ*, 702, 154
- Strauss, M. A., Fan, X., Gunn, J. E., et al. 1999, *ApJL*, 522, L61
- Thalmann, C., Carson, J., Janson, M., et al. 2009, *ApJL*, 707, L123
- Theissen, C. A. 2018, *ApJ*, 862, 173
- Thompson, M. A., Kirkpatrick, J. D., Mace, G. N., et al. 2013, *PASP*, 125, 809
- Thorstensen, J. R., & Kirkpatrick, J. D. 2003, *PASP*, 115, 1207
- Tinney, C. G., Burgasser, A. J., & Kirkpatrick, J. D. 2003, *AJ*, 126, 975

- Tinney, C. G., Burgasser, A. J., Kirkpatrick, J. D., & McElwain, M. W. 2005, *AJ*, 130, 2326
- Tinney, C. G., Kirkpatrick, J. D., Faherty, J. K., et al. 2018, *ApJS*, 236, 28
- Torres, S., Cai, M. X., Brown, A. G. A., & Portegies Zwart, S. 2019, *A&A*, 629, A139
- Tsvetanov, Z. I., Golimowski, D. A., Zheng, W., et al. 2000, *ApJL*, 531, L61
- van Leeuwen, F. 2007, *A&A*, 474, 653
- Vrba, F. J., Henden, A. A., Luginbuhl, C. B., et al. 2004, *AJ*, 127, 2948
- Warren, S. J., Mortlock, D. J., Leggett, S. K., et al. 2007, *MNRAS*, 381, 1400
- Wielen, R. 1977, *A&A*, 60, 263
- Wilson, J. C., Kirkpatrick, J. D., Gizis, J. E., et al. 2001, *AJ*, 122, 1989
- Wilson, J. C., Miller, N. A., Gizis, J. E., et al. 2003, in *IAU Symp. 211, Brown Dwarfs*, ed. E. L. Martín (San Francisco, CA: ASP), 197
- Wright, E. L., Eisenhardt, P. R. M., Mainzer, A. K., et al. 2010, *AJ*, 140, 1868
- Wright, E. L., Skrutskie, M. F., Kirkpatrick, J. D., et al. 2013, *AJ*, 145, 84
- York, D. G., Adelman, J., Anderson, J. E. J., et al. 2000, *AJ*, 120, 1579
- Zhang, Z., Burgasser, A. J., Gálvez-Ortiz, M. C., et al. 2019, *MNRAS*, 486, 1260
- Zhang, Z., Liu, M. C., Best, W. M. J., Dupuy, T. J., & Siverd, R. J. 2021, *ApJ*, 911, 7
- Zhang, Z., Pinfield, D. J., Gálvez-Ortiz, M. C., et al. 2017, *MNRAS*, 464, 3040
- Zhang, Z., Liu, M. C., Hermes, J. J., et al. 2020, *ApJ*, 891, 171
- Zuckerman, B., Bessell, M. S., Song, I., & Kim, S. 2006, *ApJ*, 649, L115
- Zuckerman, B., Song, I., & Bessell, M. S. 2004, *ApJL*, 613, L65